NAVAL POSTGRADUATE SCHOOL
MONTEREY, CALIFORNIA

THESIS

PERFORMANCE AND OPTIMAL PLACEMENT OF PIEZOCERAMIC ACTUATORS FOR SHAPE CONTROL OF A CANTILEVER BEAM

by

Kirk E. Treanor

June, 1996

Thesis Advisor: Brij N. Agrawal

Approved for public release; distribution is unlimited.

DISCLAIMER NOTICE

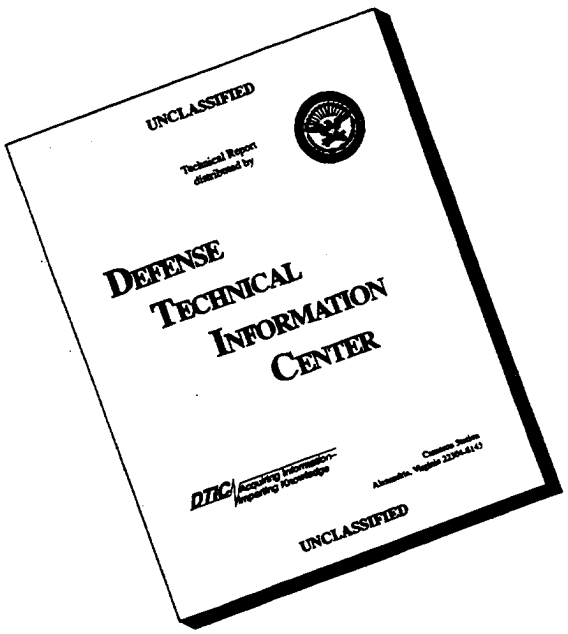

THIS DOCUMENT IS BEST QUALITY AVAILABLE. THE COPY FURNISHED TO DTIC CONTAINED A SIGNIFICANT NUMBER OF PAGES WHICH DO NOT REPRODUCE LEGIBLY.

REPORT DOCUMENTATION PAGE

Form Approved OMB No. 0704-0188

1. AGENCY USE ONLY *(Leave blank)*	2. REPORT DATE June 1996	3. REPORT TYPE AND DATES COVERED Engineer's Thesis

4. TITLE AND SUBTITLE: Performance and Optimal Placement of Piezoceramic Actuators for Shape Control of A Cantilever Beam

5. FUNDING NUMBERS

6. AUTHOR(S) Kirk E. Treanor

7. PERFORMING ORGANIZATION NAME(S) AND ADDRESS(ES)
Naval Postgraduate School
Monterey CA 93943-5000

8. PERFORMING ORGANIZATION REPORT NUMBER

9. SPONSORING/MONITORING AGENCY NAME(S) AND ADDRESS(ES)

10. SPONSORING/MONITORING AGENCY REPORT NUMBER

11. SUPPLEMENTARY NOTES The views expressed in this thesis are those of the author and do not reflect the official policy or position of the Department of Defense or the U.S. Government.

12a. DISTRIBUTION/AVAILABILITY STATEMENT
Approved for public release; distribution is unlimited.

12b. DISTRIBUTION CODE

13. ABSTRACT *(maximum 200 words)*

Shape control of spaceborne antennas can provide the ability to correct for effects such as thermal distortion and manufacturing errors as well as control the shape of an antenna's radiated beam. This thesis examines the performance of piezoceramic actuators in producing static deformation of a cantilever beam and analyzes the optimal placement of actuators to best approximate a desired deformation profile. Predictions of actuator effectiveness at producing curvature are developed using an Euler-Bernoulli model. An algorithm to determine the optimal locations and input voltages for a fixed set of actuators to achieve a desired deformation profile of a cantilever beam using embedded Nelder and Mead simplex search routines is presented and evaluated for two shape functions and various combinations of actuators. Experimental measurements show that the Euler-Bernoulli model provides a reasonable prediction of actuator performance at low input voltage but does not account for nonlinear behavior of the piezoceramic and the effects of hysteresis and transverse stresses. Further experiments demonstrate the ability of four piezoceramic actuators to produce an approximation of a parabolic deformation profile of a cantilever beam and illustrate the importance of considering these effects in determining the required actuator input voltages.

14. SUBJECT TERMS
Piezoceramic Actuator, Piezoelectric, Shape Control, Optimization

15. NUMBER OF PAGES 172

16. PRICE CODE

17. SECURITY CLASSIFICATION OF REPORT	18. SECURITY CLASSIFICATION OF THIS PAGE	19. SECURITY CLASSIFICATION OF ABSTRACT	20. LIMITATION OF ABSTRACT
Unclassified	Unclassified	Unclassified	UL

NSN 7540-01-280-5500

Standard Form 298 (Rev. 2-89)
Prescribed by ANSI Std. 239-18 298-102

Approved for public release; distribution is unlimited.

PERFORMANCE AND OPTIMAL PLACEMENT OF PIEZOCERAMIC ACTUATORS FOR SHAPE CONTROL OF A CANTILEVER BEAM

Kirk E. Treanor
Lieutenant, United States Navy
B.S., University of California Los Angeles, 1987

Submitted in partial fulfillment
of the requirements for the degree of

AERONAUTICAL AND ASTRONAUTICAL ENGINEER

from the

NAVAL POSTGRADUATE SCHOOL
June 1996

Author: _____
Kirk E. Treanor

Approved by: _____
Brij N. Agrawal, Thesis Advisor

_____
John L. Meyer, Second Reader

_____
Daniel J. Collins, Chairman
Department of Aeronautics and Astronautics

ABSTRACT

Shape control of spaceborne antennas can provide the ability to correct for effects such as thermal distortion and manufacturing errors as well as control the shape of an antenna's radiated beam. This thesis examines the performance of piezoceramic actuators in producing static deformation of a cantilever beam and analyzes the optimal placement of actuators to best approximate a desired deformation profile. Predictions of actuator effectiveness at producing curvature are developed using an Euler-Bernoulli model. An algorithm to determine the optimal locations and input voltages for a fixed set of actuators to achieve a desired deformation profile of a cantilever beam using embedded Nelder and Mead simplex search routines is presented and evaluated for two shape functions and various combinations of actuators. Experimental measurements show that the Euler-Bernoulli model provides a reasonable prediction of actuator performance at low input voltage but does not account for nonlinear behavior of the piezoceramic and the effects of hysteresis and transverse stresses. Further experiments demonstrate the ability of four piezoceramic actuators to produce an approximation of a parabolic deformation profile of a cantilever beam and illustrate the importance of considering these effects in determining the required actuator input voltages.

TABLE OF CONTENTS

ACKNOWLEDGEMENT

The author would like to gratefully acknowledge several individuals whose assistance has made the successful completion of this thesis possible. Countless thanks go to Mr. Rafford Bailey for his many hours of work spent designing the necessary hardware and constructing the beams used in the experiments. Much appreciation also goes to Mr. Doug Seivwright for his assistance in obtaining the necessary materials to build the experimental apparatus. The help and guidance of Dr. John Meyer has been invaluable in keeping focus on the ultimate objective and overcoming difficulties encountered along the way. Finally, the author wishes to express his gratitude to Dr. Brij Agrawal for his guidance and encouragement and for the opportunity to pursue an exciting and challenging area of research.

I. INTRODUCTION

A. BACKGROUND

Control of the shape of long flexible structures is of interest for a variety of space-related applications. Many spacecraft designs include slender flexible appendages as components of on board antenna systems or sensors. Maintaining the desired shape of such an appendage can be a central requirement for obtaining optimal performance from its associated system. Effects such as thermal distortion, manufacturing errors, spacecraft acceleration and vibration can all cause deviation of the shape of a component from its desired profile. Active means to counter these and other effects are therefore of considerable interest.

Piezoceramic actuators offer an attractive means to produce deformation of flexible structures. These actuators have no moving parts and require only a supplied electrical voltage to produce an electric field across the actuator material in order to function. Piezoceramics can be bonded to or, when properly insulated, embedded inside the structure they are intended to control. Applying an electric field to a piezoceramic actuator causes deformation of the piezoceramic material which, in turn, applies stress to the structure it is attached to.

While substantial research effort has been devoted to the employment and placement of piezoceramic actuators for the active suppression of structural vibrations, considerably less attention has been focused on the use and optimal placement of piezoceramics for quasi-static shape control of flexible structures. Although piezoceramics are limited to the production of relatively small structural deformations, they may be more than adequate for certain applications, such as countering thermal effects or manufacturing errors or producing a small desired deformation profile in a flexible structure.

B. SCOPE OF THESIS

This thesis examines the performance of piezoceramic actuators in producing static deformation of a thin cantilever beam and analyzes the optimal placement of actuators to best approximate a desired deformation profile. Models of common configurations of piezoceramic actuators bonded to the surface of the beam are developed from the Euler-Bernoulli model of Crawley and Anderson [Ref. 1] to compare the effectiveness of the different configurations and examine the effects of actuator thickness, width and material properties on the ability of the actuator to produce curvature of the composite actuator/beam structure. Predictions of actuator performance from the Euler-Bernoulli model are compared to experimental measurements of the tip displacement and surface strain of a cantilever beam for several actuator configurations.

An algorithm to determine the optimal locations and input voltages for a fixed set of actuators which minimize the error between the actual and desired shape of a cantilever beam under piezoceramic actuator induced deformation is presented. Optimization of the actuator locations and voltages is accomplished using the Nelder and Mead simplex search algorithm for the optimization of nonlinear functions. The MATLAB software package is used to implement and test the algorithm for two shape functions and various combinations of actuators. Capabilities and limitations of the algorithm are discussed. The predicted performance of four actuators placed in the optimum locations determined by the algorithm to approximate a parabolic beam deformation profile is compared to the results from a second set of experiments.

II. PIEZOCERAMIC MATERIAL PROPERTIES

Piezoceramics are part of a class of materials which exhibits piezoelectric behavior. Such materials have the property that material strain is produced in response to an electric field applied to the material in line with the its "poling" direction. Similarly, strain due to mechanical stresses on the material will produce an electric field in the material poling direction due to the accumulation of electrical charge on the material surfaces normal to the poling axis. This accumulated charge results in a voltage between the two surfaces. Figure 1 shows the standard coordinate system used to describe the orientation of a piezoelectric material. The poling axis is normally designated as the 3-axis, with the 1- and 2-axes indicating the principal material directions orthogonal to the poling axis.

Piezoelectric materials are typically orthotropic, meaning that the material properties are uniform along each principal material axis, but the properties along one principal axis may not be the same as those along another principal axis. Piezoceramics, however, are generally transversely isotropic, meaning that the material properties are the same in all directions in the plane orthogonal to the poling axis, depicted by the 1-2 plane in Figure 1.

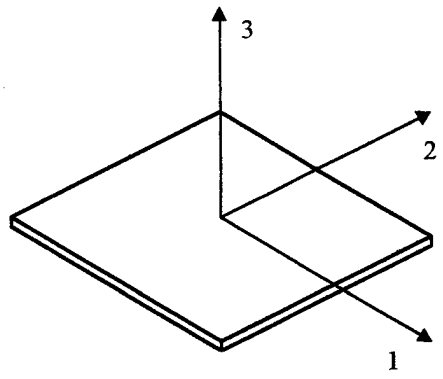

Figure 1. Piezoceramic Material Coordinate System Conventions

The strain behavior of piezoelectric materials in response to applied electric fields and the voltage produced by mechanical stresses makes piezoelectric materials suitable for use as both actuators and sensors in a variety of applications. The voltage between the two surfaces normal to the poling axis in both actuation and sensing applications requires that these two surfaces be electrically insulated from one another, hence piezoelectric materials are generally bonded to the surface of conductive metal structures with the material poling axis normal to the bond. Piezoelectric materials can, however, be embedded in electrically insulating materials, including many composites.

A. CONSTITUTIVE RELATION

The axial strains in a piezoelectric material are functions of the normal stresses applied to the material and the electric field applied in the material poling direction. These strains are given by the material constitutive relation:

$$\begin{bmatrix} \varepsilon_1 \\ \varepsilon_2 \\ \varepsilon_3 \end{bmatrix} = \begin{bmatrix} \frac{1}{E_1} & \frac{-\nu_{12}}{E_1} & \frac{-\nu_{13}}{E_1} \\ \frac{-\nu_{12}}{E_1} & \frac{1}{E_2} & \frac{-\nu_{23}}{E_2} \\ \frac{-\nu_{13}}{E_1} & \frac{-\nu_{23}}{E_2} & \frac{1}{E_3} \end{bmatrix} \begin{bmatrix} \sigma_1 \\ \sigma_2 \\ \sigma_3 \end{bmatrix} + \begin{bmatrix} d_{31} \\ d_{32} \\ d_{33} \end{bmatrix} \phi_3 \tag{2.1}$$

where the 3-direction is the poling direction of the piezoelectric material, the 1 and 2-directions are the principal material axes orthogonal to the poling direction, ε_i is the axial strain in the i-direction, E_i, ν_{ij} and d_{3i} are the material elastic moduli, Poisson ratios and piezoelectric coefficients, respectively, σ_i is the axial stress applied in the i-direction and ϕ_3 is the electric field applied in the material poling direction. The piezoelectric coefficients are generally dependent on the value of the applied electric field but are typically assigned a constant value which provides a linear approximation of the material's piezoelectric

behavior over a specified operating range. The material elastic moduli are also field dependent and are typically specified for constant electric field (short circuit) and open circuit conditions along the poling axis. The moduli for constant electric field are used in Equation 2.1. Typical values of the material properties for various types of lead zirconate titanate (PZT), the most commonly used piezoceramic material, are listed in Table 1.

Material	PZT-4	PZT-5A	PZT-8	PZT-5J	PZT-5H
DOD Type	I	II	III	V	VI
E_1, E_2 (x 10^{10} N/m^2)					
• Short Circuit	8.2	6.1	8.7	6.2	6.2
• Open Circuit	9.9	6.9	9.9	7.1	7.1
E_3 (x 10^{10} N/m^2)					
• Short Circuit	6.6	5.3	7.4	4.4	4.8
• Open Circuit	12.6	10.6	11.8	n/a	11.1
d_{31} (x 10^{-12} m/V)	-122	-171	-97	-220	-274
υ (approximate)	0.31	0.31	0.31	0.31	0.31

Table 1. Material Properties of Selected Piezoceramic Materials [After Ref. 2]

It should be noted that the piezoelectric constitutive relation is of the same form as the thermal-mechanical constitutive relation, with the piezoelectric coefficients corresponding to the material coefficients of thermal expansion and the electric field applied in the poling direction corresponding to the difference in material temperature from its reference temperature. This fact proves useful in modeling piezoelectric material behavior using finite element software which includes thermal-mechanical models but not piezoelectric models.

B. ACTUATOR STRESS

If the piezoceramic material is under a state of plane stress in the plane orthogonal to the poling axis, i.e. $\sigma_3 = 0$, then the expression for the transverse strains in Equation 2.1 can be simplified to:

$$\begin{bmatrix} \varepsilon_1 \\ \varepsilon_2 \end{bmatrix} = \begin{bmatrix} \frac{1}{E_1} & \frac{-\nu_{12}}{E_1} \\ \frac{-\nu_{12}}{E_1} & \frac{1}{E_2} \end{bmatrix} \begin{bmatrix} \sigma_1 \\ \sigma_2 \end{bmatrix} + \begin{bmatrix} d_{31} \\ d_{32} \end{bmatrix} \phi_3 \tag{2.2}$$

which can be solved for the transverse normal stresses:

$$\begin{bmatrix} \sigma_1 \\ \sigma_2 \end{bmatrix} = \begin{bmatrix} Q_{11} & Q_{12} \\ Q_{12} & Q_{22} \end{bmatrix} \begin{bmatrix} \varepsilon_1 - d_{31}\phi_3 \\ \varepsilon_2 - d_{32}\phi_3 \end{bmatrix} \tag{2.3}$$

where the reduced stiffnesses Q_{ij} are given by:

$$\begin{aligned} Q_{11} &= \frac{E_1}{1-\nu_{12}\nu_{21}} \\ Q_{12} &= \frac{\nu_{21}E_1}{1-\nu_{12}\nu_{21}} = \frac{\nu_{12}E_2}{1-\nu_{12}\nu_{21}} \\ Q_{22} &= \frac{E_2}{1-\nu_{12}\nu_{21}} \end{aligned} \tag{2.4}$$

and the material Poisson ratios are related by:

$$\nu_{21} = \frac{E_2}{E_1}\nu_{12} \tag{2.5}$$

Equations 2.1 through 2.5 apply to orthotropic piezoelectric materials and must be used for materials such as polyvinylidene flouride (PVDF) film which are not transversely isotropic in the plane orthogonal to the poling axis. Transversely isotropic materials such as PZT ceramics have the same properties in all directions in the 1-2 plane, i.e.

$$\begin{aligned} E_1 &= E_2 \\ \nu_{12} &= \nu_{21} \\ d_{31} &= d_{32} \end{aligned} \tag{2.6}$$

which allows Equation 2.3 to be further simplified to:

$$\begin{bmatrix} \sigma_1 \\ \sigma_2 \end{bmatrix} = \begin{bmatrix} Q_{11} & Q_{12} \\ Q_{12} & Q_{11} \end{bmatrix} \begin{bmatrix} \varepsilon_1 - d_{31}\phi_3 \\ \varepsilon_2 - d_{31}\phi_3 \end{bmatrix} \tag{2.7}$$

where:

$$\begin{aligned} Q_{11} &= \frac{E_1}{1-\nu_{12}^2} \\ Q_{12} &= \frac{\nu_{12}E_1}{1-\nu_{12}^2} \end{aligned} \tag{2.8}$$

If the material is under a state of uniaxial stress along the 1-axis, i.e. $\sigma_2 = \sigma_3 = 0$ in Equation 2.1, then the expression for the axial strain along the 1-axis can be reduced to:

$$\varepsilon_1 = \frac{\sigma_1}{E_1} + d_{31}\phi_3 \tag{2.9}$$

which can be solved for the normal stress along the 1-axis:

$$\sigma_1 = E_1(\varepsilon_1 - d_{31}\phi_3) \tag{2.10}$$

The plot of Equation 2.10 in Figure 2 is illustrative of the performance of a piezoelectric material as an actuator. An unconstrained piezoelectric material will have normal strain ε_1 equal to the *actuation strain* $d_{31}\phi_3$ and will therefore produce no normal stress σ_1. In contrast, a piezoelectric material constrained to have no normal strain ε_1 will produce the material's *blocked* normal stress:

$$\sigma_{1\,\text{blocked}} = -E_1 d_{31}\phi_3 \tag{2.11}$$

In general, the normal stress in a piezoelectric actuator bonded to or embedded in a deformable structure will be somewhere between zero and the blocked normal stress, as determined by the material properties and geometry of the actuator and structure.

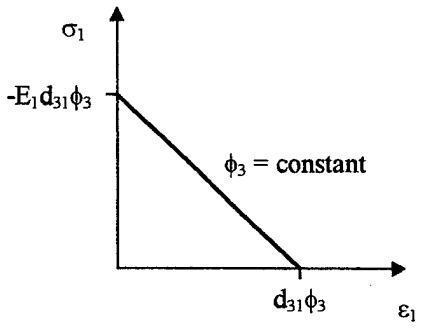

Figure 2. Axial Stress vs. Strain For Piezoelectric Material Under Uniaxial Stress

III. EULER-BERNOULLI MODEL OF BEAM DEFORMATION DUE TO SURFACE-BONDED PIEZOCERAMIC ACTUATORS

Piezoceramics can be used as actuators to produce curvature of a section of a beam. Voltage applied to a piezoceramic actuator bonded to the surface of a beam as shown in Figure 3 will induce normal strain of the same sign in both the 1- and 2-directions. The beam will resist expansion of the piezoceramic to its full actuation strain, producing normal stress in the piezoceramic which will cause curvature of the composite actuator/beam about the *x*- and *z*-axes. The curvature about the *z*-axis for a configuration such as that shown in Figure 3 will be significantly greater than the curvature about the *x*-axis due to the difference in the moments of inertia of the respective beam cross-sections. The resulting stress state in the actuator and the beam can be assumed to be plane stress provided that the material dimensions in the 3-direction are much smaller than the corresponding dimensions in the 1- and 2-directions. The normal stresses in the piezoceramic for the plane stress condition are coupled in the 1- and 2-directions by the Poisson effect, as indicated by Equation 2.7. Solution of the coupled equations requires the use of a complex plate theory model, but a simple approximation of the curvature about the z-axis can be obtained using Euler-Bernoulli assumptions.

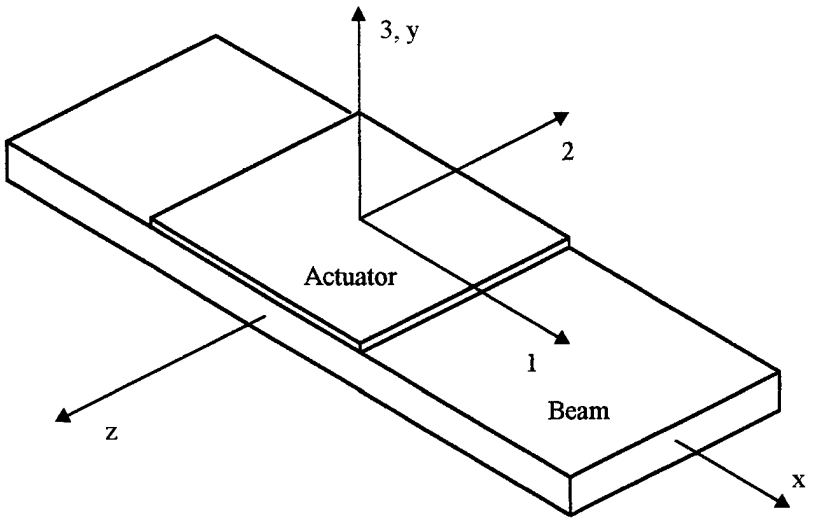

Figure 3. Piezoceramic Actuator Bonded to Beam

Euler-Bernoulli beam theory assumes that the transverse components of normal stress σ_2 and σ_3 are negligible compared to the axial component σ_1 and hence uses Equation 2.10 to determine the normal stress in the piezoceramic along the beam axis. Comparison of Equations 2.7 and 2.10 reveals that the Equation 2.10 provides a lower estimate of the axial stress than Equation 2.7 for a given normal strain ε_1 and applied electric field ϕ_3. The Euler-Bernoulli model therefore gives a conservative approximation of the bending moment produced by the actuator about the beam's z-axis for a given curvature of the beam about that axis.

Crawley and Anderson [Ref. 1] compared two models of beam curvature due to induced strain actuation by piezoceramic actuators bonded to beam structures. The first model, initially presented by Crawley and de Luis [Ref. 2], assumed uniform axial strain in a pair of piezoceramic actuators bonded symmetrically to the outer surfaces of a beam undergoing actuator-induced bending. The second model assumed that the beam behaves as an Euler-Bernoulli beam, with a linear distribution of axial strain throughout the composite actuator-beam cross-section, as shown in Figure 4. The predicted beam curvature under both models was compared to that predicted by a detailed two-dimensional finite element model. The Euler-Bernoulli model was found to provide results that are within 0.1% of the finite element model over the full range of possible actuator-to-beam thickness ratios, while the uniform strain model results diverged significantly for actuator thicknesses greater than about 20% of that of the beam. The Euler-Bernoulli model was therefore judged to provide a much more accurate prediction of beam curvature produced by surface bonded piezoceramic actuators.

Chaudry and Rogers [Ref. 4] performed a similar analysis of an actuator bonded to one side of a beam using a thermal-mechanical finite element model incorporating two-dimensional linear plane stress elements to model the effect of the actuator's piezoelectric behavior. The Euler-Bernoulli and finite element models were again found to be in close agreement, differing by at most 3.9% for actuator-to-beam thickness ratios of 1 or less.

Bronowicki and Betros [Ref. 5] refer to experimental work conducted by Griffin and Denoyer [Ref. 6] which demonstrated that the tip displacement of a beam with a pair

of piezoceramic actuators mounted symmetrically on opposite sides was 8% less than predicted by the Euler-Bernoulli model. The difference between the predicted and measured displacements was within the range of measurement and manufacturing tolerances of the experiment.

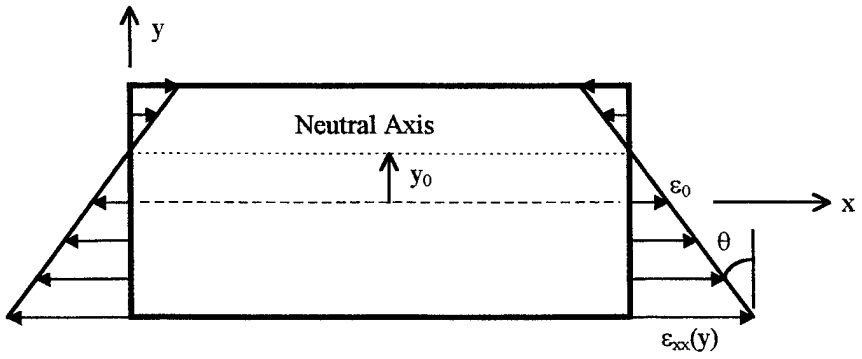

Figure 4. Linear Strain Distribution for Euler-Bernoulli Beam

All of the above references support the use of Euler-Bernoulli assumptions as a suitable model for analysis of the effectiveness of piezoceramic actuators in producing curvature of the composite actuator/beam. The development of this model by Crawley and Anderson [Ref. 1] was used as a basis for comparison of various actuator configurations in this thesis.

A. GENERAL FORMULATION

Crawley and Anderson [Ref. 1] expressed the total strain energy in an Euler-Bernoulli beam with attached or embedded piezoceramic actuators as:

$$U = \frac{1}{2}\int_0^l \left\{ \begin{bmatrix} \varepsilon_0 & \kappa \end{bmatrix} \begin{bmatrix} (EA)_c & (ES)_c \\ (ES)_c & (EI)_c \end{bmatrix} \begin{bmatrix} \varepsilon_0 \\ \kappa \end{bmatrix} - 2\begin{bmatrix} P_\Lambda & M_\Lambda \end{bmatrix} \begin{bmatrix} \varepsilon_0 \\ \kappa \end{bmatrix} \right\} dx \qquad (3.1)$$

where l is the length, ε_0 is the axial strain at $y = 0$, as shown in Figure 4, and κ is the curvature of the actuator/beam section, which can be approximated by:

$$\kappa = \frac{d\theta}{dx} \qquad (\theta << 1) \tag{3.2}$$

The total area stiffness $(EA)_c$, the first moment of inertia $(ES)_c$ and the second moment of inertia $(EI)_c$ of the composite actuator/beam cross-section are respectively given by:

$$(EA)_c = \int_y E(y)w(y)dy \tag{3.3}$$

$$(ES)_c = \int_y E(y)w(y)ydy \tag{3.4}$$

$$(EI)_c = \int_y E(y)w(y)y^2dy \tag{3.5}$$

where $E(y)$ is the elastic modulus and $w(y)$ is the width of the composite actuator beam material as a function of the coordinate y. The first term inside the integral in Equation 3.1, with the 1/2 multiplication factor, represents the strain energy per unit length for a composite beam with the specified cross-sectional properties composed of materials which exhibit linear stress-strain behavior in accordance with Hooke's Law. The second term and 1/2 multiplication factor represent a reduction in the strain energy per unit length due to the portion of the material strain which is induced by the piezoelectric effect rather than applied stress.

The resultant force P_Λ and resultant moment M_Λ due to the actuation strain Λ are respectively determined from:

$$P_\Lambda = \int_y E(y)\Lambda(y)w(y)dy \tag{3.6}$$

$$M_\Lambda = \int_y E(y)\Lambda(y)w(y)ydy \tag{3.7}$$

where the actuation strain Λ is determined by the actuator piezoelectric charge constant d_{31}, the actuator thickness t_p and the actuator input voltage V applied in the poling direction of the piezoceramic:

$$\Lambda = d_{31}\frac{V}{t_p} \tag{3.8}$$

If the actuator and beam properties are constant over the length of the actuator/beam section, Equation 3.1 can be integrated to give:

$$U = \frac{1}{2}l\left[\varepsilon_0{}^2(EA)_c + 2\varepsilon_0\kappa(ES)_c + \kappa^2(EI)_c - 2P_\Lambda\varepsilon_0 - 2M_\Lambda\kappa\right] \tag{3.9}$$

Equations for the axial strain ε_0 at y=0 and the curvature κ can then be obtained by differentiating Equation 3.9 with respect to ε_0 and κ and using Castigliano's First Theorem:

$$\frac{\partial U}{\partial qi} = Q_i \quad (i = 1,2,\ldots,n) \tag{3.10}$$

where q_i is the ith displacement and Q_i is the ith generalized external force. If no external forces or moments are applied to the beam, substitution of Equation 3.9 into Equation 3.10 gives:

$$\frac{\partial U}{\partial \varepsilon_0} = \frac{1}{2} l\left[2\varepsilon_0 (EA)_c + 2\kappa (ES)_c - 2P_\Lambda\right] = 0$$
$$\frac{\partial U}{\partial \kappa} = \frac{1}{2} l\left[2\varepsilon_0 (ES)_c + 2\kappa (EI)_c - 2M_\Lambda\right] = 0 \tag{3.11}$$

which can be solved to obtain expressions for the axial strain at $y = 0$ and the curvature of the composite beam:

$$\varepsilon_0 = \frac{P_\Lambda (EI)_c - M_\Lambda (ES)_c}{(EA)_c (EI)_c - (ES)_c^{\,2}}$$
$$\kappa = \frac{M_\Lambda}{(EI)_c} - \frac{(ES)_c}{(EI)_c}\left[\frac{P_\Lambda (EI)_c - M_\Lambda (ES)_c}{(EA)_c (EI)_c - (ES)_c^{\,2}}\right] \tag{3.12}$$

If the composite beam cross-section is symmetrical with respect to the z-axis, then the first moment of inertia of the cross-section is zero and Equations 3.12 simply to:

$$\varepsilon_0 = \frac{P_\Lambda}{(EA)_c}$$
$$\kappa = \frac{M_\Lambda}{(EI)_c} \tag{3.13}$$

The location of the neutral axis, which has zero axial strain as shown in Figure 4, can be determined by solving:

$$\varepsilon_{xx} = \varepsilon_0 - \kappa y = 0 \tag{3.14}$$

for y, giving:

$$y_0 = \frac{\varepsilon_0}{\kappa} \tag{3.15}$$

B. MODELS OF SELECTED ACTUATOR/BEAM CONFIGURATIONS

Piezoceramic actuators are typically bonded to beams in one of four configurations: a single actuator, a pair of actuators bonded symmetrically to opposite sides of the beam, a stacked pair of actuators bonded to one side of the beam and stacked pairs of actuators bonded symmetrically to opposite sides of the beam. Prepackaged actuators, such as the PZT QuickPacks from Active Control eXperts, Inc., which have the piezoceramics and wiring encased in an insulating matrix material, can also be bonded to one or both sides of a beam. It is of interest to compare the effectiveness of each of these configurations in producing curvature of the composite beam. The general formulation of the Euler-Bernoulli model is applied to each of these configurations in the following subsections. While the bond between an actuator and a beam is often negligibly thin when compared to the thicknesses of the beam and actuator, Baz and Poh [Ref. 7] noted that the thickness and material properties of the bond may contribute significantly to the composite beam's mechanical behavior. The dimensions and modulus of the bond material are therefore included in the models for completeness. For simplicity, all piezoceramic actuators in the models with more than one actuator are assumed to have the same dimensions.

1. Beam Deformation Due To Single Piezoceramic Actuator.

Figure 5 shows a schematic representation of a piezoceramic actuator bonded to a section of a beam which extends in the $\pm x$-direction. The total area stiffness for the composite single actuator configuration is obtained by substitution of the elastic moduli E_i and dimensions w_i and t_i into Equation 3.3, where no subscript, the subscript b and the subscript p denote the properties of the beam, bond and piezoceramic actuator, respectively:

$$(EA)_c = \int_{-\frac{t}{2}}^{\frac{t}{2}} Ewdy + \int_{\frac{t}{2}}^{\frac{t}{2}+t_b} E_b w_b dy + \int_{\frac{t}{2}+t_b}^{\frac{t}{2}+t_b+t_p} E_p w_p dy$$
$$= Ewt + E_b w_b t_b + E_p w_p t_p \tag{3.16}$$

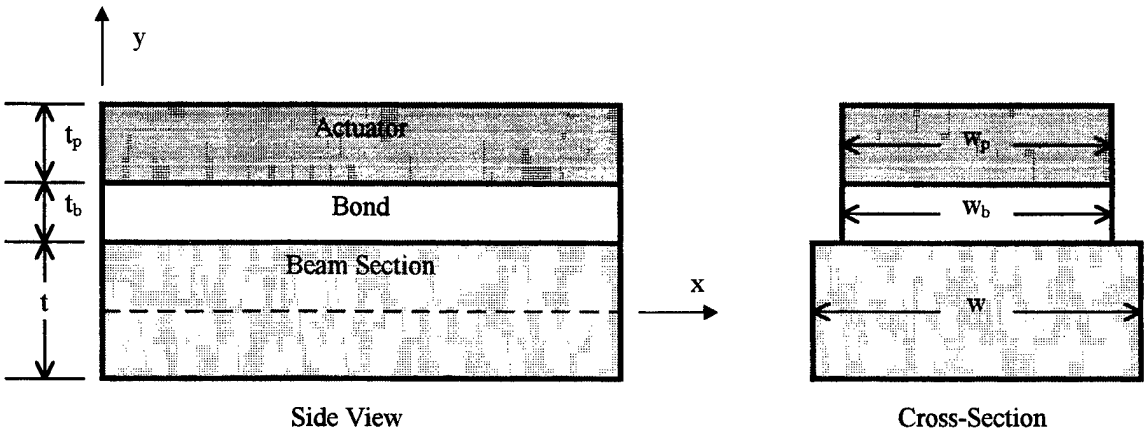

Figure 5. Schematic of Single Piezoceramic Actuator Bonded to Beam

The first and second moments of inertia of the composite beam cross-section are similarly obtained from Equations 3.4 and 3.5:

$$(ES)_c = \int_{-\frac{t}{2}}^{\frac{t}{2}} Ewydy + \int_{\frac{t}{2}}^{\frac{t}{2}+t_b} E_b w_b ydy + \int_{\frac{t}{2}+t_b}^{\frac{t}{2}+t_b+t_p} E_p w_p ydy$$
$$= E_b w_b t_b \left(\frac{t}{2} + \frac{t_b}{2}\right) + E_p w_p t_p \left(\frac{t}{2} + t_b + \frac{t_p}{2}\right) \tag{3.17}$$

$$(EI)_c = \int_{-\frac{t}{2}}^{\frac{t}{2}} Ewy^2 dy + \int_{\frac{t}{2}}^{\frac{t}{2}+t_b} E_b w_b y^2 dy + \int_{\frac{t}{2}+t_b}^{\frac{t}{2}+t_b+t_p} E_p w_p y^2 dy$$

$$= \frac{Ewt^3}{12} + E_b w_b t_b \left[\left(\frac{t}{2}\right)^2 + \frac{t}{2} t_b + \frac{t_b^2}{3} \right] \tag{3.18}$$

$$+ E_p w_p t_p \left[\left(\frac{t}{2} + t_b\right)^2 + \left(\frac{t}{2} + t_b\right) t_p + \frac{t_p^2}{3} \right]$$

The resultant force P_Λ and resultant moment M_Λ due to an actuator input voltage V are obtained from Equations 3.6, 3.7 and 3.8:

$$P_\Lambda = \int_{\frac{t}{2}+t_b}^{\frac{t}{2}+t_b+t_p} E_p \Lambda w_p dy = E_p d_{31} w_p V \tag{3.19}$$

$$M_\Lambda = \int_{\frac{t}{2}+t_b}^{\frac{t}{2}+t_b+t_p} E_p \Lambda w_p y dy = E_p d_{31} w_p \left[\frac{t}{2} + t_b + \frac{t_p}{2} \right] V \tag{3.20}$$

Since the composite beam cross-section is not symmetrical with respect to the z-axis, an actuator input voltage will produce both non-zero axial strain ε_0 at $y = 0$ and curvature κ about the z-axis, as given by Equations 3.12, with the location of the neutral axis given by Equation 3.15.

2. Beam Deformation Due To Symmetric Piezoceramic Actuator Pair

Figure 6 shows a schematic representation of a symmetric piezoceramic actuator pair bonded to a section of a beam which extends in the $\pm x$-direction. The total area

stiffness and first and second moments of inertia for a beam with a symmetric actuator pair can be computed as for the single actuator configuration using Equations 3.3 through 3.5:

$$\begin{aligned}(EA)_c &= \int_{-\left(\frac{t}{2}+t_b+t_p\right)}^{-\left(\frac{t}{2}+t_b\right)} E_p w_p dy + \int_{-\left(\frac{t}{2}+t_b\right)}^{-\frac{t}{2}} E_b w_b dy + \int_{-\frac{t}{2}}^{\frac{t}{2}} E w dy + \int_{\frac{t}{2}}^{\frac{t}{2}+t_b} E_b w_b dy + \int_{\frac{t}{2}+t_b}^{\frac{t}{2}+t_b+t_p} E_p w_p dy \\ &= Ewt + 2E_b w_b t_b + 2E_p w_p t_p\end{aligned} \tag{3.21}$$

$$\begin{aligned}(ES)_c &= \int_{-\left(\frac{t}{2}+t_b+t_p\right)}^{-\left(\frac{t}{2}+t_b\right)} E_p w_p y dy + \int_{-\left(\frac{t}{2}+t_b\right)}^{-\frac{t}{2}} E_b w_b y dy + \int_{-\frac{t}{2}}^{\frac{t}{2}} E w y dy \\ &\quad + \int_{\frac{t}{2}}^{\frac{t}{2}+t_b} E_b w_b y dy + \int_{\frac{t}{2}+t_b}^{\frac{t}{2}+t_b+t_p} E_p w_p y dy \\ &= 0\end{aligned} \tag{3.22}$$

$$\begin{aligned}(EI)_c &= \int_{-\left(\frac{t}{2}+t_b+t_p\right)}^{-\left(\frac{t}{2}+t_b\right)} E_p w_p y^2 dy + \int_{-\left(\frac{t}{2}+t_b\right)}^{-\frac{t}{2}} E_b w_b y^2 dy + \int_{-\frac{t}{2}}^{\frac{t}{2}} E w y^2 dy \\ &\quad + \int_{\frac{t}{2}}^{\frac{t}{2}+t_b} E_b w_b y^2 dy + \int_{\frac{t}{2}+t_b}^{\frac{t}{2}+t_b+t_p} E_p w_p y^2 dy \\ &= \frac{Ewt^3}{12} + 2E_b w_b t_b \left[\left(\frac{t}{2}\right)^2 + \frac{t}{2}t_b + \frac{t_b^2}{3}\right] \\ &\quad + 2E_p w_p t_p \left[\left(\frac{t}{2}+t_b\right)^2 + \left(\frac{t}{2}+t_b\right)t_p + \frac{t_p^2}{3}\right]\end{aligned} \tag{3.23}$$

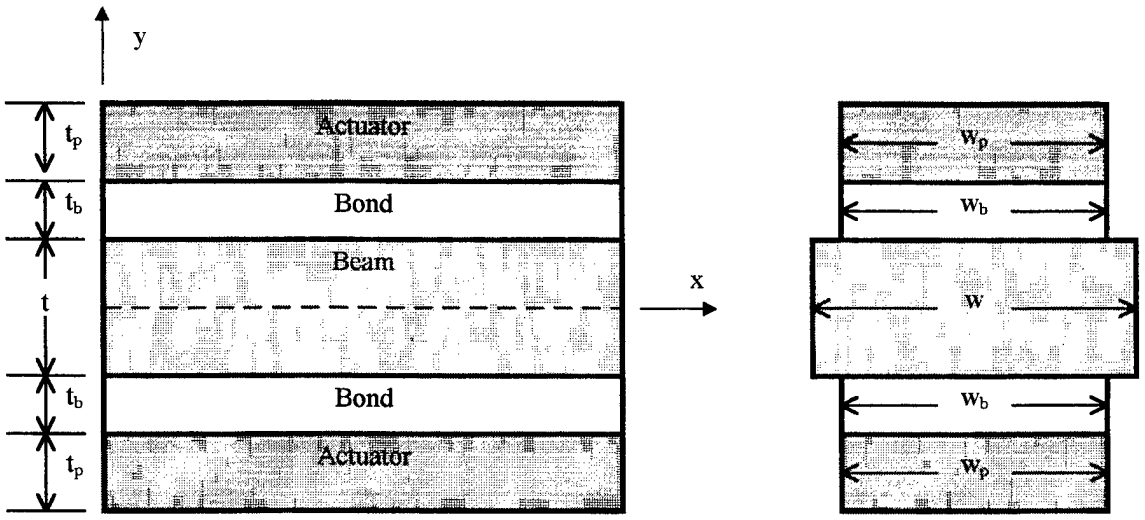

Figure 6. Schematic of Symmetric Piezoceramic Actuator Pair Bonded to Beam

The resultant force P_Λ and resultant moment M_Λ, as given by Equations 3.6, 3.7 and 3.8, depend on the input voltages V_1 to the actuator on the $+y$ side and V_2 to the actuator on the $-y$ side of the beam:

$$P_\Lambda = \int_{\frac{t}{2}+t_b}^{\frac{t}{2}+t_b+t_p} E_p \Lambda_1 w_p dy + \int_{-\left(\frac{t}{2}+t_b+t_p\right)}^{-\left(\frac{t}{2}+t_b\right)} E_p \Lambda_2 w_p dy$$
$$= E_p d_{31} w_p \left(V_1 + V_2\right) \tag{3.24}$$

$$M_\Lambda = \int_{\frac{t}{2}+t_b}^{\frac{t}{2}+t_b+t_p} E_p \Lambda_1 w_p y dy + \int_{-\left(\frac{t}{2}+t_b+t_p\right)}^{-\left(\frac{t}{2}+t_b\right)} E_p \Lambda_2 w_p y dy$$
$$= E_p d_{31} w_p \left[\frac{t}{2} + t_b + \frac{t_p}{2}\right]\left(V_1 - V_2\right) \tag{3.25}$$

Since the composite actuator/beam cross-section is symmetric with respect to the z-axis, the axial strain at $y = 0$ and curvature about the z-axis are given by Equations 3.13. Substitution of Equations 3.24 and 3.25 into Equations 3.13 gives:

$$\varepsilon_0 = \frac{E_p d_{31} w_p (V_1 + V_2)}{(EA)_c}$$
$$\kappa = \frac{E_p d_{31} w_p \left[\frac{t}{2} + t_b + \frac{t_p}{2}\right](V_1 - V_2)}{(EI)_c} \tag{3.26}$$

Thus, equal voltages applied to each actuator will produce axial strain with no curvature and input voltages of equal magnitude and opposite polarity will produce curvature with no axial strain at $y = 0$. Input voltages of unequal magnitude will produce a combination of curvature and axial strain at $y = 0$.

3. Beam Deformation Due To Stacked Pair of Piezoceramic Actuators

Figure 7 shows a schematic representation of a stacked piezoceramic actuator pair bonded to a section of a beam which extends in the $\pm x$-direction. The total area stiffness and first and second moments of inertia for a beam with a stacked actuator pair are determined by substitution of the appropriate cross-sectional dimensions and properties into Equations 3.3 through 3.5:

$$\begin{aligned}(EA)_c &= \int_{-\frac{t}{2}}^{\frac{t}{2}} E w dy + \int_{\frac{t}{2}}^{\frac{t}{2}+t_b} E_b w_b dy + \int_{\frac{t}{2}+t_b}^{\frac{t}{2}+t_b+t_p} E_p w_p dy + \int_{\frac{t}{2}+t_b+t_p}^{\frac{t}{2}+2t_b+t_p} E_b w_b dy + \int_{\frac{t}{2}+2t_b+t_p}^{\frac{t}{2}+2t_b+2t_p} E_p w_p dy \\ &= Ewt + 2E_b w_b t_b + 2E_p w_p t_p\end{aligned} \tag{3.27}$$

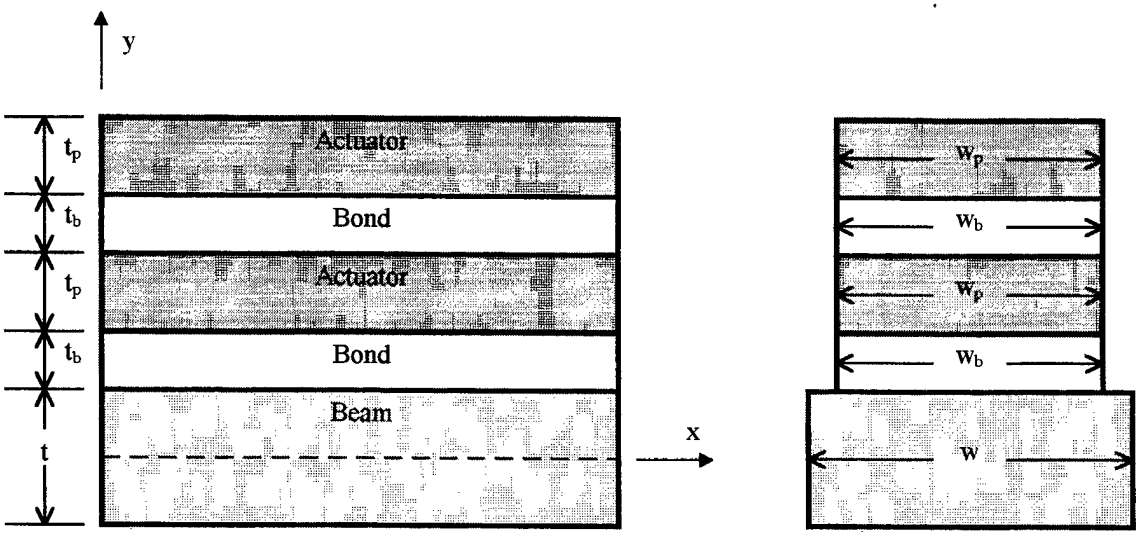

Figure 7. Schematic of Stacked Piezoceramic Actuator Pair Bonded to Beam

$$
\begin{aligned}
(ES)_c = & \int_{-\frac{t}{2}}^{\frac{t}{2}} Ewydy + \int_{\frac{t}{2}}^{\frac{t}{2}+t_b} E_b w_b ydy + \int_{\frac{t}{2}+t_b}^{\frac{t}{2}+t_b+t_p} E_p w_p ydy \\
& + \int_{\frac{t}{2}+t_b+t_p}^{\frac{t}{2}+2t_b+t_p} E_b w_b ydy + \int_{\frac{t}{2}+2t_b+t_p}^{\frac{t}{2}+2t_b+2t_p} E_p w_p ydy \\
& = E_b w_b t_b \left(t + 2t_b + t_p\right) + E_p w_p t_p \left(t + 3t_b + 2t_p\right)
\end{aligned}
\tag{3.28}
$$

$$
\begin{aligned}
(EI)_c &= \int_{-\frac{t}{2}}^{\frac{t}{2}} Ewy^2 dy + \int_{\frac{t}{2}}^{\frac{t}{2}+t_b} E_b w_b y^2 dy + \int_{\frac{t}{2}+t_b}^{\frac{t}{2}+t_b+t_p} E_p w_p y^2 dy \\
&\quad + \int_{\frac{t}{2}+t_b+t_p}^{\frac{t}{2}+2t_b+t_p} E_b w_b y^2 dy + \int_{\frac{t}{2}+2t_b+t_p}^{\frac{t}{2}+2t_b+2t_p} E_p w_p y^2 dy \\
&= \frac{Ewt^3}{12} + E_b w_b t_b \left[\left(\frac{t}{2}\right)^2 + \left(\frac{t}{2}+t_b+t_p\right) + \left(t+\frac{5}{3}t_b+t_p\right) t_b \right] \\
&\quad + E_p w_p t_p \left[\left(\frac{t}{2}+t_b\right)^2 + \left(\frac{t}{2}+2t_b+t_p\right)^2 + \left(t+3t_b+\frac{5}{3}t_p\right) t_p \right]
\end{aligned}
\tag{3.29}
$$

The resultant force P_A and resultant moment M_A, as given by Equations 3.6, 3.7 and 3.8, depend on the input voltages V_1 to the inner actuator and V_2 to the outer actuator:

$$
\begin{aligned}
P_A &= \int_{\frac{t}{2}+t_b}^{\frac{t}{2}+t_b+t_p} E_p \Lambda_1 w_p dy + \int_{\frac{t}{2}+2t_b+t_p}^{\frac{t}{2}+2t_b+2t_p} E_p \Lambda_2 w_p dy \\
&= E_p d_{31} w_p \left(V_1 + V_2\right)
\end{aligned}
\tag{3.30}
$$

$$
\begin{aligned}
M_A &= \int_{\frac{t}{2}+t_b}^{\frac{t}{2}+t_b+t_p} E_p \Lambda_1 w_p y dy + \int_{\frac{t}{2}+2t_b+t_p}^{\frac{t}{2}+2t_b+2t_p} E_p \Lambda_2 w_p y dy \\
&= E_p d_{31} w_p \left[\left(\frac{t}{2}+t_b+\frac{t_p}{2}\right) V_1 + \left(\frac{t}{2}+2t_b+\frac{3t_p}{2}\right) V_2 \right]
\end{aligned}
\tag{3.31}
$$

Since the composite actuator/beam cross-section is not symmetric with respect to the z-axis, the axial strain at $y = 0$ and curvature about the z-axis are given by Equations 3.12. Actuator input voltages will, in general, produce both non-zero axial strain ε_0 at $y = 0$ and curvature κ about the z-axis, with the location of the neutral axis given by Equation 3.15.

4. Beam Curvature Due To A Symmetric Pair of Stacked Piezoceramic Actuators

Figure 8 shows a schematic representation of a symmetric pair of stacked piezoceramic actuators bonded to a section of a beam which extends in the $\pm x$-direction. The total area stiffness and first and second moments of inertia for a beam with a stacked actuator pair are determined by substitution of the appropriate cross-sectional dimensions and properties into Equations 3.3 through 3.5:

$$\begin{aligned}(EA)_c = &\int_{-\left(\frac{t}{2}+2t_b+2t_p\right)}^{-\left(\frac{t}{2}+2t_b+t_p\right)} E_p w_p dy + \int_{-\left(\frac{t}{2}+2t_b+t_p\right)}^{-\left(\frac{t}{2}+t_b+t_p\right)} E_b w_b dy + \int_{-\left(\frac{t}{2}+t_b+t_p\right)}^{-\left(\frac{t}{2}+t_b\right)} E_p w_p dy \\ &+ \int_{-\left(\frac{t}{2}+t_b\right)}^{-\frac{t}{2}} E_b w_b dy + \int_{-\frac{t}{2}}^{\frac{t}{2}} Ew dy + \int_{\frac{t}{2}}^{\frac{t}{2}+t_b} E_b w_b dy \\ &+ \int_{\frac{t}{2}+t_b}^{\frac{t}{2}+t_b+t_p} E_p w_p dy + \int_{\frac{t}{2}+t_b+t_p}^{\frac{t}{2}+2t_b+t_p} E_b w_b dy + \int_{\frac{t}{2}+2t_b+t_p}^{\frac{t}{2}+2t_b+2t_p} E_p w_p dy \\ &= Ewt + 4E_b w_b t_b + 4E_p w_p t_p\end{aligned} \tag{3.32}$$

$$\begin{aligned}(ES)_c = &\int_{-\left(\frac{t}{2}+2t_b+2t_p\right)}^{-\left(\frac{t}{2}+2t_b+t_p\right)} E_p w_p y dy + \int_{-\left(\frac{t}{2}+2t_b+t_p\right)}^{-\left(\frac{t}{2}+t_b+t_p\right)} E_b w_b y dy + \int_{-\left(\frac{t}{2}+t_b+t_p\right)}^{-\left(\frac{t}{2}+t_b\right)} E_p w_p y dy \\ &+ \int_{-\left(\frac{t}{2}+t_b\right)}^{-\frac{t}{2}} E_b w_b y dy + \int_{-\frac{t}{2}}^{\frac{t}{2}} Ewy dy + \int_{\frac{t}{2}}^{\frac{t}{2}+t_b} E_b w_b y dy \\ &+ \int_{\frac{t}{2}+t_b}^{\frac{t}{2}+t_b+t_p} E_p w_p y dy + \int_{\frac{t}{2}+t_b+t_p}^{\frac{t}{2}+2t_b+t_p} E_b w_b y dy + \int_{\frac{t}{2}+2t_b+t_p}^{\frac{t}{2}+2t_b+2t_p} E_p w_p y dy \\ &= 0\end{aligned} \tag{3.33}$$

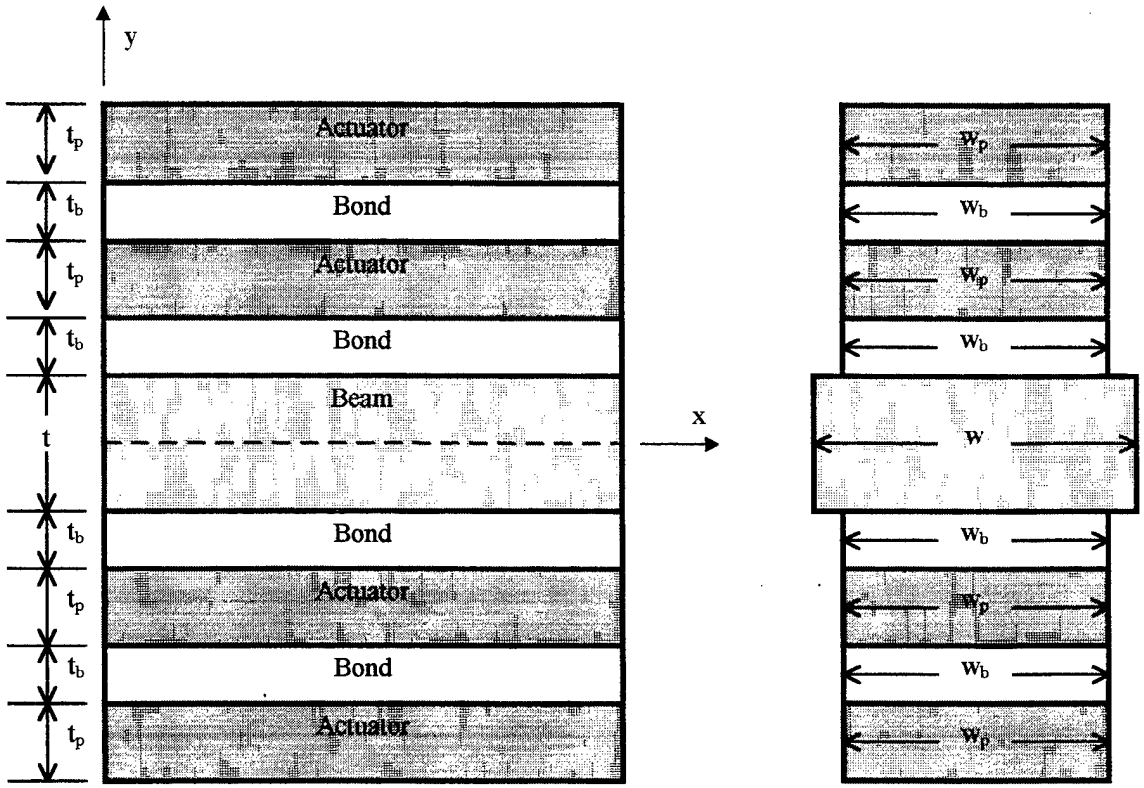

Figure 8. Schematic of Symmetric Pair of Stacked Piezoceramic Actuators Bonded to Beam

$$
\begin{aligned}
(EI)_c = & \int_{-\left(\frac{t}{2}+2t_b+2t_p\right)}^{-\left(\frac{t}{2}+2t_b+t_p\right)} E_p w_p y^2 dy + \int_{-\left(\frac{t}{2}+2t_b+t_p\right)}^{-\left(\frac{t}{2}+t_b+t_p\right)} E_b w_b y^2 dy + \int_{-\left(\frac{t}{2}+t_b+t_p\right)}^{-\left(\frac{t}{2}+t_b\right)} E_p w_p y^2 dy \\
& + \int_{-\left(\frac{t}{2}+t_b\right)}^{-\frac{t}{2}} E_b w_b y^2 dy + \int_{-\frac{t}{2}}^{\frac{t}{2}} E w y^2 dy + \int_{\frac{t}{2}}^{\frac{t}{2}+t_b} E_b w_b y^2 dy \\
& + \int_{\frac{t}{2}+t_b}^{\frac{t}{2}+t_b+t_p} E_p w_p y^2 dy + \int_{\frac{t}{2}+t_b+t_p}^{\frac{t}{2}+2t_b+t_p} E_b w_b y^2 dy + \int_{\frac{t}{2}+2t_b+t_p}^{\frac{t}{2}+2t_b+2t_p} E_p w_p y^2 dy \\
& = \frac{E w t^3}{12} + 2E_b w_b t_b \left[\left(\frac{t}{2}\right)^2 + \left(\frac{t}{2}+t_b+t_p\right) + \left(t+\frac{5}{3}t_b+t_p\right) t_b \right] \\
& + 2E_p w_p t_p \left[\left(\frac{t}{2}+t_b\right)^2 + \left(\frac{t}{2}+2t_b+t_p\right)^2 + \left(t+3t_b+\frac{5}{3}t_p\right) t_p \right]
\end{aligned}
\tag{3.34}
$$

The resultant force P_A and resultant moment M_A, as given by Equations 3.6, 3.7 and 3.8, depend on the input voltages V_1 and V_2 to the inner actuators and V_3 and V_4 to the outer actuators, where the odd numbered voltages are applied to the actuators on the $+y$ side and the even numbered voltages are applied to the actuators on the $-y$ side of the beam, respectively:

$$
\begin{aligned}
P_A = & \int_{-\left(\frac{t}{2}+2t_b+2t_p\right)}^{-\left(\frac{t}{2}+2t_b+t_p\right)} E_p \Lambda_4 w_p dy + \int_{-\left(\frac{t}{2}+t_b+t_p\right)}^{-\left(\frac{t}{2}+t_b\right)} E_p \Lambda_2 w_p dy \\
& + \int_{\frac{t}{2}+t_b}^{\frac{t}{2}+t_b+t_p} E_p \Lambda_1 w_p dy + \int_{\frac{t}{2}+2t_b+t_p}^{\frac{t}{2}+2t_b+2t_p} E_p \Lambda_3 w_p dy \\
& = E_p d_{31} w_p \left(V_1 + V_2 + V_3 + V_4\right)
\end{aligned}
\tag{3.35}
$$

$$M_\Lambda = \int_{-\left(\frac{t}{2}+2t_b+2t_p\right)}^{-\left(\frac{t}{2}+t_b\right)} E_p \Lambda_4 w_p y dy + \int_{-\left(\frac{t}{2}+t_b+t_p\right)}^{-\left(\frac{t}{2}+t_b\right)} E_p \Lambda_2 w_p y dy$$
$$+ \int_{\frac{t}{2}+t_b}^{\frac{t}{2}+t_b+t_p} E_p \Lambda_1 w_p y dy + \int_{\frac{t}{2}+2t_b+t_p}^{\frac{t}{2}+2t_b+2t_p} E_p \Lambda_3 w_p y dy \qquad (3.36)$$
$$= E_p d_{31} w_p \left[\left(\frac{t}{2} + t_b + \frac{t_p}{2} \right)(V_1 - V_2) + \left(\frac{t}{2} + 2t_b + \frac{3t_p}{2} \right)(V_3 - V_4) \right]$$

Since the composite actuator/beam cross-section is symmetric with respect to the z-axis, the axial strain at $y = 0$ and curvature about the z-axis are given by Equations 3.13. Substitution of Equations 3.35 and 3.36 into Equations 3.13 gives:

$$\varepsilon_0 = \frac{E_p d_{31} w_p (V_1 + V_2 + V_3 + V_4)}{(EA)_c}$$
$$\kappa = \frac{E_p d_{31} w_p \left[\left(\frac{t}{2} + t_b + \frac{t_p}{2} \right)(V_1 - V_2) + \left(\frac{t}{2} + 2t_b + \frac{3t_p}{2} \right)(V_3 - V_4) \right]}{(EI)_c} \qquad (3.37)$$

Hence, beam curvature with no axial strain at $y = 0$ can be obtained by setting $V_1 = -V_2$ and $V_3 = -V_4$. Similarly, pure axial strain with no beam curvature is achieved when $V_1 = V_2$ and $V_3 = V_4$.

5. Beam Deformation Due To Single ACX QuickPack Actuator

Figure 9 shows a schematic representation of a single ACX QuickPack actuator bonded to a section of a beam which extends in the $\pm x$-direction. A QuickPack actuator consists of a stacked pair of piezoceramic wafers encased in a matrix material.

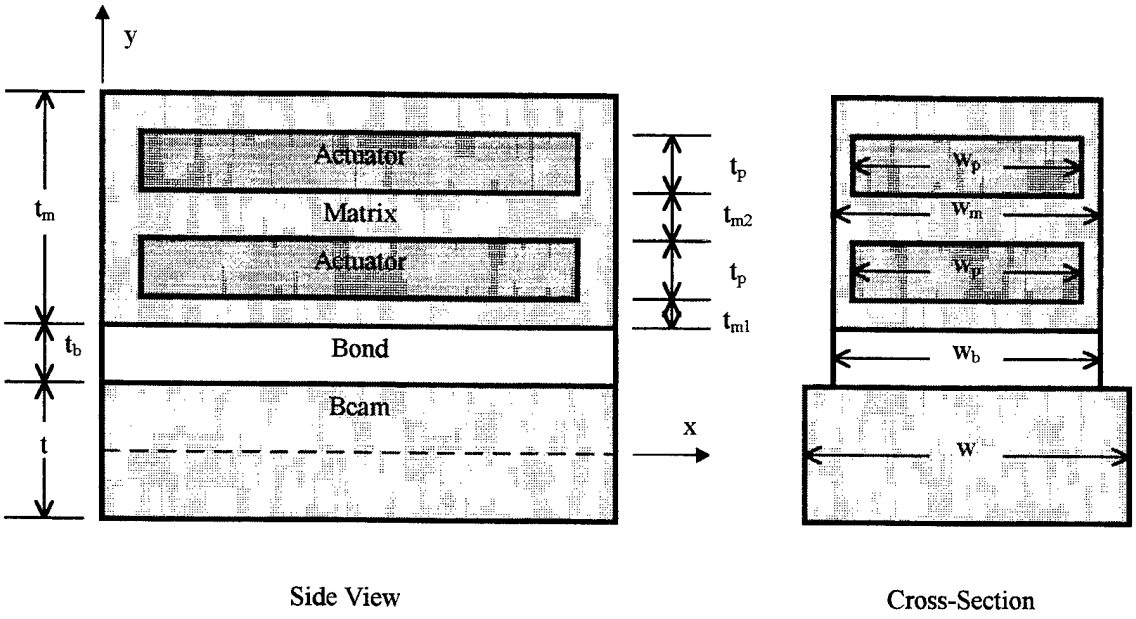

Figure 9. Schematic of Single ACX QuickPack Actuator Bonded to Beam

The total area stiffness and first and second moments of inertia for a beam with a single ACX QuickPack actuator are determined by substitution of the appropriate cross-sectional dimensions and properties into Equations 3.3 through 3.5:

$$\begin{aligned}(EA)_c &= \int_{-\frac{t}{2}}^{\frac{t}{2}} Ew\,dy + \int_{\frac{t}{2}}^{\frac{t}{2}+t_b} E_b w_b\,dy + \int_{\frac{t}{2}+t_b}^{\frac{t}{2}+t_b+t_m} E_m w_m\,dy \\ &+ \int_{\frac{t}{2}+t_b+t_{m1}}^{\frac{t}{2}+t_b+t_{m1}+t_p} \left(E_p - E_m\right) w_p\,dy + \int_{\frac{t}{2}+t_b+t_{m1}+t_{m2}+t_p}^{\frac{t}{2}+t_b+t_{m1}+t_{m2}+2t_p} \left(E_p - E_m\right) w_p\,dy \\ &= Ewt + E_b w_b t_b + E_m w_m t_m + 2\left(E_p - E_m\right) w_p t_p\end{aligned} \tag{3.38}$$

$$
\begin{aligned}
(ES)_c &= \int_{-\frac{t}{2}}^{\frac{t}{2}} Ewy\,dy + \int_{\frac{t}{2}}^{\frac{t}{2}+t_b} E_b w_b y\,dy + \int_{\frac{t}{2}+t_b}^{\frac{t}{2}+t_b+t_m} E_m w_m y\,dy \\
&+ \int_{\frac{t}{2}+t_b+t_{m1}}^{\frac{t}{2}+t_b+t_{m1}+t_p} \left(E_p - E_m\right) w_p y\,dy + \int_{\frac{t}{2}+t_b+t_{m1}+t_p}^{\frac{t}{2}+t_b+t_{m1}+t_{m2}+2t_p} \left(E_p - E_m\right) w_p y\,dy \\
&= E_b w_b t_b \left(\frac{t}{2} + \frac{t_b}{2}\right) + E_m w_m t_m \left(\frac{t}{2} + t_b + \frac{t_m}{2}\right) \\
&+ \left(E_p - E_m\right) w_p t_p \left(t + 2t_b + 2t_{m1} + t_{m2} + 2t_p\right)
\end{aligned}
\tag{3.39}
$$

$$
\begin{aligned}
(EI)_c &= \int_{-\frac{t}{2}}^{\frac{t}{2}} Ewy^2\,dy + \int_{\frac{t}{2}}^{\frac{t}{2}+t_b} E_b w_b y^2\,dy + \int_{\frac{t}{2}+t_b}^{\frac{t}{2}+t_b+t_m} E_m w_m y^2\,dy \\
&+ \int_{\frac{t}{2}+t_b+t_{m1}}^{\frac{t}{2}+t_b+t_{m1}+t_p} \left(E_p - E_m\right) w_p y^2\,dy + \int_{\frac{t}{2}+t_b+t_{m1}+t_p}^{\frac{t}{2}+t_b+t_{m1}+t_{m2}+2t_p} \left(E_p - E_m\right) w_p y^2\,dy \\
&= \frac{Ewt^3}{12} + E_b w_b t_b \left[\left(\frac{t}{2}\right) + \left(\frac{t}{2}\right) t_b + \frac{{t_b}^2}{3}\right] \\
&+ E_m w_m t_m \left[\left(\frac{t}{2} + t_b\right)^2 + \left(\frac{t}{2} + t_b\right) t_m + \frac{{t_m}^2}{3}\right] \\
&+ \left(E_p - E_m\right) w_p t_p \left[\begin{array}{l} \left(\frac{t}{2} + t_b + t_{m1}\right)^2 + \left(\frac{t}{2} + t_b + t_{m1} + t_{m2} + t_p\right)^2 \\ + \left(t + 2t_b + 2t_{m1} + t_{m2} + \frac{5t_p}{3}\right) t_p \end{array}\right]
\end{aligned}
\tag{3.40}
$$

The resultant force P_A and resultant moment M_A, as given by Equations 3.6, 3.7 and 3.8, depend on the input voltages V_1 to the inner actuator and V_2 to the outer actuator:

$$P_\Lambda = \int_{\frac{t}{2}+t_b+t_{m1}}^{\frac{t}{2}+t_b+t_{m1}+t_p} E_p \Lambda_1 w_p dy + \int_{\frac{t}{2}+t_b+t_{m1}+t_{m2}+t_p}^{\frac{t}{2}+t_b+t_{m1}+t_{m2}+2t_p} E_p \Lambda_2 w_p dy$$
$$= E_p d_{31} w_p (V_1 + V_2) \tag{3.41}$$

$$M_\Lambda = \int_{\frac{t}{2}+t_b+t_{m1}}^{\frac{t}{2}+t_b+t_{m1}+t_p} E_p \Lambda_1 w_p y dy + \int_{\frac{t}{2}+t_b+t_{m1}+t_{m2}+t_p}^{\frac{t}{2}+t_b+t_{m1}+t_{m2}+2t_p} E_p \Lambda_2 w_p y dy$$
$$= E_p d_{31} w_p \left[\left(\frac{t}{2} + t_b + t_{m1} + \frac{t_p}{2} \right) V_1 + \left(\frac{t}{2} + t_b + t_{m1} + t_{m2} + \frac{3t_p}{2} \right) V_2 \right] \tag{3.42}$$

Since the composite actuator/beam cross-section is not symmetric with respect to the z-axis, the axial strain at $y = 0$ and curvature about the z-axis are given by Equations 3.12. Actuator input voltages will, in general, produce both non-zero axial strain ε_0 at $y = 0$ and curvature κ about the z-axis, with the location of the neutral axis given by Equation 3.15.

6. Beam Deformation Due To Symmetric Pair of ACX QuickPack Actuators

Figure 9 shows a schematic representation of a symetric ACX QuickPack actuator pair bonded to a section of a beam which extends in the $\pm x$-direction. The total area stiffness and first and second moments of inertia for a beam with a symmetric ACX QuickPack actuator pair are determined by substitution of the appropriate cross-sectional dimensions and properties into Equations 3.3 through 3.5:

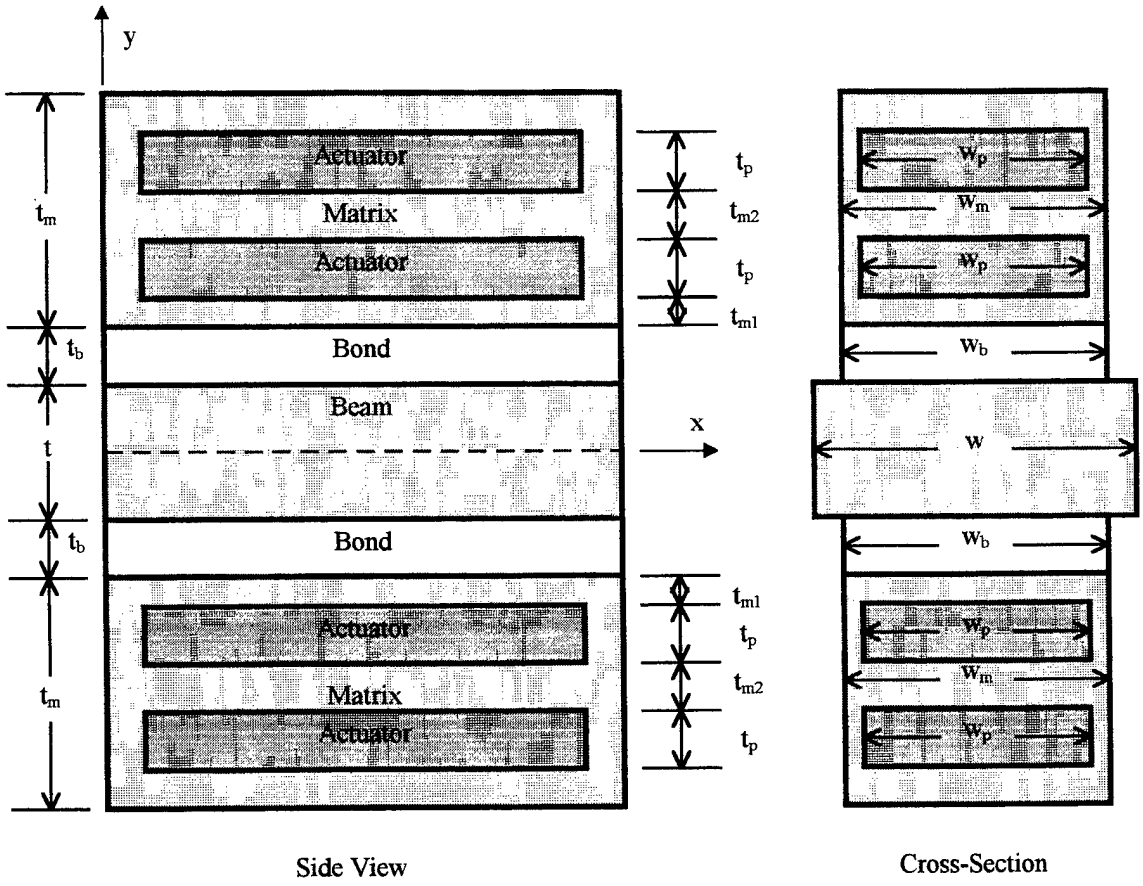

Figure 10. Schematic of Symmetric ACX QuickPack Actuator Pair Bonded to Beam

$$
\begin{aligned}
(EA)_c = & \int_{-\left(\frac{t}{2}+t_b+t_{m1}+t_{m2}+2t_p\right)}^{-\left(\frac{t}{2}+t_b+t_{m1}+t_{m2}+t_p\right)} \left(E_p - E_m\right) w_p dy + \int_{-\left(\frac{t}{2}+t_b+t_{m1}+t_p\right)}^{-\left(\frac{t}{2}+t_b+t_{m1}\right)} \left(E_p - E_m\right) w_p dy \\
& + \int_{-\left(\frac{t}{2}+t_b+t_m\right)}^{-\left(\frac{t}{2}+t_b\right)} E_m w_m dy + \int_{-\left(\frac{t}{2}+t_b\right)}^{-\frac{t}{2}} E_b w_b dy \\
& + \int_{-\frac{t}{2}}^{\frac{t}{2}} E w dy + \int_{\frac{t}{2}}^{\frac{t}{2}+t_b} E_b w_b dy + \int_{\frac{t}{2}+t_b}^{\frac{t}{2}+t_b+t_m} E_m w_m dy \\
& + \int_{\frac{t}{2}+t_b+t_{m1}}^{\frac{t}{2}+t_b+t_{m1}+t_p} \left(E_p - E_m\right) w_p dy + \int_{\frac{t}{2}+t_b+t_{m1}+t_{m2}+t_p}^{\frac{t}{2}+t_b+t_{m1}+t_{m2}+2t_p} \left(E_p - E_m\right) w_p dy \\
& = Ewt + 2E_b w_b t_b + 2E_m w_m t_m + 4\left(E_p - E_m\right) w_p t_p
\end{aligned}
\tag{3.43}
$$

$$
\begin{aligned}
(ES)_c = & \int_{-\left(\frac{t}{2}+t_b+t_{m1}+t_{m2}+2t_p\right)}^{-\left(\frac{t}{2}+t_b+t_{m1}+t_{m2}+t_p\right)} \left(E_p - E_m\right) w_p y dy + \int_{-\left(\frac{t}{2}+t_b+t_{m1}+t_p\right)}^{-\left(\frac{t}{2}+t_b+t_{m1}\right)} \left(E_p - E_m\right) w_p y dy \\
& + \int_{-\left(\frac{t}{2}+t_b+t_m\right)}^{-\left(\frac{t}{2}+t_b\right)} E_m w_m y dy + \int_{-\left(\frac{t}{2}+t_b\right)}^{-\frac{t}{2}} E_b w_b y dy \\
& \int_{-\frac{t}{2}}^{\frac{t}{2}} E w y dy + \int_{\frac{t}{2}}^{\frac{t}{2}+t_b} E_b w_b y dy + \int_{\frac{t}{2}+t_b}^{\frac{t}{2}+t_b+t_m} E_m w_m y dy \\
& + \int_{\frac{t}{2}+t_b+t_{m1}}^{\frac{t}{2}+t_b+t_{m1}+t_p} \left(E_p - E_m\right) w_p y dy + \int_{\frac{t}{2}+t_b+t_{m1}+t_{m2}+t_p}^{\frac{t}{2}+t_b+t_{m1}+t_{m2}+2t_p} \left(E_p - E_m\right) w_p y dy \\
& = 0
\end{aligned}
\tag{3.44}
$$

$$
\begin{aligned}
(EI)_c = & \int_{-\left(\frac{t}{2}+t_b+t_{m1}+t_{m2}+2t_p\right)}^{-\left(\frac{t}{2}+t_b+t_{m1}+t_{m2}+t_p\right)} \left(E_p - E_m\right) w_p y^2 dy + \int_{-\left(\frac{t}{2}+t_b+t_{m1}+t_p\right)}^{-\left(\frac{t}{2}+t_b+t_{m1}\right)} \left(E_p - E_m\right) w_p y^2 dy \\
& + \int_{-\left(\frac{t}{2}+t_b+t_m\right)}^{-\left(\frac{t}{2}+t_b\right)} E_m w_m y^2 dy + \int_{-\left(\frac{t}{2}+t_b\right)}^{-\frac{t}{2}} E_b w_b y^2 dy \\
& + \int_{-\frac{t}{2}}^{\frac{t}{2}} E w y^2 dy + \int_{\frac{t}{2}}^{\frac{t}{2}+t_b} E_b w_b y^2 dy + \int_{\frac{t}{2}+t_b}^{\frac{t}{2}+t_b+t_m} E_m w_m y^2 dy \\
& + \int_{\frac{t}{2}+t_b+t_{m1}}^{\frac{t}{2}+t_b+t_{m1}+t_p} \left(E_p - E_m\right) w_p y^2 dy + \int_{\frac{t}{2}+t_b+t_{m1}+t_p}^{\frac{t}{2}+t_b+t_{m1}+t_{m2}+2t_p} \left(E_p - E_m\right) w_p y^2 dy \\
= & \frac{E w t^3}{12} + 2E_b w_b t_b \left[\left(\frac{t}{2}\right) + \left(\frac{t}{2}\right) t_b + \frac{t_b^{\,2}}{3}\right] \\
& + 2E_m w_m t_m \left[\left(\frac{t}{2}+t_b\right)^2 + \left(\frac{t}{2}+t_b\right) t_m + \frac{t_m^{\,2}}{3}\right] \\
& + 2\left(E_p - E_m\right) w_p t_p \left[\begin{array}{l} \left(\frac{t}{2}+t_b+t_{m1}\right)^2 + \left(\frac{t}{2}+t_b+t_{m1}+t_{m2}+t_p\right)^2 \\ + \left(t+2t_b+2t_{m1}+t_{m2}+\frac{5t_p}{3}\right) t_p \end{array}\right]
\end{aligned}
\tag{3.45}
$$

The resultant force P_A and resultant moment M_A, as given by Equations 3.6, 3.7 and 3.8, depend on the input voltages V_1 and V_2 to the inner actuators and V_3 and V_4 to the outer actuators, where the odd numbered voltages are applied to the actuators on the $+y$ side and the even numbered voltages are applied to the actuators on the $-y$ side of the beam, respectively:

$$
\begin{aligned}
P_\Lambda = & \int_{-\left(\frac{t}{2}+t_b+t_{m1}+t_{m2}+2t_p\right)}^{-\left(\frac{t}{2}+t_b+t_{m1}+t_{m2}+t_p\right)} E_p\Lambda_2 w_p dy + \int_{-\left(\frac{t}{2}+t_b+t_{m1}+t_p\right)}^{-\left(\frac{t}{2}+t_b+t_{m1}\right)} E_p\Lambda_1 w_p dy \\
& + \int_{\frac{t}{2}+t_b+t_{m1}}^{\frac{t}{2}+t_b+t_{m1}+t_p} E_p\Lambda_1 w_p dy + \int_{\frac{t}{2}+t_b+t_{m1}+t_{m2}+t_p}^{\frac{t}{2}+t_b+t_{m1}+t_{m2}+2t_p} E_p\Lambda_2 w_p dy \\
& = E_p d_{31} w_p \left(V_1 + V_2 + V_3 + V_4\right)
\end{aligned}
\tag{3.46}
$$

$$
\begin{aligned}
M_\Lambda = & \int_{-\left(\frac{t}{2}+t_b+t_{m1}+t_{m2}+2t_p\right)}^{-\left(\frac{t}{2}+t_b+t_{m1}+t_{m2}+t_p\right)} E_p\Lambda_2 w_p y dy + \int_{-\left(\frac{t}{2}+t_b+t_{m1}+t_p\right)}^{-\left(\frac{t}{2}+t_b+t_{m1}\right)} E_p\Lambda_1 w_p y dy \\
& + \int_{\frac{t}{2}+t_b+t_{m1}}^{\frac{t}{2}+t_b+t_{m1}+t_p} E_p\Lambda_1 w_p y dy + \int_{\frac{t}{2}+t_b+t_{m1}+t_{m2}+t_p}^{\frac{t}{2}+t_b+t_{m1}+t_{m2}+2t_p} E_p\Lambda_2 w_p y dy \\
& = E_p d_{31} w_p \left[\begin{array}{l} \left(\frac{t}{2}+t_b+t_{m1}+\frac{t_p}{2}\right)\left(V_1 - V_2\right) \\ + \left(\frac{t}{2}+t_b+t_{m1}+t_{m2}+\frac{3t_p}{2}\right)\left(V_3 - V_4\right) \end{array} \right]
\end{aligned}
\tag{3.47}
$$

Since the composite actuator/beam cross-section is symmetric with respect to the z-axis, the axial strain at $y = 0$ and curvature about the z-axis are given by Equations 3.13. Substitution of Equations 3.46 and 3.47 into Equations 3.13 gives:

$$
\begin{aligned}
\varepsilon_0 &= \frac{E_p d_{31} w_p \left(V_1 + V_2 + V_3 + V_4\right)}{\left(EA\right)_c} \\
\kappa &= \frac{E_p d_{31} w_p \left[\begin{array}{l} \left(\frac{t}{2}+t_b+t_{m1}+\frac{t_p}{2}\right)\left(V_1 - V_2\right) \\ + \left(\frac{t}{2}+t_b+t_{m1}+t_{m2}+\frac{3t_p}{2}\right)\left(V_3 - V_4\right) \end{array} \right]}{\left(EI\right)_c}
\end{aligned}
\tag{3.48}
$$

Hence, beam curvature with no axial strain at $y = 0$ can be obtained by setting $V_1 = -V_2$ and $V_3 = -V_4$. Similarly, pure axial strain with no beam curvature is achieved when $V_1 = V_2$ and $V_3 = V_4$.

C. ACTUATOR EFFECTIVENESS

The results Euler-Bernoulli models of actuator produced curvature for the single, symmetric pair, single stacked and symmetric stacked pair configurations were compared for different thicknesses of an aluminum beam. All actuator configurations were assumed to cover the entire width of the beam and the bond between the piezoceramics and the beam was assumed to be negligibly thin. Material properties for Navy Type II PZT were used for the piezoceramic and a maximum applied electric field of 20 volts/mil, a typical operating limit, was applied to all actuators. Figure 11 shows the curvature of the composite actuator/beam as a function of the thickness of the individual piezoceramic elements for a 0.79 mm (0.031 in) thick beam. It can be clearly seen from Figure 11 that the symmetric actuator configurations are more effective at producing beam curvature than those with actuators on one side of the beam. This is due to the concentration of the piezoceramic at the outer edges of the composite beam for the symmetric configurations, where the actuator stress contributes most effectively to a bending moment about the central axis of the beam. An optimum piezoceramic thickness for each actuator type is also evident. Thicker than optimum actuators contribute more to the stiffness of the composite beam cross-section than to actuator bending moment and hence result in lower than optimum curvature. The optimum thicknesses for the two stacked configurations here are exactly half those of the corresponding single actuator configurations due to the assumption of negligible bond thickness. The stacked configurations therefore require half the input voltage of the single actuator configurations to achieve a given electric field across the piezoceramic to produce a desired level of actuation strain.

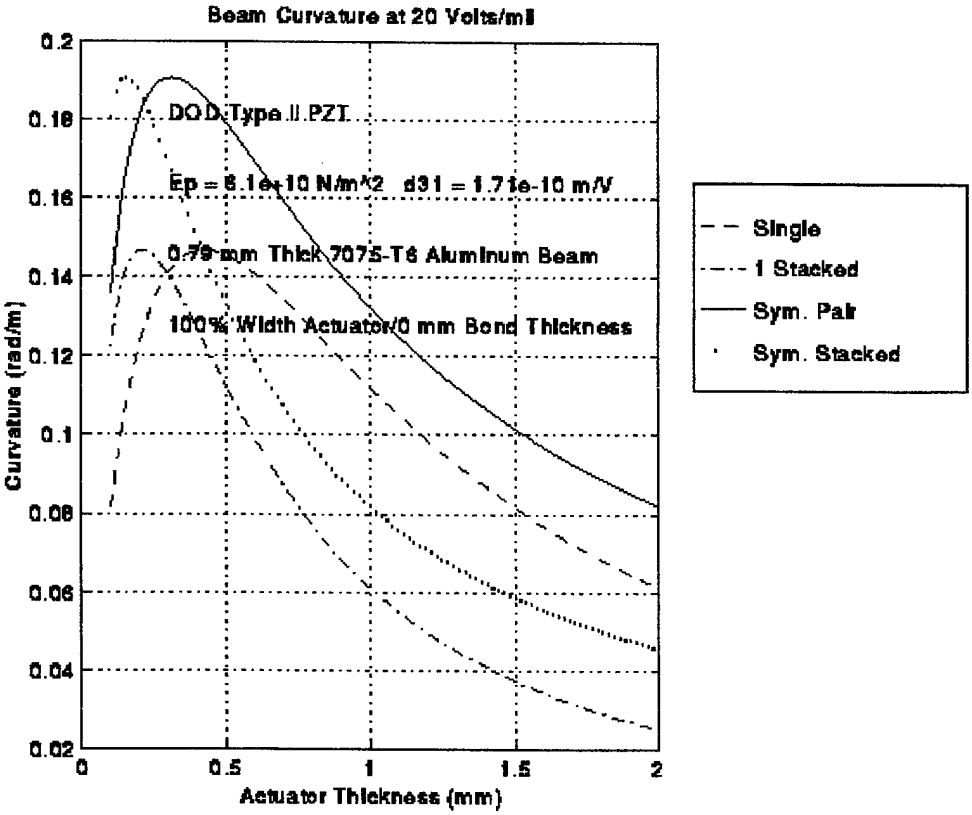

Figure 11. Beam Curvature vs. Piezoceramic Thickness and Actuator Type for 0.79 mm Aluminum Beam and 20 Volts/mil Electric Field applied to Actuators

Figure 12 depicts the performance of the same actuators as in Figure 11 for an aluminum beam with twice the thickness. The optimum thickness of the actuators for each configuration is found to correspondingly double, however, the attainable curvature of the 1.58 mm beam is only half that attainable for the 0.79 mm beam at the 20 volts/mil electric field limitation. This is due to the maximum actuation strain of the piezoceramic remaining constant. The limit on actuation strain for a given piezoceramic results in an inverse relationship between beam thickness and the curvature attainable using an actuator of optimum thickness.

Figure 13 and Figure 14 show the same information as Figure 11 and Figure 12, respectively, but with the actuator thickness plotted as a percentage of the thickness of the aluminum beam. Figure 15 and Figure 16 show the effect of actuator width for a constant

actuator thickness of 0.26 mm and beam thicknesses of 0.79 mm and 1.58 mm respectively. Full width actuators are clearly the most effective in producing beam curvature for all actuator configurations. The reason for this can be seen by examining the curvature equation in Equations 3.26, or the equivalent equation for other actuator configurations. Actuator width appears as a factor of the entire numerator but of only one term in the denominator, given by Equation 3.23. Increasing actuator width therefore always results in an increase in beam curvature, provided all other terms remain constant.

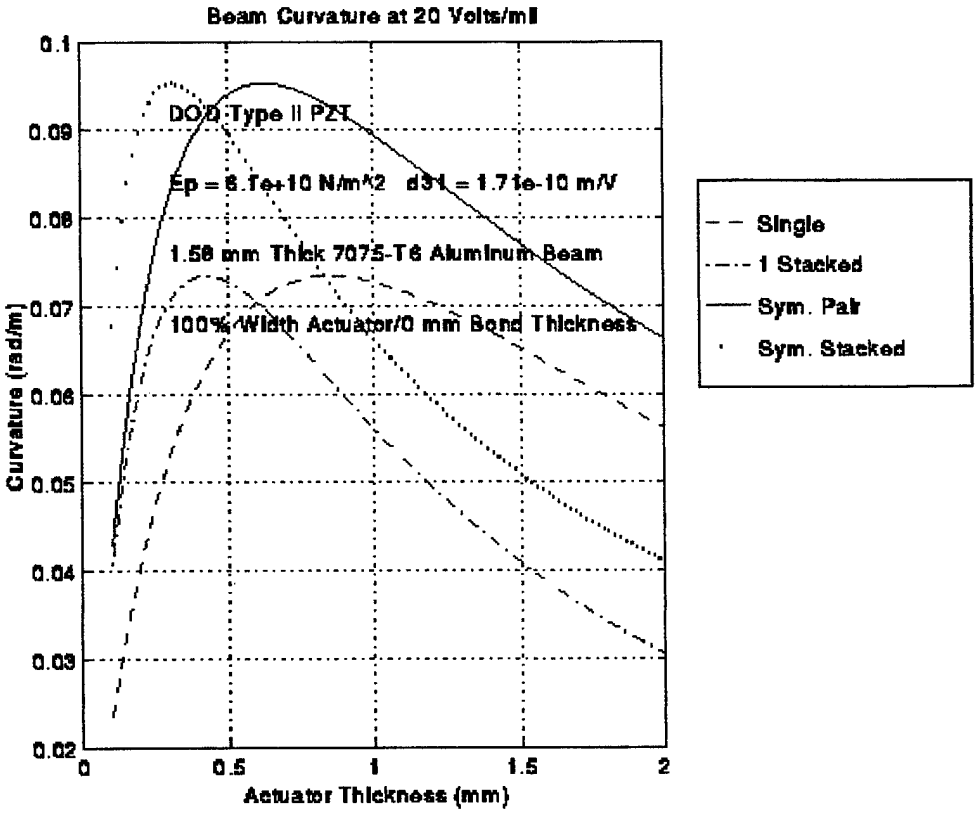

Figure 12. Beam Curvature vs. Piezoceramic Thickness and Actuator Type for 1.58 mm Aluminum Beam and 20 Volts/mil Electric Field applied to Actuators

Examination of Equation 3.26 also reveals the material properties desirable in a piezoceramic actuator. High material modulus E_p, piezoelectric coefficient d_{31} and operating voltage, or equivalently operating electric field, all result in increased actuator effectiveness. In general, the higher the product of these three properties, the more effective the actuator.

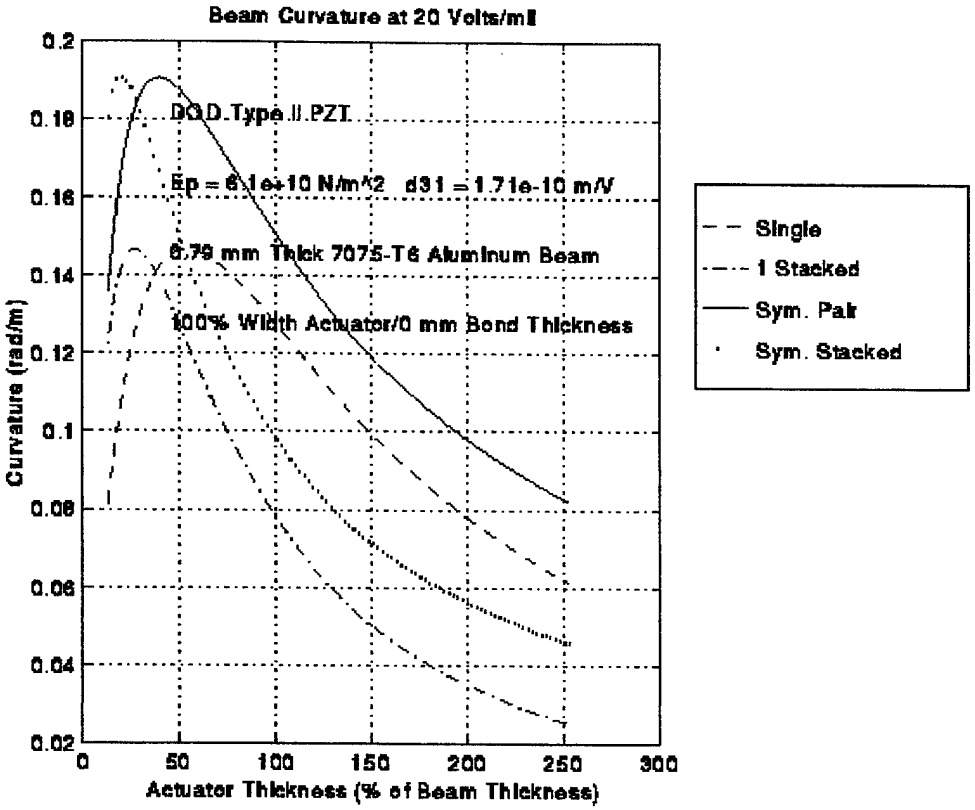

Figure 13. Beam Curvature vs. Piezoceramic Thickness as a Percentage of Beam Thickness and Actuator Type for 0.79 mm Aluminum Beam and 20 Volts/mil Electric Field applied to Actuators

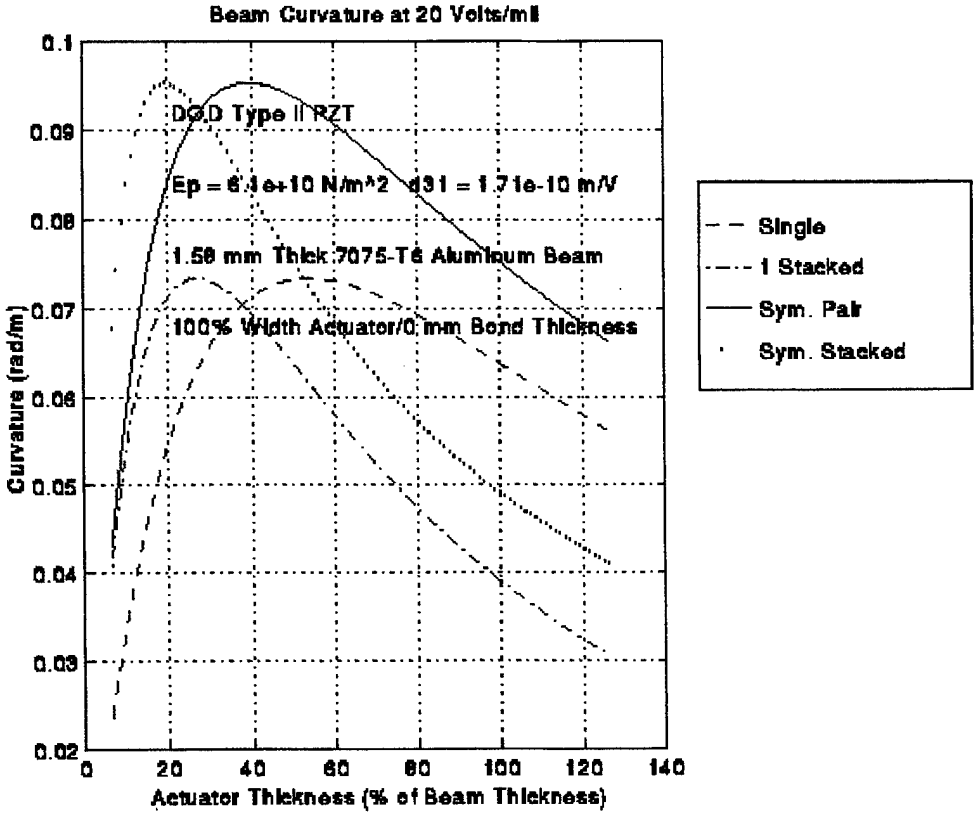

Figure 14. Beam Curvature vs. Piezoceramic Thickness as a Percentage of Beam Thickness and Actuator Type for 1.58 mm Aluminum Beam and 20 Volts/mil Electric Field applied to Actuators

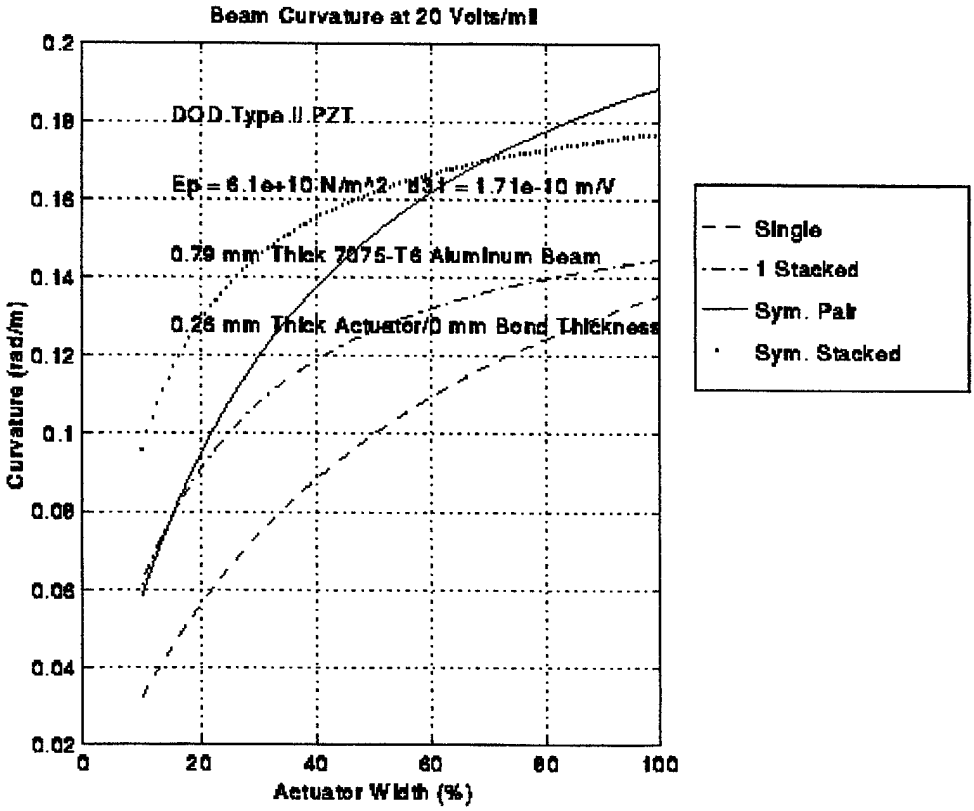

Figure 15. Beam Curvature vs. Piezoceramic Actuator Width and Type for 0.79 mm Aluminum Beam and 20 Volts/mil Electric Field applied to Actuators

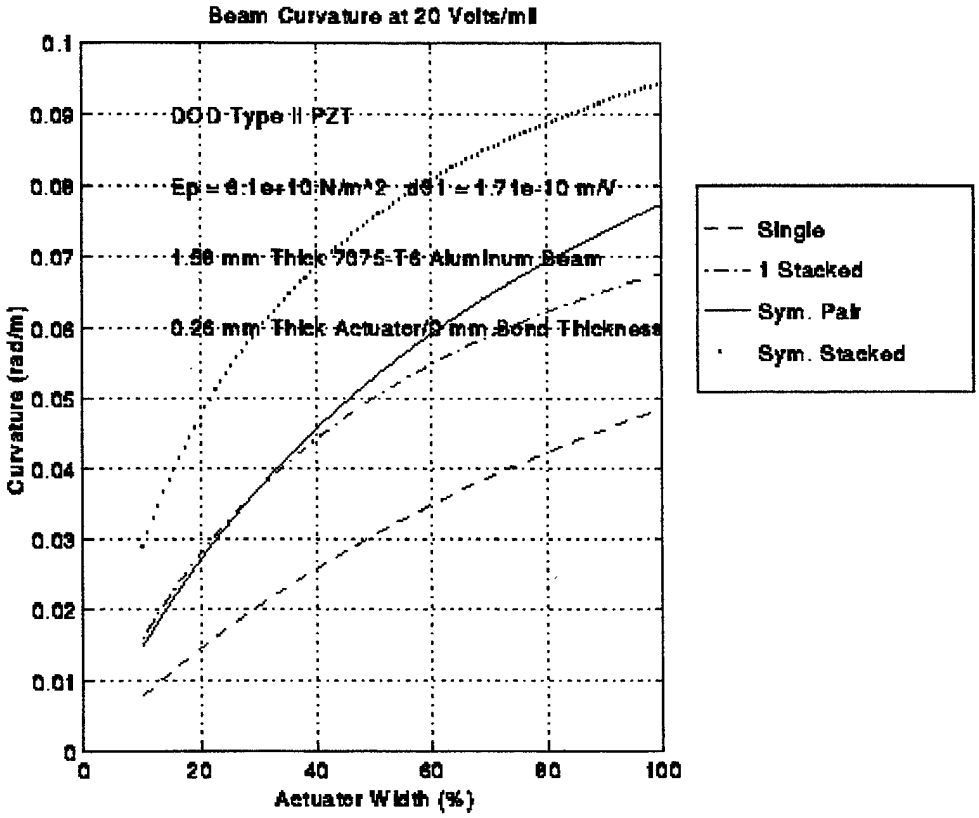

Figure 16. Beam Curvature vs. Piezoceramic Actuator Width and Type for 1.58 mm Aluminum Beam and 20 Volts/mil Electric Field applied to Actuators

IV. ACTUATOR PLACEMENT

A. DEFORMATION OF EULER-BERNOULLI BEAM UNDER ACTUATOR BENDING MOMENT

1. Transverse Deflection of a Beam Segment due to an Actuator Moment

A section of laminated beam with uniform cross-sectional properties throughout its length will deform with uniform curvature over its length when subjected to a pure bending moment. For small displacements, defined as beam slope much less than 1, this behavior can be approximated by:

$$\frac{d^2 v_0}{dx^2} = \frac{M_k}{(EI)_k} \qquad \left(x_k \le x \le x_k + l_k, \frac{dv_0}{dx} << 1 \right) \tag{4.1}$$

where x is the coordinate along the length of the beam, x_k is the x coordinate of the start of beam segment k, l_k is the x length of the beam segment, $v_0(x)$ is the transverse displacement of the beam's neutral axis in the y-direction, M_k is the bending moment applied to beam segment k about its neutral axis and

$$(EI)_k = \sum_i E_i I_i \tag{4.2}$$

is the flexural rigidity of the composite beam segment about its neutral axis. E_i and I_i are the Young's modulus and moment of inertia about the beam segment neutral axis of the ith lamina on segment k.

The transverse displacement at any point x on beam segment k can be obtained by integrating Equation 4.1 twice over the length of the segment. Integrating once gives the slope of the beam segment as a function of x:

$$v_0'(x) = \frac{dv_0(x)}{dx} = v_0'(x_k) + \frac{M_k}{(EI)_k}(x - x_k) \qquad (x_k \le x \le x_k + l_k) \qquad (4.3)$$

Integrating a second time gives:

$$v_0(x) = v_0(x_k) + v_0'(x_k)(x - x_k) + \frac{M_k}{2(EI)_k}(x - x_k)^2 \qquad (x_k \le x \le x_k + l_k) \qquad (4.4)$$

Thus, for small displacements, the transverse displacement along the length of a beam segment is a function of the displacement and slope at the start of the beam segment, the curvature of the beam segment due to the actuator moment and the position x-x_k on the beam segment.

2. Transverse Deflection of Complete Beam due to Actuator Moments

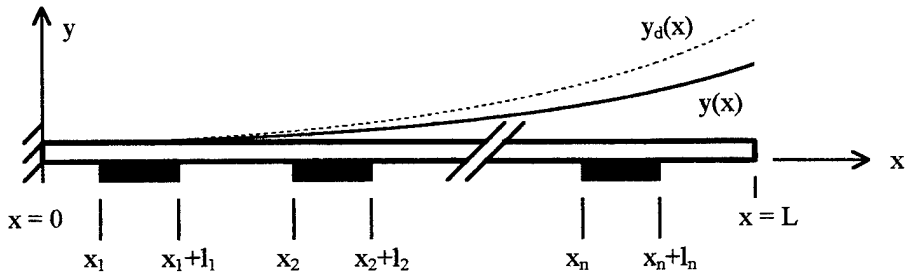

Figure 17. Beam with Attached Piezoceramic Actuators

Figure 17 shows a cantilever beam with n piezoceramic actuators bonded to the beam at locations x_i (i = 1,2,...,n). If the actuators are perfectly bonded to the beam over

their entire lengths and an actuator's bending moment is proportional to its input voltage, then each actuator will produce a beam curvature per unit voltage:

$$K_k = \frac{M_k}{(EI)_k V_k} = \frac{\kappa_k}{V_k} \qquad (k = 1,2,\ldots,n) \tag{4.5}$$

over its respective beam segment, where V_k is the input voltage of actuator k and κ_k is the curvature of the corresponding composite actuator/beam section. A suitable value for K_k for a given actuator/beam configuration can be obtained as discussed in Chapter II.

If the deformation of the beam is static and no external loads are applied, then the deformation of the beam is strictly a function of the actuator locations, lengths, actuator/beam section curvatures per unit voltage and actuator input voltages. The static deformation of the beam on actuator k can be obtained by substituting Equation 4.5 into Equations 4.3 and 4.4, giving:

$$v_0'(x) = v_0'(x_k) + K_k V_k (x - x_k) \qquad (x_k \le x \le x_k + l_k) \tag{4.6}$$

$$v_0(x) = v_0(x_k) + v_0'(x_k)(x - x_k) + \frac{K_k V_k}{2}(x - x_k)^2 \qquad (x_k \le x \le x_k + l_k) \tag{4.7}$$

Similarly, since the sections of the beam between the actuators have no applied moments, and hence zero curvature, the static deformation of the beam between actuator k and $k+1$ can be obtained from Equations 4.3 and 4.4 with the moment terms set to zero. Thus,

$$v_0'(x) = v_0'(x_k + l_k) \qquad (x_k + l_k \le x \le x_{k+1}) \tag{4.8}$$

$$v_0(x) = v_0(x_k + l_k) + v_0'(x_k + l_k)[x - (x_k + l_k)] \qquad (x_k + l_k \le x \le x_{k+1}) \tag{4.9}$$

Equations 4.6 through 4.9 include the terms $v_0(x_k)$, $v_0'(x_k)$, $v_0(x_k+l_k)$ and $v_0'(x_k+l_k)$, which depend on the effects of actuators 1 through *k-1* but not actuators *k+1* through *n*. Thus, a complete expression for the transverse deflection of the beam as a function of x can be obtained using Equations 4.6 through 4.9 by starting at the root of the beam (x=0) and working outward to the tip (x=L).

Replacing the variable v_0 with y, the slope y' and displacement y of the beam are both zero prior to the first actuator:

$$\left.\begin{aligned} y'(x) &= \frac{dy}{dx} = 0 \\ y(x) &= 0 \end{aligned}\right\} \quad (0 \le x \le x_1)$$

The slope and displacement of the beam for x on the first actuator are functions of x and the properties of the first actuator only:

$$\left.\begin{aligned} y'(x) &= y'(x_1) + K_1V_1(x - x_1) \\ &= 0 + K_1V_1(x - x_1) \\ &= K_1V_1(x - x_1) \\ y(x) &= y(x_1) + y'(x_1)(x - x_1) + \frac{K_1V_1}{2}(x - x_1)^2 \\ &= 0 + 0 + \frac{K_1V_1}{2}(x - x_1)^2 \\ &= \frac{K_1V_1}{2}(x - x_1)^2 \end{aligned}\right\} \quad (x_1 \le x \le x_1 + l_1)$$

The slope for x between the first and second actuators is the slope achieved at the end of the first actuator while the displacement for x in this range is the displacement at the end of the first actuator plus the slope at the end of the first actuator times the distance from the end of the first actuator:

$$\left.\begin{aligned} y'(x) &= y'\left(x_1 + l_1\right) \\ &= K_1 V_1 l_1 \\ y(x) &= y\left(x_1 + l_1\right) + y'\left(x_1 + l_1\right)\left[x - \left(x_1 + l_1\right)\right] \\ &= \frac{K_1 V_1}{2} l_1^{\,2} + K_1 V_1 l_1\left[x - \left(x_1 + l_1\right)\right] \\ &= K_1 V_1 l_1\left[x - x_1 - \frac{l_1}{2}\right] \end{aligned}\right\} \quad \left(x_1 + l_1 \le x \le x_2\right)$$

Continuing in this manner leads to the following general slope and transverse displacement relations for a beam with *n* attached piezoceramic actuators:

a) For* x *prior to the first actuator

$$\left.\begin{aligned} y'(x) &= 0 \\ y(x) &= 0 \end{aligned}\right\} \quad \left(0 \le x \le x_1\right) \tag{4.10}$$

b) For* x *on the first actuator

$$\left.\begin{aligned} y'(x) &= K_1 V_1\left(x - x_1\right) \\ y(x) &= \frac{K_1 V_1}{2}\left(x - x_1\right)^2 \end{aligned}\right\} \quad \left(x_1 \le x \le x_1 + l_1\right) \tag{4.11}$$

***c) For* x *on actuator* k**

$$\left.\begin{aligned} y'(x) &= K_k V_k\left(x - x_k\right) + \sum_{i=1}^{k-1} K_i V_i l_i \\ y(x) &= \frac{K_k V_k}{2}\left(x - x_k\right)^2 + \sum_{i=1}^{k-1} K_i V_i l_i\left(x - x_i - \frac{l_i}{2}\right) \end{aligned}\right\} \quad \begin{pmatrix} x_k \le x \le x_k + l_k \\ k = 2,3,\ldots,n \end{pmatrix} \tag{4.12}$$

***d) For* x *between actuator* k *and* k+1**

$$\left.\begin{aligned} y'(x) &= \sum_{i=1}^{k} K_i V_i l_i \\ y(x) &= \sum_{i=1}^{k} K_i V_i l_i\left(x - x_i - \frac{l_i}{2}\right) \end{aligned}\right\} \quad \begin{pmatrix} x_k + l_k \le x \le x_{k+1} \\ k = 1,2,\ldots,n-1 \end{pmatrix} \tag{4.13}$$

e) For **x** *between actuator* **n** *and the free end of the beam* **(x = L)**

$$\left.\begin{aligned} y'(x) &= \sum_{i=1}^{n} K_i V_i l_i \\ y(x) &= \sum_{i=1}^{n} K_i V_i l_i \left(x - x_i - \frac{l_i}{2} \right) \end{aligned}\right\} \quad \left(x_n + l_n \le x \le L \right) \tag{4.14}$$

B. OPTIMIZATION PROBLEM IN KUHN-TUCKER FORM

It is desired to determine the optimum placement of piezoceramic actuators to approximate a desired beam shape function under actuator-induced deformation. Optimization requires a suitable cost function to serve as a measure of performance for a given actuator configuration. The optimum actuator configuration achieves the absolute minimum value of the cost function among all possible values of the input variables. For piezoceramic actuators, these input variables can be expressed as actuator position, length, input voltage, and beam curvature per unit actuator input voltage.

An appropriate cost function for measuring actuator performance in static deflection of a cantilever beam is:

$$J = \int_0^L \left[y(x) - y_d(x) \right]^2 dx \tag{4.15}$$

where x is the coordinate along the length of the beam and $y(x)$ and $y_d(x)$ are the actual and desired transverse beam deflections at each point along the beam, respectively, as shown in Figure 17. Values of x range from 0 at the constrained end to L at the unconstrained end of the beam. Equation 4.15 is minimized by the combination of input variables that produces a $y(x)$ which provides a continuous "least squares" fit to the desired shape function over the length of the beam.

The actuator locations and lengths are constrained by:

$$
\begin{aligned}
& x_1 \geq 0 \\
& x_i \geq x_{i-1} + l_{i-1} \quad (i = 2,3,\ldots,n) \\
& x_n + l_n \leq L \\
& l_i \geq 0 \quad (i = 1,2,\ldots,n)
\end{aligned}
\tag{4.16}
$$

where n is the number of actuators and x_i and l_i are the locations and lengths of the actuators as shown in Figure 17. Equations 4.16 ensure that all actuators are located entirely on the beam with no overlap and that all have nonnegative length. Constraints on the maximum actuator lengths can also be included. Furthermore, the input voltages to the piezoceramic actuators must lie within an operating range specified by:

$$
V_{\min} \leq V_i \leq V_{\max} \quad (i = 1,2,\ldots,n) \tag{4.17}
$$

where V_{min} and V_{max} are the actuator's minimum and maximum operating voltage and V_i is the input voltage to the ith actuator.

The problem of optimizing Equation 1 within the constraints of Equations 4.16 and 4.17 can be expressed in Kuhn-Tucker (KT) form [Ref. 8] as: *Minimize Equation 4.15 subject to:*

$$
\begin{aligned}
& g_1(\underline{z}) = -x_1 \leq 0 \\
& g_i(\underline{z}) = x_{i-1} + l_{i-1} - x_i \leq 0 \quad (i = 2,3,\ldots,n) \\
& g_{n+1}(\underline{z}) = x_n + l_n - L \leq 0 \\
& g_{n+1+i}(\underline{z}) = -l_i \leq 0 \quad (i = 1,2,\ldots,n) \\
& g_{2n+1+i}(\underline{z}) = (V_i - V_{\min})(V_i - V_{\max}) \leq 0 \quad (i = 1,2,\ldots,n)
\end{aligned}
\tag{4.18}
$$

where the vector of input variables, $\underline{z}$, is given by

$$
\underline{z} = [x_1 \ldots x_n, l_1 \ldots l_n, V_1 \ldots V_n]^T \tag{4.19}
$$

A KT problem is typically solved by constructing a Lagrangian, given by:

$$L = J(\underline{z}) + \mu_1 g_1(\underline{z}) + \mu_2 g_2(\underline{z}) + \ldots + \mu_m g_m(\underline{z}) \tag{4.20}$$

and solving the system of equations:

$$\begin{aligned} &\frac{\partial L}{\partial \underline{z}} = \frac{\partial J(\underline{z})}{\partial \underline{z}} + \mu_1 \frac{\partial g_1(\underline{z})}{\partial \underline{z}} + \mu_2 \frac{\partial g_2(\underline{z})}{\partial \underline{z}} + \ldots + \mu_m \frac{\partial g_m(\underline{z})}{\partial \underline{z}} = \underline{0} \\ &\mu_i \begin{cases} = 0 & \text{if } g_i(\underline{z}) < 0 \\ > 0 & \text{if } g_i(\underline{z}) = 0 \end{cases} \quad (i = 1,2,\ldots,m) \end{aligned} \tag{4.21}$$

where m is the number of constraint equations. Equations 4.21 with all μ_i terms set to 0 may have no solutions or one or more solutions for the values of the input variables, with each solution corresponding to a local minimum or maximum of Equation 4.15. A local minimum may or may not be the global minimum, if a global minimum exists. If Equation 4.15 has either no finite global minimum or a global minimum outside the constrained range of input variables, the minimum value of Equation 1 over the allowable range of input variables may lie on a constraint boundary. The μ_i terms in Equations 4.20 and 4.21 allow for the possibility that the minimum value of the cost function in Equation 4.15 over the bounded range of possible input variables specified by Equation 4.18 lies on one or more constraint boundaries. The minimum value of the cost function on constraint boundary i can be found by including μ_i as an additional variable to be solved for in the $\underline{z}$ vector and adding the corresponding constraint equation $g_i=0$ to the system of equations to be solved in Equations 4.21. Differentiating Equation 4.20 with respect to the additional variable μ_i can be seen to return the appropriate constraint equation.

C. SELECTED SHAPE FUNCTIONS FOR ANALYSIS

An analytical expression for the cost function to be minimized can be obtained by substituting Equations 4.10 through 4.14 into Equation 4.15, provided that all terms involving the desired beam shape function $y_d(x)$ are integrable. Two suitable shape functions were selected for evaluation of optimal actuator placement. The first, a parabolic shape function given by:

$$y_d(x) = Cx^2 \tag{4.22}$$

was selected as a due to its mathematical simplicity and its applicability to common structures such as antennas. This shape function has uniform curvature C over the length of the beam. A second shape function given by:

$$y_d(x) = C[1 - \cos(mx)] \tag{4.23}$$

where $m = \pi/L$, was chosen to analyze the effect of non-uniform desired curvature and an inflection point on the optimization process. This function has curvature:

$$y_d''(x) = \frac{C\pi^2}{L^2}\cos\left(\frac{\pi x}{L}\right) \tag{4.24}$$

which is positive over the first half of the beam and negative over the second half. The inflection point for this function is at $x = 0.5L$, where the curvature is zero.

Substituting Equation 4.22 and Equations 4.10 through 4.14 into Equation 4.15 gives an expression for the cost function associated with the parabolic desired shape:

$$
\begin{aligned}
J = {} & \frac{C^2 x_1^{\,5}}{5} \\
& + \sum_{k=1}^{n} \left\{ \begin{array}{l} (a_{2k} - C)^2 \dfrac{(x_k + l_k)^5 - x_k^{\,5}}{5} + 2(a_{2k} - C) a_{1k} \dfrac{(x_k + l_k)^4 - x_k^{\,4}}{4} \\ + \left[2(a_{2k} - C) a_{0k} + a_{1k}^{\,2} \right] \dfrac{(x_k + l_k)^3 - x_k^{\,3}}{3} \\ + 2 a_{1k} a_{0k} \dfrac{(x_k + l_k)^2 - x_k^{\,2}}{2} + a_{0k}^{\,2} l_k \end{array} \right\} \\
& + \sum_{k=1}^{n-1} \left\{ \begin{array}{l} C^2 \dfrac{x_{k+1}^{\,5} - (x_k + l_k)^5}{5} - 2C b_{1k} \dfrac{x_{k+1}^{\,4} - (x_k + l_k)^4}{4} \\ + (-2C b_{0k} + b_{1k}^{\,2}) \dfrac{x_{k+1}^{\,3} - (x_k + l_k)^3}{3} + 2 b_{1k} b_{0k} \dfrac{x_{k+1}^{\,2} - (x_k + l_k)^2}{2} \\ + b_{0k}^{\,2} (x_{k+1} - x_k - l_k) \end{array} \right\} \\
& + C^2 \frac{L^5 - (x_n + l_n)^5}{5} - 2C b_{1n} \frac{L^4 - (x_n + l_n)^4}{4} \\
& + (-2C b_{0n} + b_{1n}^{\,2}) \frac{L^3 - (x_n + l_n)^3}{3} + 2 b_{1n} b_{0n} \frac{L^2 - (x_n + l_n)^2}{2} \\
& + b_{0n}^{\,2} (L - x_n - l_n)
\end{aligned}
\tag{4.25}
$$

where the coefficients a_{ij} and b_{ij} are obtained by rewriting the beam displacements in Equations 4.10 through 4.14 as polynomials in x:

For x prior to the first actuator:

$$y(x) = 0 \qquad (0 \le x \le x_1) \tag{4.26}$$

For x on actuator k:

$$y(x) = a_{2k} x^2 + a_{1k} x + a_{0k} \qquad \begin{pmatrix} x_k \le x \le x_k + l_k \\ k = 1,2,\ldots,n \end{pmatrix} \tag{4.27}$$

For x between actuator k and $k+1$:

$$y(x) = b_{1k}x + b_{0k} \qquad \begin{pmatrix} x_k + l_k \le x \le x_{k+1} \\ k = 1,2,\ldots,n-1 \end{pmatrix} \tag{4.28}$$

For x between actuator n and the free end of the beam ($x = L$):

$$y(x) = b_{1n}x + b_{0n} \qquad \left(x_n + l_n \le x \le L\right) \tag{4.29}$$

giving:

$$\begin{aligned}
a_{2k} &= \frac{K_k V_k}{2} \qquad (k = 1,2,\ldots,n) \\
a_{1k} &= \begin{cases} -K_1 V_1 x_1 & (k = 1) \\ -K_k V_k x_k + \sum_{i=1}^{k-1} K_i V_i l_i & (k = 2,3,\ldots,n) \end{cases} \\
a_{01} &= \begin{cases} \dfrac{K_1 V_1 x_1^{\,2}}{2} & (k = 1) \\ \dfrac{K_k V_k x_k^{\,2}}{2} - \sum_{i=1}^{k-1} K_i V_i l_i \left(x_i + \dfrac{l_i}{2}\right) & (k = 2,3,\ldots,n) \end{cases} \\
b_{1k} &= \sum_{i=1}^{k} K_i V_i l_i \qquad (k = 1,2,\ldots,n) \\
b_{0k} &= -\sum_{i=1}^{k} K_i V_i l_i \left(x_i + \frac{l_i}{2}\right) \qquad (k = 1,2,\ldots,n)
\end{aligned} \tag{4.30}$$

An equation for the cost function associated with the second shape function can similarly be obtained by substituting Equation 4.23 and 4.26 through 4.30 into Equation 4.15, giving:

$$J = C^2\left[x_1 - \frac{2}{m}\sin(mx_1) + \frac{L}{2} + \frac{1}{4m}\sin(2mL)\right]$$

$$+\sum_{k=1}^{n}\left\{\begin{aligned}
&a_{2k}{}^2\frac{(x_k+l_k)^5 - x_k{}^5}{5} + 2a_{2k}a_{1k}\frac{(x_k+l_k)^4 - x_k{}^4}{4}\\
&+\left[2a_{2k}(a_{0k}-C) + a_{1k}{}^2\right]\frac{(x_k+l_k)^3 - x_k{}^3}{3}\\
&+2a_{1k}(a_{0k}-C)\frac{(x_k+l_k)^2 - x_k{}^2}{2} + (a_{0k}-C)^2 l_k\\
&+\frac{4a_{2k}C}{m^2}\left[(x_k+l_k)\cos(m(x_k+l_k)) - x_k\cos(mx_k)\right]\\
&+2a_{2k}C\left[\left(\frac{(x_k+l_k)^2}{m} - \frac{2}{m^3}\right)\sin(m(x_k+l_k)) - \left(\frac{x_k}{m} - \frac{2}{m^3}\right)\sin(mx_k)\right]\\
&+\frac{2a_{1k}C}{m^2}\left[\cos(m(x_k+l_k)) - \cos(mx_k)\right]\\
&+\frac{2a_{1k}C}{m}\left[(x_k+l_k)\sin(m(x_k+l_k)) - x_k\sin(mx_k)\right]\\
&+\frac{2(a_{0k}-C)C}{m}\left[\sin(m(x_k+l_k)) - \sin(mx_k)\right]
\end{aligned}\right\}$$

$$+\sum_{k=1}^{n-1}\left\{\begin{aligned}
&b_{1k}{}^2\frac{x_{k+1}{}^3 - (x_k+l_k)^3}{3} + 2b_{1k}(b_{0k}-C)\frac{x_{k+1}{}^2 - (x_k+l_k)^2}{2}\\
&+(b_{0k}-C)^2(x_{k+1} - x_k - l_k)\\
&+\frac{2b_{1k}C}{m^2}\left[\cos(mx_{k+1}) - \cos(m(x_k+l_k))\right]\\
&+\frac{2b_{1k}C}{m}\left[x_{k+1}\sin(mx_{k+1}) - (x_k+l_k)\sin(m(x_k+l_k))\right]\\
&+\frac{2(b_{0k}-C)C}{m}\left[\sin(mx_{k+1}) - \sin(m(x_k+l_k))\right]
\end{aligned}\right\}$$

(continued on next page)

$$
\begin{aligned}
&+ b_{1n}{}^2 \frac{L^3 - (x_n + l_n)^3}{3} + 2b_{1n}(b_{0n} - C)\frac{L^2 - (x_n + l_n)^2}{2} \\
&+ (b_{0n} - C)^2 (L - x_n - l_n) \\
&+ \frac{2b_{1n}C}{m^2}\left[\cos(mL) - \cos\left(m(x_n + l_n)\right)\right] \\
&+ \frac{2b_{1n}C}{m}\left[L\sin(mL) - (x_n + l_n)\sin\left(m(x_n + l_n)\right)\right] \\
&+ \frac{2(b_{0n} - C)C}{m}\left[\sin(mL) - \sin\left(m(x_n + l_n)\right)\right]
\end{aligned}
\tag{4.31}
$$

D. ALGORITHM FOR SOLUTION OF OPTIMIZATION PROBLEM FOR ACTUATORS WITH FIXED DIMENSIONS AND PROPERTIES

The MATLAB software package was used for development of an algorithm to optimize actuator placement and voltage for a given shape function and fixed actuator and beam dimensions and properties. The shape functions of Equations 4.22 and 4.23, with Equations 4.25 and 4.31, respectively as corresponding cost functions, were used for evaluation. Inspection of Equation 4.25, with appropriate substitutions from Equations 4.30, reveals that its terms are up to fifth order polynomials in the actuator locations x_i and lengths l_i multiplied by second order polynomials in the actuator curvatures K_iV_i. Equation 4.31 is similar, with sine and cosine terms replacing some of the polynomial terms. If the actuator dimensions and properties are fixed, then the lengths l_i and curvatures per unit input voltage will be constant values. Either cost function is therefore minimized by optimizing the remaining variables x_i and V_i. Equivalently, if only the actuator lengths are specified, the cost function is minimized by optimizing the actuator locations x_i and curvatures $\kappa_i = K_iV_i$. The actuator configuration and cross-sectional properties can then be chosen to maximize the actuator curvature per unit voltage as discussed in Chapter III.

The MATLAB Optimization Toolbox includes three functions intended for the optimization of multivariable functions. Two functions, *fminu* and *fmins*, perform unconstrained optimization of the input variables of a cost function, while one function,

constr, performs optimization of the input variables subject to constraints on their values. *Fmins* uses the simplex search algorithm developed by Nelder and Mead. *Fminu* uses the quasi-Newton method of Broyden, Fletcher, Goldfarb and Shanno (BFGS) with a mixed quadratic and cubic line search procedure to determine a search direction at each iteration. *Constr* also uses a BFGS quasi-Newton method to solve a quadratic subproblem at each iteration of a sequential quadratic programming routine. Grace [Ref. 9] provides a thorough description of the BFGS and sequential quadratic programming algorithms but omits detailed discussion of the Nelder and Mead technique.

Initial attempts to optimize actuator placement and voltages simultaneously using *constr* and *fminu* proved unsuccessful. These algorithms returned unreliable results with minimal change in the initial actuator locations and voltages specified for each test, regardless of the settings of the tolerances on the input variables and cost function evaluations and other options associated with the functions. *Fmins* produced much better results in general but was found to return erroneous results for some sets of initial conditions for three or more actuators. The likelihood of erroneous results increased directly with the number of actuators evaluated. A more robust method of optimizing actuator locations was therefore judged to be needed.

A revised approach to the optimization problem was developed, drawing on the work of Clark and Fuller [Ref. 10] and Wang, Burdisso and Fuller [Ref. 11] to optimize actuator locations for structural acoustic control. The latter group noted that the mathematical inconsistency in order of the voltages and actuator locations in their objective function formulation requires independent solution for the voltages and locations. Both groups therefore determined optimum actuator voltages for each set of actuator locations evaluated in their algorithms to determine optimum actuator placement. A similar approach can be applied to this problem by using an outer optimization algorithm to determine the actuator locations which minimize Equation 4.25 or 4.31 with an embedded algorithm to determine the optimum actuator input voltages for each set of actuator positions evaluated. The cost function for the outer algorithm thus becomes a fifth order polynomial in the actuator locations x_i, with sine and cosine terms if Equation

4.31 is used, while the cost function for the embedded voltage optimization algorithm becomes a second order polynomial in the actuator input voltages V_i.

A two-stage solution algorithm to determine the optimum actuator locations and voltages for a given set of actuator and beam dimensions and properties was implemented as described above using MATLAB. The algorithm was tested using either *constr*, *fminu* or *fmins* to perform the required optimization. Both *constr* and *fminu* were again found to return unreliable results with almost no change in the specified initial conditions but the *fmins* simplex search routine was found to be highly reliable, converging to the same results for a given number of actuators and set of actuator and beam dimensions and properties, over a wide range of specified initial actuator positions. This is consistent with the observations of Parkinson and Hutchinson [Refs. 12, 13], who noted that the Nelder and Mead Simplex (NMS) algorithm has proven to be robust, although less efficient than some unconstrained optimization algorithms. A block diagram of the algorithm incorporating *fmins* is shown in Figure 18. The outer stage of the algorithm uses *fmins* to perform a simplex search to determine the actuator positions, starting from an initial estimate, which minimize the cost function to a set tolerance. The inner stage of the algorithm uses *fmins* to determine the optimum actuator input voltages for each set of actuator positions evaluated by the outer stage. The effect of actuator input voltage is therefore completely transparent to the outer stage, while the actuator locations are fixed for each evaluation of the inner stage.

The use of the unconstrained optimization algorithm *fmins* to solve the constrained actuator location and voltage optimization problems is acceptable provided that the optimum solution is at the global minimum of the cost function and does not violate any of the constraints. Since the integrand of Equation 4.15 is always non-negative, the value of the cost function will also be non-negative and the cost function will have a global minimum. The algorithm presented here is therefore suitable for shape functions which do not result in actuator overlap and which require actuator input voltages within the allowable range. Complex desired shape functions with significant curvature variation over distances on the order of an actuator length or less might result in solutions with

actuator overlap, requiring that the NMS routine be modified to include constraints or replaced with another suitable constrained optimization algorithm for both voltage and position optimization.

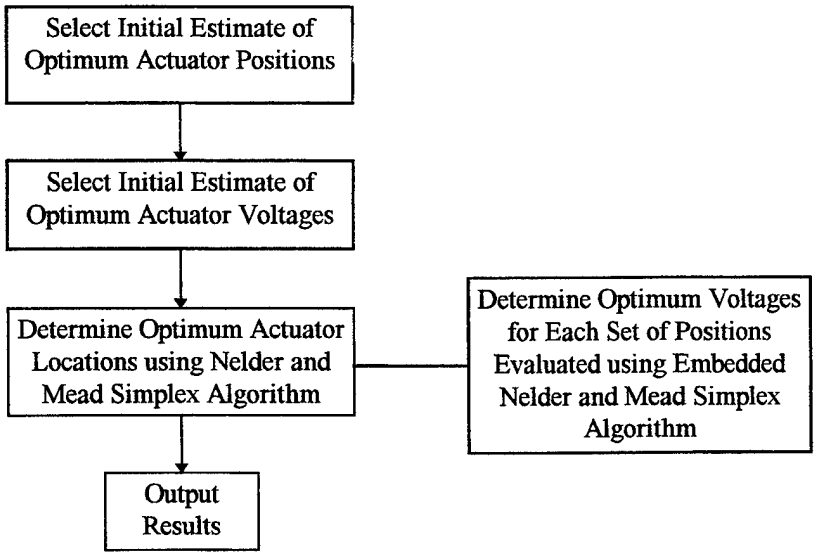

Figure 18. Actuator Placement Optimization Algorithm

E. VALIDATION OF OPTIMIZATION ALGORITHM

1. Results for Parabolic Shape Function

The optimization algorithm was implemented using the MATLAB program *actplace.m* and its associated subroutines, which are presented in the appendix. The program was tasked with determining the optimum locations for between one and five actuators on a one meter long cantilever beam to best approximate a desired parabolic beam shape with a tip displacement equal to 0.1% of the beam length. The beam was specified to have the properties of 7075-T6 aluminum, a length of 1 meter, a width of 5.08

cm (2.00 in.) and a thickness of 1.575 mm (0.062 in.). The beam curvature per unit actuator input voltage was calculated for a symmetrically mounted pair of 0.26 mm (10 mil) thick Navy Type II piezoceramic actuators covering 75% of the width of the beam. Each actuator length was fixed at 10% of the overall beam length. The algorithm was tested with at least four sets of arbitrarily selected initial actuator locations for each number of actuators to ensure convergence to the same optimum values. The initial configurations tested included all actuators clustered at the root of the beam, all actuators clustered at the center of the beam and actuators distributed over the length of the beam. An additional test was performed with the initial actuator locations within a few percent of beam length of the optimum locations found on previous trials for comparison of the number of floating point operations required to reach convergence. Initial actuator voltages were the optimum voltages for the initial actuator locations for each case, determined using *fmins*, except where noted.

The results for each number of actuators are tabulated with respect to each set of initial conditions in Table 2 through Table 6. The optimization algorithm proved to have minimal sensitivity to the initial actuator locations specified for up to five actuators, with two exceptions denoted by asterisks in Table 5 and Table 6. Grouping the initial locations for four actuators adjacent to one another at the center of the beam and using optimum voltages for this initial configuration as an initial estimate for all voltage evaluations prevented the inner voltage optimization algorithm from converging within the set maximum of 10,000 iterations at some point during the optimization process. Using the same actuator locations with initial voltage estimates of 0 produced erroneous results with some actuator overlap, as shown in the Run 2 column of Table 5. Similarly, grouping the initial locations for five actuators adjacent to one another at the root of the beam produced erroneous results with the first actuator overhanging the fixed end of the beam, as shown in the Run 1 column of Table 6. For both of these cases, slightly changing the initial conditions to allow 1 to 2% of beam length spacing between the initial actuator positions produced results consistent with those for the remaining sets of initial conditions tested, as shown in the Run 5 columns of the respective tables. The optimum actuator positions

obtained in the remaining cases for each number of actuators differed by at most 10^{-4}, which was the set tolerance on the actuator locations for termination of the *fmins* function. The optimum deformed beam shape is plotted versus the desired parabolic shape for each number of actuators in Figure 19 through Figure 23.

The results of the actuator voltage optimization algorithm were compared to the results of exhaustive searches of all possible combinations of discrete sets of actuator voltages, for the one, two and three actuator cases. The actuator voltages were varied discretely over specified ranges for actuator locations fixed at the optimum locations found by the placement optimization algorithm. Figure 24 through Figure 27 show plots of the variation of error with actuator input voltage. For all cases, the error due to the voltages obtained from the optimization was less than the smallest error obtained by the discrete search. Additionally, the voltages obtained from the optimization algorithm coincide with the locations of the minimum error in the corresponding plots.

The results of the actuator placement optimization algorithms were similarly compared to the results of exhaustive searches of all possible combinations of discrete sets of actuator locations for the one, two and three actuator cases. The actuator locations were varied discretely over specified ranges and the optimum actuator input voltages were determined for each combination of actuator locations using the voltage optimization algorithm. Figure 28 through Figure 31 show plots of the variation of error with actuator location. As for the voltages, the error due to the actuator locations obtained from the optimization was less than the smallest error obtained by the discrete search and the locations obtained from the optimization algorithm coincide with the locations of the minimum error in the corresponding plots. Table 7 shows the results for three actuators which can be compared to the results of the optimal placement algorithm in Table 4.

The comparison of the slopes of Figure 25 through Figure 27 and Figure 29 through Figure 31 illustrates the relative importance of each of the actuators in determining the error between the actual and desired beam shapes. The location and input voltage, or equivalently curvature, of actuator 1, the actuator closest to the cantilevered end of the beam have the most significant effect. Similarly, the location and input voltage

of actuator 2 have a greater impact than those of actuator 3. This is consistent with the fact that each actuator affects the shape of the beam from its location to the beam's free end but has no effect on the shape of the beam between the cantilevered end and its location. Actuator 1 therefore affects the greatest portion of the beam's length, followed by actuator 2, then 3, etc.

2. Results for Second Shape Function

Following evaluation of the optimization algorithm's performance with the parabolic shape function, the algorithm was tasked with determining the optimum location for between one and four actuators to best approximate the beam shape given by Equation 4.23 with a beam tip displacement again equal to 0.1% of the beam length. The beam and actuators were given the same dimensions and properties as in the previous tests. The algorithm was tested with at least four sets of initial actuator locations for each number of actuators to check convergence to the same optimum values. The initial configurations tested again included all actuators clustered at the root of the beam, all actuators clustered at the center of the beam, actuators distributed over the length of the beam and initial locations within a few percent of beam length of the optimum locations found on previous trials. Initial actuator voltages were the optimum voltages for the initial actuator locations for each case.

The results of the tests for the shape function of Equation 4.23 are presented in Figure 32 through Figure 36 and Table 8 through Table 11. The optimization algorithm showed greater sensitivity to initial conditions for this shape function than for the parabola, particularly for the four actuator test, but again converged to essentially the same results for a variety of sets of initial conditions for each number of actuators. Several sets of initial conditions prevented the inner voltage optimization algorithm from converging within the set maximum of 10,000 iterations at some point during the optimization process. Grouping the initial actuator positions at the root of the beam resulted in the algorithm converging on local minima of the cost function for the two and

four actuator cases, as shown in the Run 1 column of the respective tables. While the result of the two actuator case for these initial conditions, with the first actuator overhanging the fixed end of the beam, is obviously erroneous, the result of the four actuator case is a valid local minimum. Comparison of the actuator locations which result in the global minimum of the cost function in Figure 35 and the actuator locations resulting in the local minimum in Figure 36 illustrates this.

The curvature of the desired shape function, given by Equation 4.24, is decreasingly positive from the root to the midpoint of the beam and then increasingly negative from the midpoint to the free end of the beam. It can thus be qualitatively seen that actuators must be located in the regions of high desired curvature near the ends of the beam to most closely approximate the desired shape. Similarly, actuators in the low curvature region near the midpoint of the beam provide relatively little benefit in reducing the cost function. The combination of three actuators producing successively lower curvatures near the root and one actuator producing a high curvature in the opposite direction near the free end of the beam in Figure 36 provides a relatively good approximation of the shape function over its high-curvature portion near the root of the beam but a poorer approximation of the shape function over its high-curvature portion near the free end. In contrast, the combination of two actuators near the root and two actuators near the free end of the beam in Figure 35 provides a slightly poorer approximation of the shape function over its high-curvature portion near the root of the beam but a much better approximation of the shape function over its high-curvature portion near the free end, resulting in a lower overall value of the cost function than the arrangement in Figure 36. Grouping the initial actuator positions near the root of the beam prevented the optimization algorithm from moving more than one actuator past the inflection point in the desired shape function at $x = 0.5L$. However, the initial conditions for runs 4 through 6 in Table 11, which start two actuators on each side of the inflection point, allow the optimization algorithm to achieve the correct optimum positions.

3. General Observations

The two shape functions considered here illustrate the importance of properly selecting initial conditions for the optimization algorithm. Allowing some space between initial actuator locations was proven to be beneficial, but not always required to obtain convergence. The presence of inflection points or significant variations in the curvature of the desired shape function can result in actuator locations producing a local minimum in the error cost function and must therefore be considered in selecting initial conditions. Knowledge of the approximate locations of the optimum actuator positions should be used if possible, and multiple sets of initial conditions should be evaluated to ensure the minimum obtained is the global minimum. Exhaustive searches of discrete sets of actuator locations can be helpful in selecting initial conditions, but such searches become increasingly computationally intensive as the number of actuators is increased.

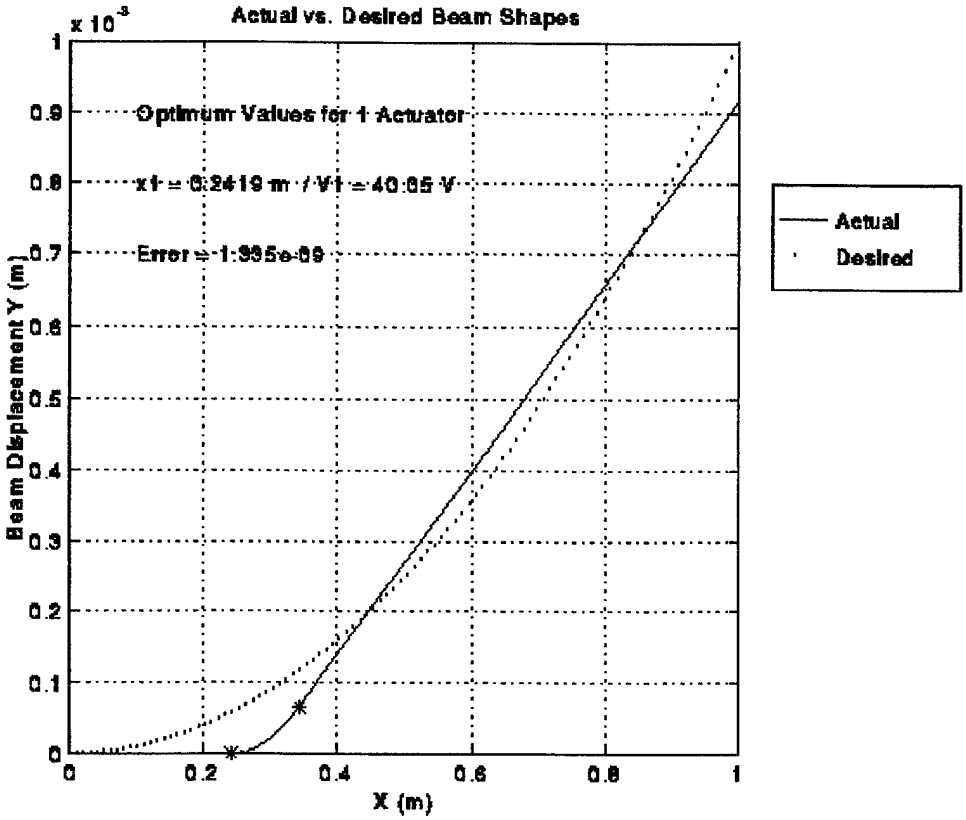

Figure 19. Optimal Location for One 10% Length Actuator for Parabolic Desired Shape

Run Number	1	2	3	4
Initial Actuator Location (m)	0	0.2	0.6	0.25
Initial Actuator Voltage (V)	25.23	36.71	104.59	40.74
Optimum Actuator Location (m)	0.2419	0.2420	0.2419	0.2419
Optimum Actuator Voltage (V)	40.05	40.05	40.05	40.05
Error (10^{-9})	1.335	1.335	1.335	1.335
Operations (10^{5})	3.08	1.53	2.93	1.10

Table 2. Optimization Algorithm Results for One 10% Length Actuator for Parabolic Desired Shape

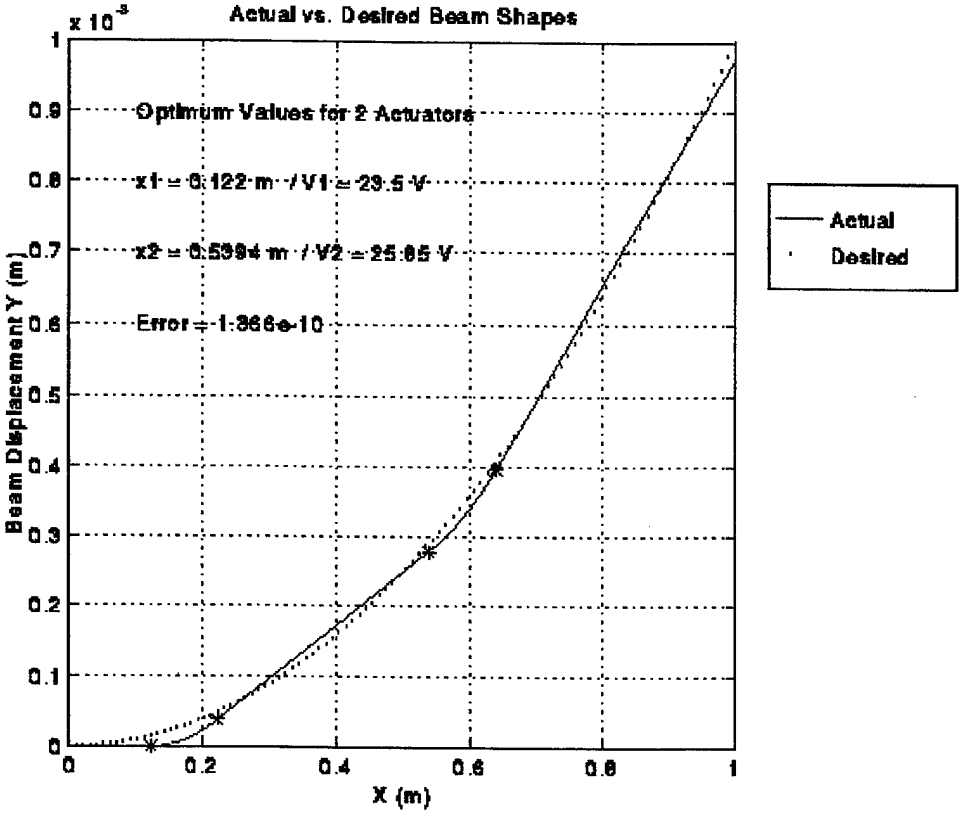

Figure 20. Optimal Locations for Two 10% Length Actuators for Parabolic Desired Shape

Run Number	1	2	3	4
Initial Actuator Locations (m)	0.0 0.1	0.4 0.5	0.25 0.65	0.1 0.5
Initial Actuator Voltages (V)	-26.64 61.55	94.79 -50.78	37.66 12.97	20.85 26.95
Optimum Actuator Locations (m)	0.1220 0.5394	0.1220 0.5394	0.1220 0.5394	0.1220 0.5394
Optimum Actuator Voltages (V)	23.50 24.85	23.50 24.85	23.50 24.85	23.50 24.85
Error (10^{-10})	1.366	1.366	1.366	1.366
Operations (10^{6})	2.88	1.72	1.55	0.83

Table 3. Optimization Algorithm Results for Two 10% Length Actuators for Parabolic Desired Shape

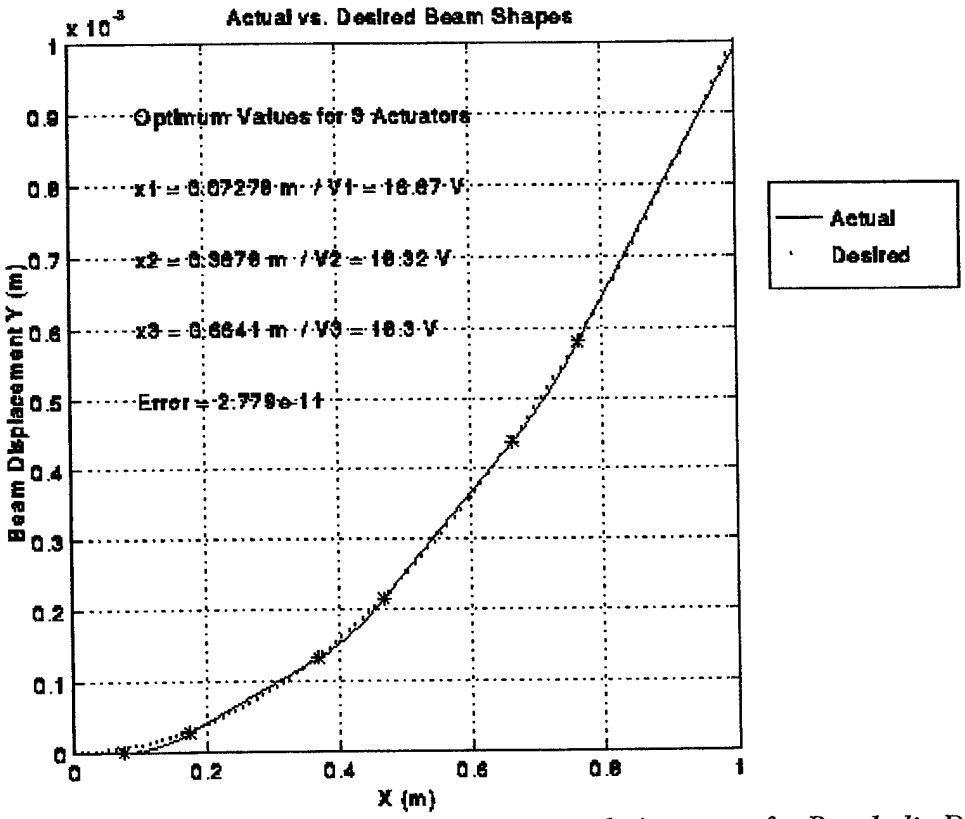

Figure 21. Optimal Locations for Three 10% Length Actuators for Parabolic Desired Shape

Run Number	1	2	3	4	5	6
Initial Actuator Locations (m)	0.0 0.1 0.2	0.35 0.45 0.55	0.20 0.45 0.70	0.1 0.4 0.7	0.05 0.35 0.65	0.075 0.370 0.665
Initial Actuator Voltages (V)	16.61 -40.88 62.52	100.09 -99.82 50.20	31.45 4.58 19.22	19.40 17.62 17.94	14.69 19.48 18.51	16.89 18.18 18.25
Optimum Actuator Locations (m)	0.0728 0.3678 0.6641	0.0728 0.3678 0.6641	0.0728 0.3678 0.6642	0.0728 0.3678 0.6641	0.0728 0.3678 0.6642	0.0728 0.3678 0.6641
Optimum Actuator Voltages (V)	16.67 18.32 18.30	16.67 18.32 18.30	16.67 18.32 18.30	16.67 18.32 18.30	16.67 18.32 18.30	16.67 18.32 18.30
Error (10^{-11})	2.779	2.779	2.779	2.779	2.779	2.779
Operations (10^6)	20.3	8.63	8.39	4.48	5.48	3.17

Table 4. Optimization Algorithm Results for Three 10% Length Actuators for Parabolic Desired Shape

Run Number	1	2*	3	4	5
Initial Actuator Locations (m)	0.0 0.1 0.2 0.3	0.3 0.4 0.5 0.6	0.1 0.3 0.6 0.8	0.05 0.25 0.50 0.75	0.28 0.39 0.51 0.62
Initial Actuator Voltages (V)	-22.33 70.51 -47.54 38.53	0 0 0 0	17.51 12.75 17.92 8.98	12.58 13.23 16.22 14.35	64.31 -44.41 15.55 16.00
Optimum Actuator Locations (m)	0.0462 0.2742 0.5038 0.7334	0.0794 0.3700 0.6141 0.7697	0.0462 0.2743 0.5039 0.7335	0.0462 0.2742 0.5038 0.7334	0.0462 0.2743 0.5039 0.7335
Optimum Actuator Voltages (V)	12.95 14.19 14.20 14.18	17.35 16.87 12.17 9.74	12.95 14.20 14.19 14.18	12.94 14.19 14.20 14.18	12.95 14.20 14.20 14.18
Error (10^{-12})	7.528	16.48	7.528	7.528	7.528
Operations (10^7)	7.88	7.83	2.69	1.78	5.27

Table 5. Optimization Algorithm Results for Four 10% Length Actuators for Parabolic Desired Shape

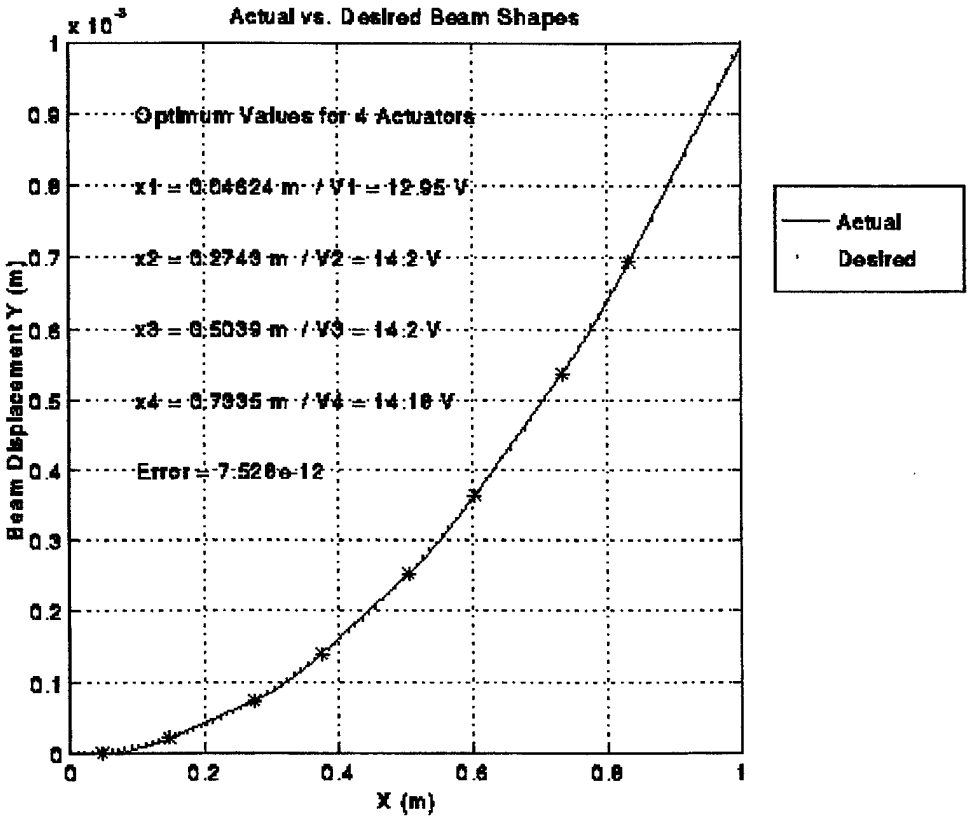

Figure 22. Optimal Locations for Four 10% Length Actuators for Parabolic Desired Shape

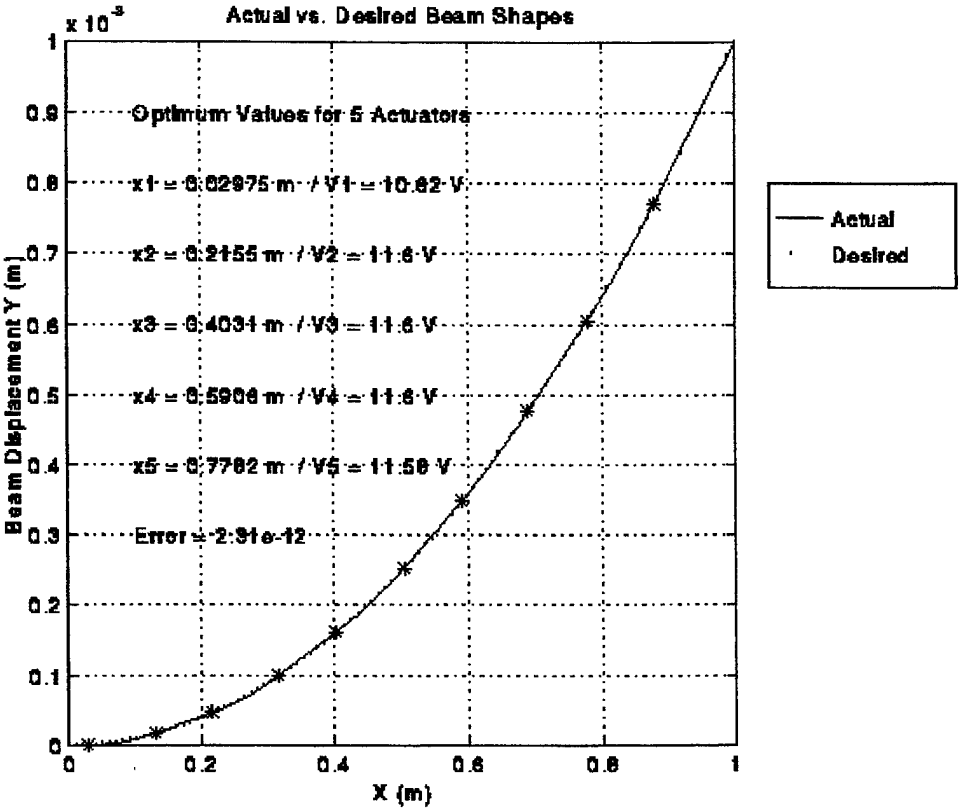

Figure 23. Optimal Locations for Five 10% Length Actuators for Parabolic Desired Shape

Run Number	1*	2	3	4	5
Initial Actuator Locations (m)	0.0 0.1 0.2 0.3 0.4	0.25 0.35 0.45 0.55 0.65	0.05 0.25 0.45 0.65 0.85	0.05 0.20 0.40 0.60 0.80	0.00 0.11 0.22 0.33 0.44
Initial Actuator Voltages (V)	-1.54 31.37 -30.73 26.74 17.24	27.22 12.93 13.58 -16.96 8.83	11.59 16.55 4.06 23.07 -7.16	11.25 6.56 25.93 -3.48 12.04	11.33 -2.36 3.04 17.09 14.88
Optimum Actuator Locations (m)	-0.0100 0.1531 0.3548 0.5575 0.7610	0.0298 0.2155 0.4031 0.5907 0.7782	0.0298 0.2155 0.4031 0.5906 0.7782	0.0298 0.2155 0.4031 0.5907 0.7782	0.0298 0.2156 0.4031 0.5906 0.7782
Optimum Actuator Voltages (V)	6.39 12.38 12.51 12.56 12.57	10.62 11.60 11.60 11.60 11.58	10.62 11.60 11.60 11.60 11.58	10.62 11.60 11.60 11.59 11.58	10.62 11.60 11.59 11.59 11.58
Error (10^{-12})	3.688	2.310	2.310	2.310	2.310
Operations (10^{7})	15.7	14.5	7.52	6.80	24.5

Table 6. Optimization Algorithm Results for Five 10% Length Actuators for Parabolic Desired Shape

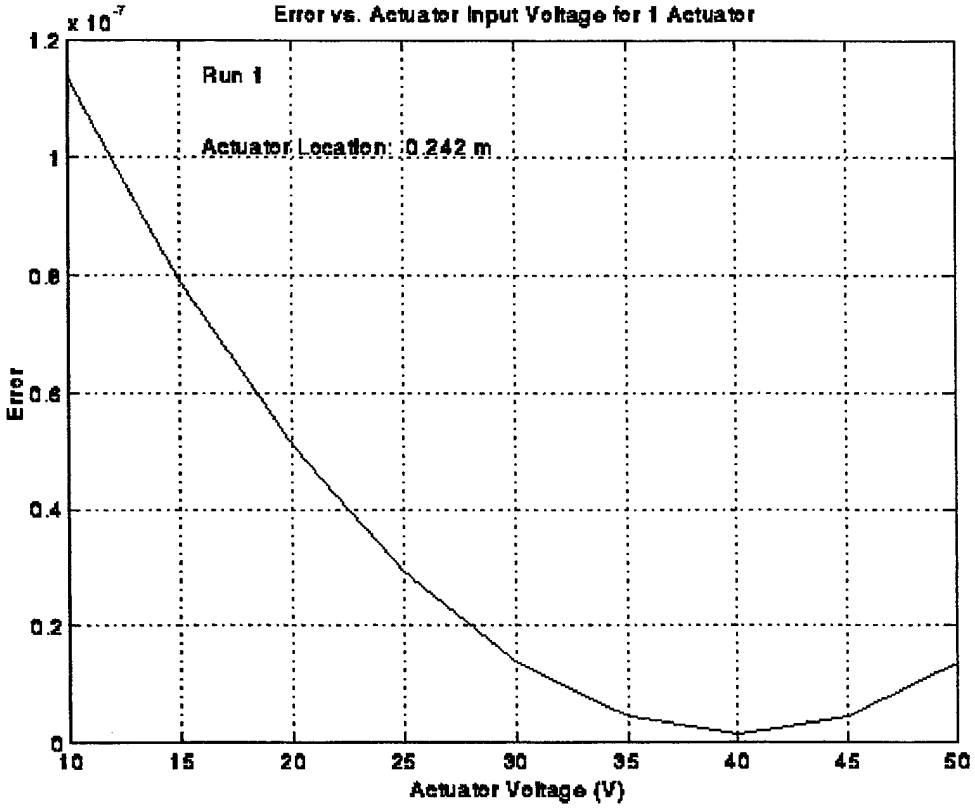

Figure 24. Variation of Error with Input Voltage for One Actuator at Optimum Location for Parabolic Desired Shape

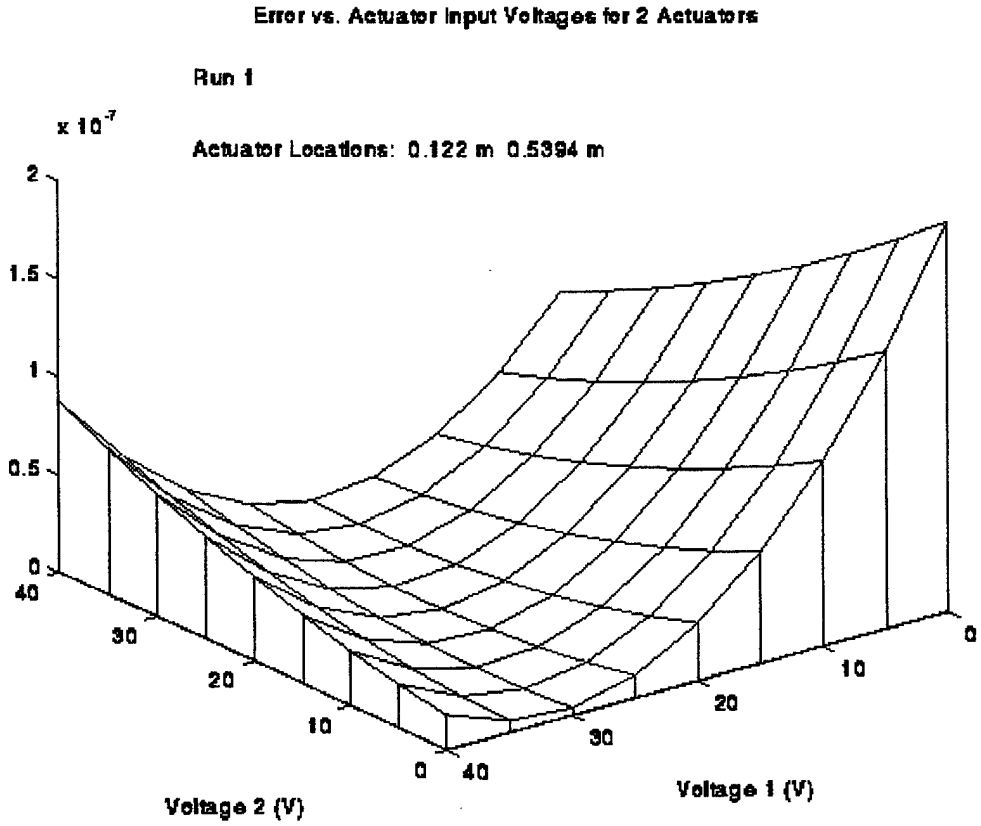

Figure 25. Variation of Error with Input Voltages for Two Actuators at Optimum Locations for Parabolic Desired Shape

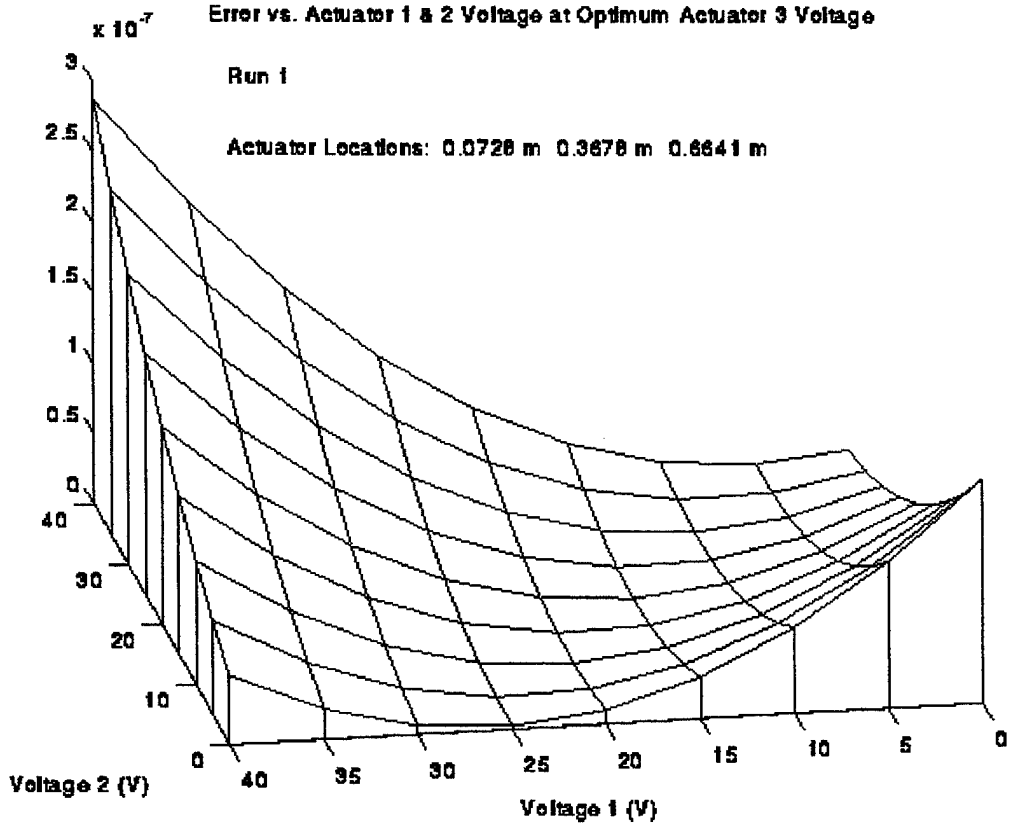

Figure 26. Variation of Error with Actuator 1 and 2 Input Voltages for Three Actuators at Optimum Locations and Optimum Actuator 3 Input Voltage for Parabolic Desired Shape

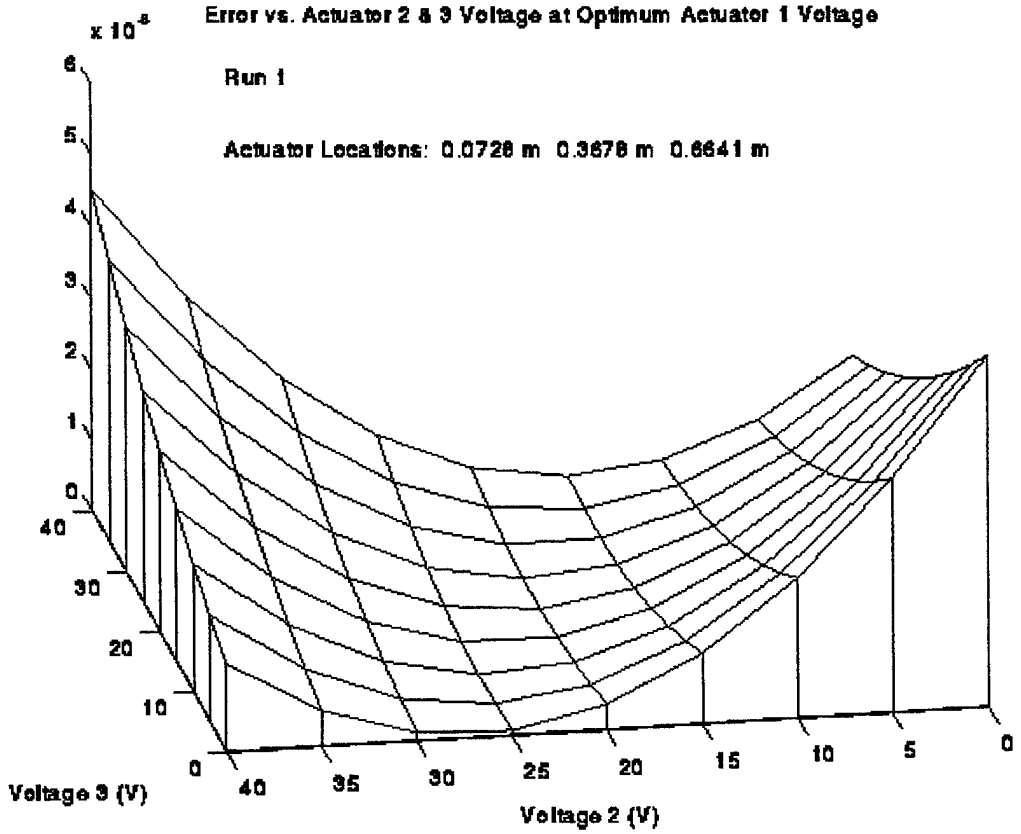

Figure 27. Variation of Error with Actuator 2 and 3 Input Voltages for Three Actuators at Optimum Locations and Optimum Actuator 1 Input Voltage for Parabolic Desired Shape

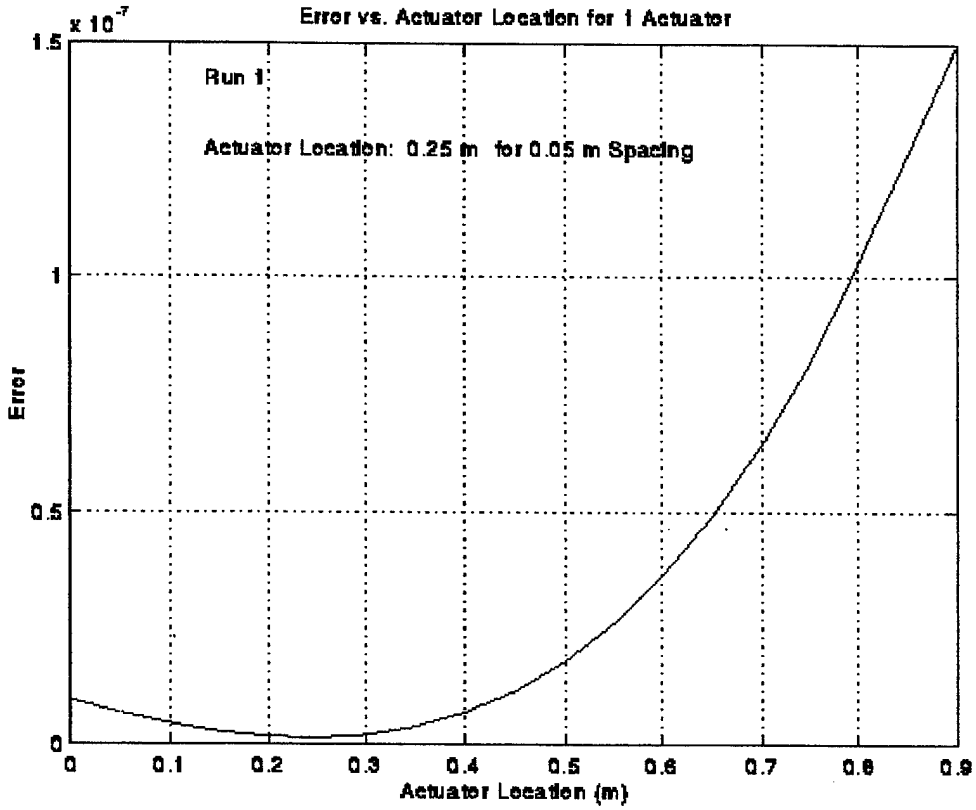

Figure 28. Variation of Error with Actuator Location for One Actuator for Parabolic Desired Shape

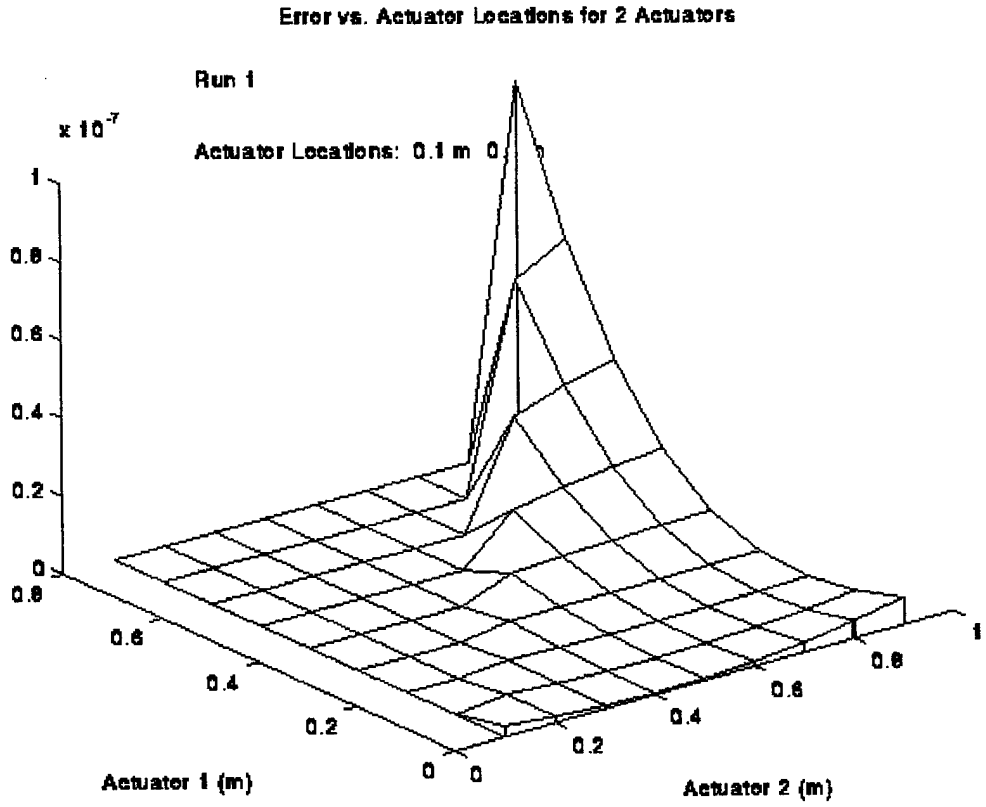

Figure 29. Variation of Error with Actuator Location for Two Actuators for Parabolic Desired Shape

Run Number	1	2	3	4	5	6
Actuator Location Ranges (m)	0.0-0.7 0.1-0.8 0.2-0.9	0.0-0.4 0.2-0.6 0.5-0.9	0.00-0.20 0.25-0.45 0.55-0.75	0.000-0.100 0.325-0.425 0.625-0.725	0.05-0.10 0.35-0.40 0.65-0.70	0.055-0.095 0.355-0.395 0.655-0.695
Spacing Between Discrete Actuator Locations (m)	0.1	0.05	0.025	0.0125	0.00625	0.005
Discrete Actuator Locations for Minimum Error (m)	0.1 0.4 0.7	0.05 0.35 0.65	0.075 0.375 0.675	0.075 0.375 0.675	0.07500 0.36875 0.66625	0.075 0.370 0.665
Optimum Actuator Voltages (V)	19.40 17.62 17.94	15.88 19.48 18.50	16.96 18.68 18.13	16.96 18.68 18.13	16.87 18.06 18.28	16.89 18.18 18.25
Error ($\times 10^{-11}$)	3.674	3.210	2.806	2.806	2.786	2.783

Table 7. Results of Discrete Actuator Placement Algorithm for Three Actuators for Parabolic Desired Shape

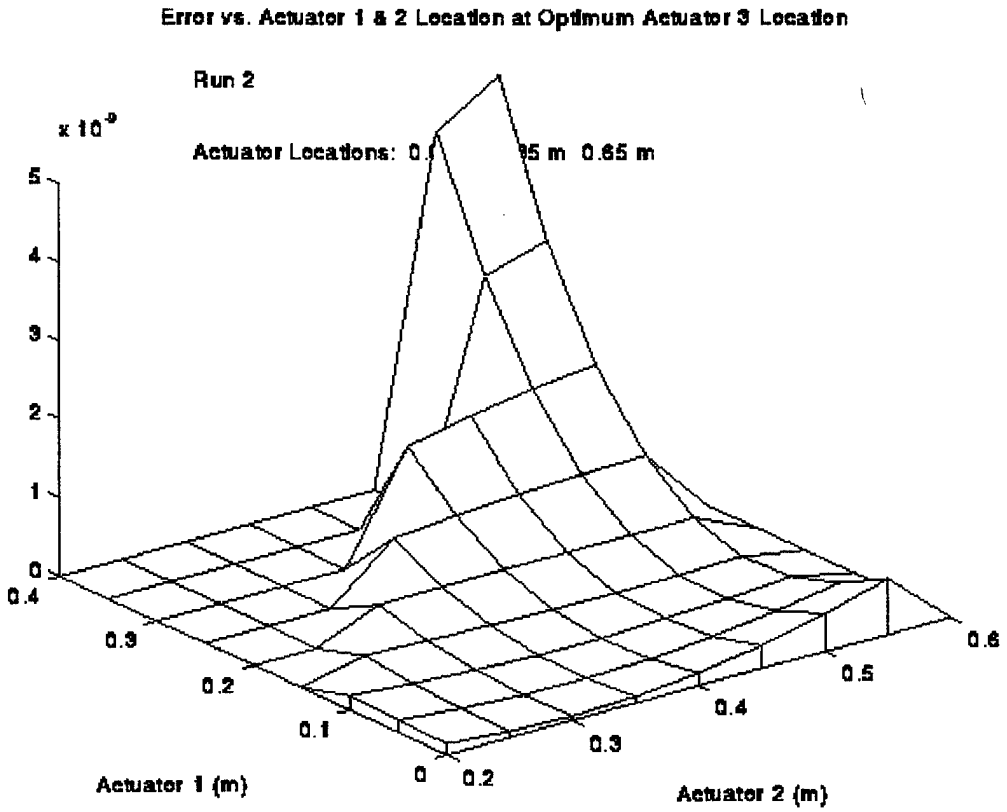

Figure 30. Variation of Error with Actuator 1 and 2 Location for Three Actuators with Actuator 3 at Optimum Location for Parabolic Desired Shape

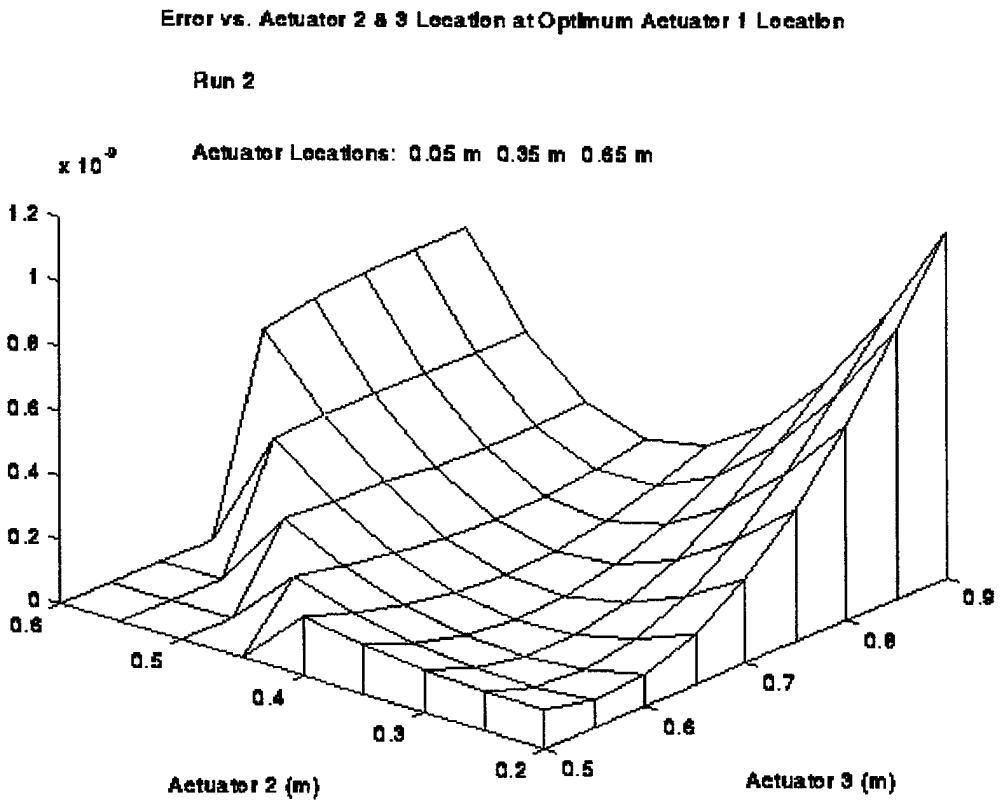

Figure 31. Variation of Error with Actuator 2 and 3 Location for Three Actuators with Actuator 1 at Optimum Location for Parabolic Desired Shape

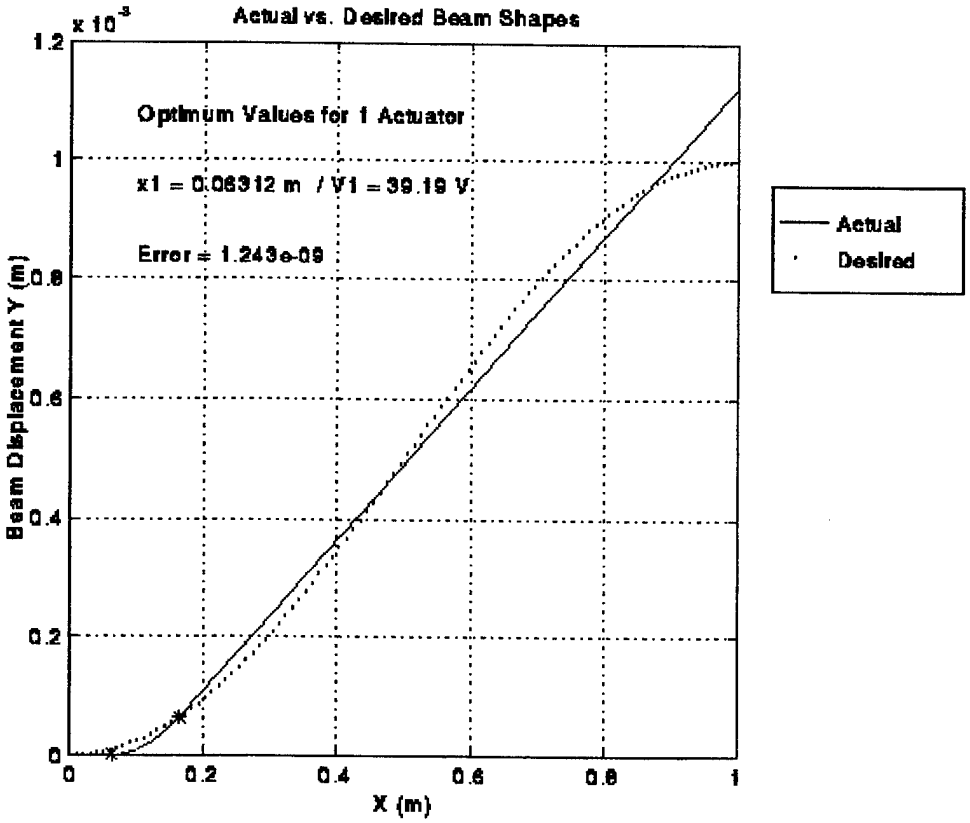

Figure 32. Optimal Location for One 10% Length Actuator for Equation 4.23 Desired Shape

Run Number	1	2	3	4
Initial Actuator Location (m)	0	0.2	0.6	0.1
Initial Actuator Voltage (V)	35.29	49.93	126.64	41.74
Optimum Actuator Location (m)	0.0631	0.0631	0.0632	0.0631
Optimum Actuator Voltage (V)	39.19	39.19	39.19	39.19
Error (10^{-9})	1.243	1.243	1.243	1.243
Operations (10^{5})	4.47	4.22	5.90	2.86

Table 8. Optimization Algorithm Results for One 10% Length Actuator for Equation 4.23 Desired Shape

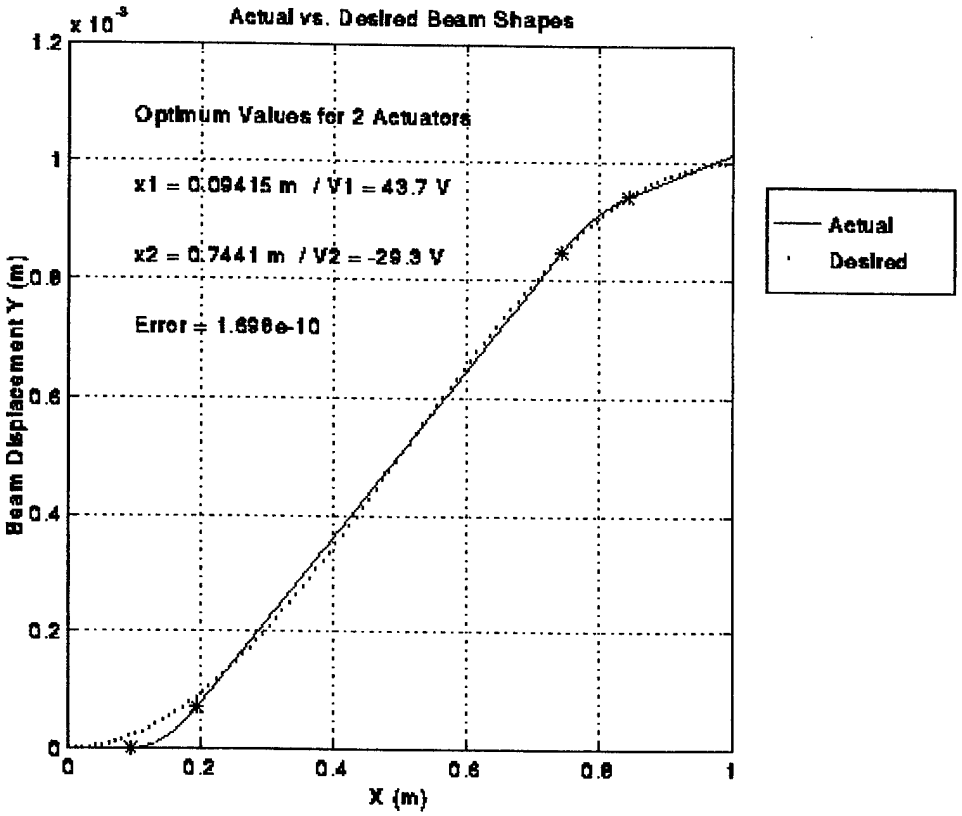

Figure 33. Optimal Locations for Two 10% Length Actuators for Equation 4.23 Desired Shape

Run Number	1*	2	3	4	5
Initial Actuator Locations (m)	0.0 0.1	0.4 0.5	0.25 0.65	0.1 0.25	0.1 0.75
Initial Actuator Voltages (V)	13.64 25.70	214.07 -190.42	67.89 -54.75	50.72 -12.17	44.21 -31.68
Optimum Actuator Locations (m)	-0.0100 0.0989	0.0942 0.7441	0.0942 0.7441	0.0941 0.7441	0.0942 0.7441
Optimum Actuator Voltages (V)	12.08 27.27	43.70 -29.32	43.70 -29.31	43.70 -29.31	43.70 -29.30
Error (10^{-10})	12.25	1.698	1.698	1.698	1.698
Operations (10^6)	2.28	3.96	2.96	3.41	1.81

Table 9. Optimization Algorithm Results for Two 10% Length Actuators for Equation 4.23 Desired Shape

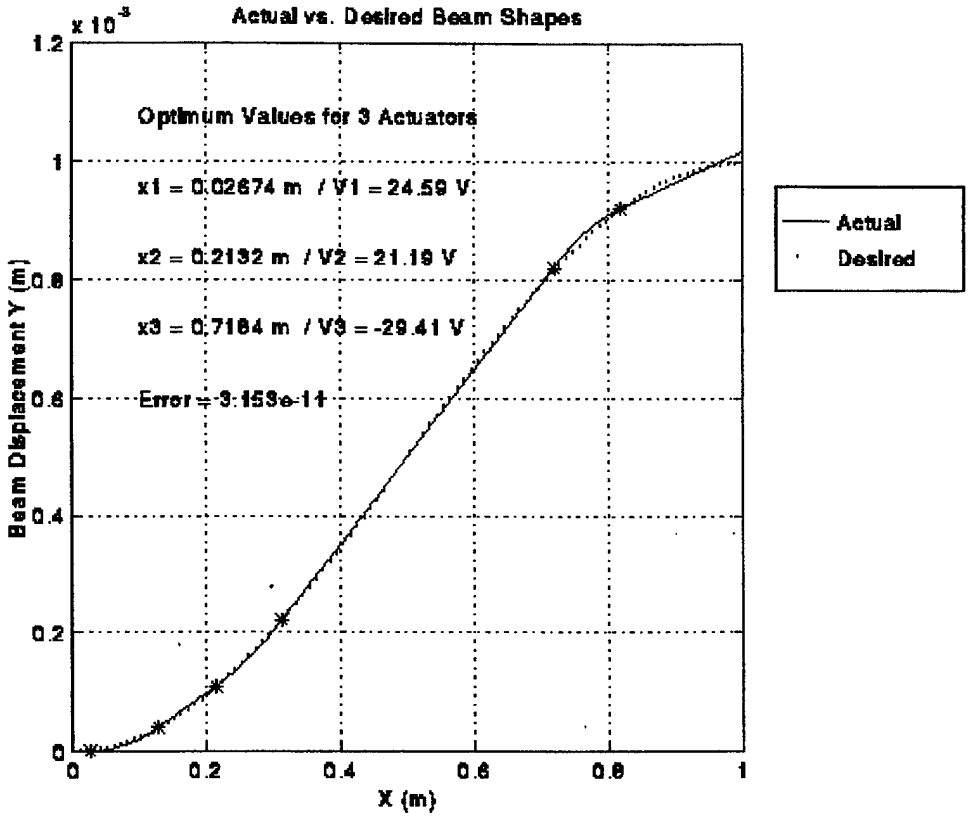

Figure 34. Optimal Locations for Three 10% Length Actuators for Equation 4.23 Desired Shape

Run Number	1	2	3*	4	5
Initial Actuator Locations (m)	0.0 0.1 0.2	0.35 0.45 0.55	0.20 0.45 0.70	0.1 0.4 0.7	0.05 0.20 0.70
Initial Actuator Voltages (V)	21.44 11.32 6.28	195.57 -183.43 18.63	66.51 -26.36 -19.35	43.49 3.27 -28.43	27.29 18.43 -26.67
Optimum Actuator Locations (m)	0.0268 0.2133 0.7184	0.0268 0.2133 0.7184	Did Not Converge	0.0268 0.2133 0.7184	0.0267 0.2132 0.7184
Optimum Actuator Voltages (V)	24.60 21.18 -29.42	24.60 21.18 -29.42		24.61 21.17 -29.42	24.59 21.19 -29.41
Error (10^{-11})	3.153	3.153		3.153	3.153
Operations (10^{7})	2.45	2.97		1.51	0.84

Table 10. Optimization Algorithm Results for Three 10% Length Actuators for Equation 4.23 Desired Shape

Run Number	1*	2*	3*	4	5	6
Initial Actuator Locations (m)	0.0 0.1 0.2 0.3	0.3 0.4 0.5 0.6	0.1 0.3 0.6 0.8	0.1 0.3 0.5 0.7	0.0 0.2 0.7 0.9	0.05 0.25 0.65 0.85
Initial Actuator Voltages (V)	17.07 2.89 42.39 -24.74	151.41 -109.40 -12.45 1.26	42.46 4.64 -11.57 -26.61	41.55 7.65 -6.15 -22.63	19.74 26.31 -27.09 3.80	30.18 17.04 -19.37 -21.98
Optimum Actuator Locations (m)	0.0041 0.1199 0.2463 0.7161	Did Not Converge	Did Not Converge	0.0303 0.2273 0.6514 0.8153	0.0303 0.2273 0.6513 0.8152	0.0303 0.2273 0.6513 0.8152
Optimum Actuator Voltages (V)	16.73 15.69 13.57 -29.47			25.76 20.92 -16.05 -21.81	25.76 20.93 -16.04 -21.81	25.76 20.92 -16.04 -21.81
Error (10^{-12})	27.88			8.540	8.540	8.540
Operations (10^{7})	10.7			6.41	5.85	3.38

Table 11. Optimization Algorithm Results for Four 10% Length Actuators for Equation 4.23 Desired Shape

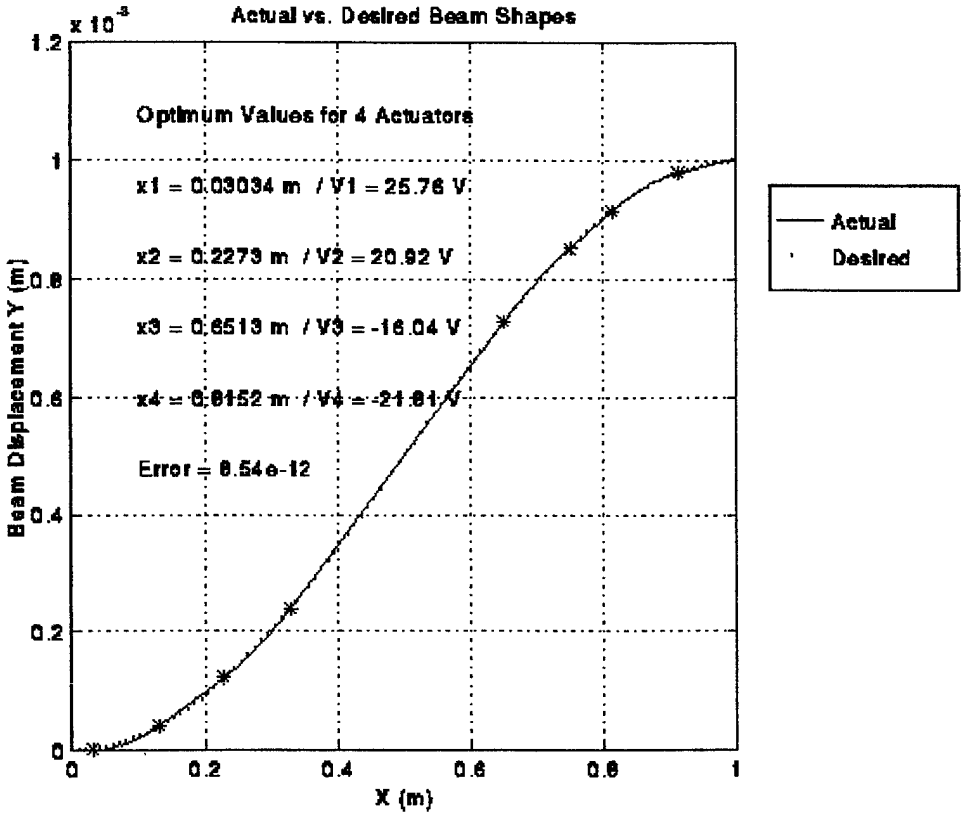

Figure 35. Optimal Locations for Four 10% Length Actuators for Equation 4.23 Desired Shape

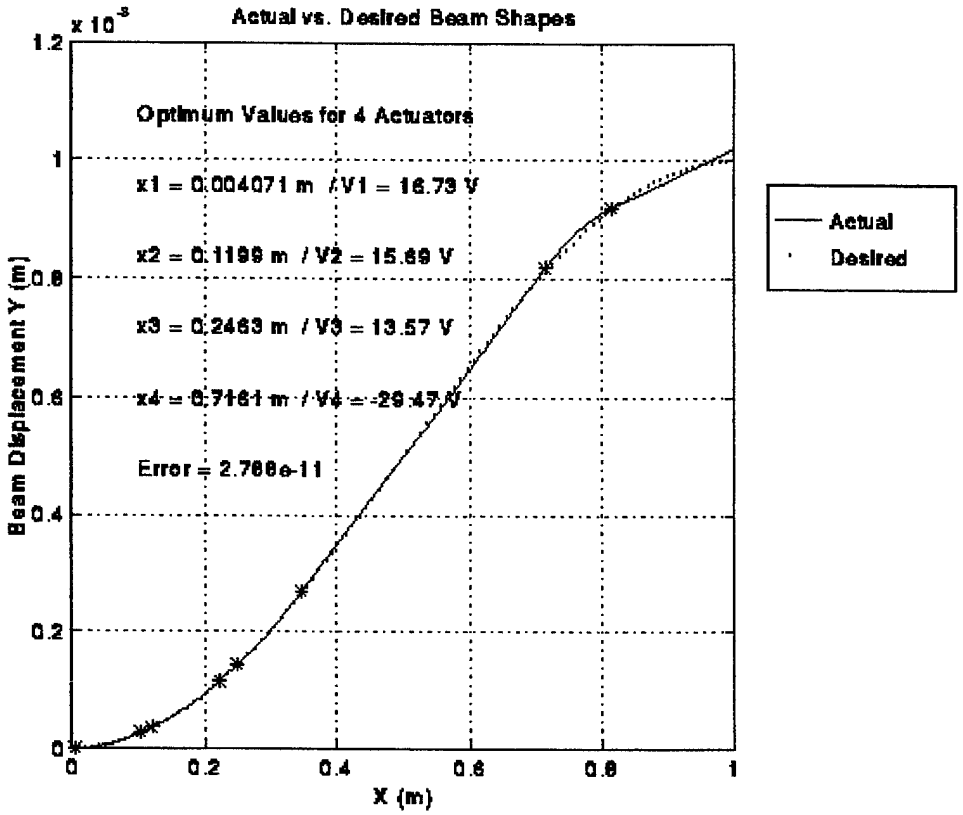

Figure 36. Actuator Locations Resulting in Local Minimum of Cost Function for Equation 4.23 Desired Shape

F. EFFECT OF NUMBER OF ACTUATORS FOR A GIVEN TOTAL ACTUATOR LENGTH

The optimization algorithm was run for a total length of actuators equal to 50% of the beam length divided into one, two, three, four or five actuators to analyze the effect of dividing a given total actuator length into increasing numbers of smaller actuators. The algorithm was tasked with determining the optimum location for the actuators on a 0.7875 mm (0.031 in.) thick 7075-T6 aluminum cantilever beam to best approximate a desired parabolic beam shape with a tip displacement equal to 0.1% of the beam length. The beam curvature per unit actuator input voltage was calculated for a symmetrically mounted pair of 0.26 mm (10 mil) thick Navy Type II piezoceramic actuators covering

75% of the width of the beam. The results for each number of actuators are tabulated in Table 12 and plotted in Figure 37 through Figure 41. These results demonstrate that increasing the number of actuators making up the total actuator length contributes substantially to minimizing the error in approximating the desired shape. Doubling the number of actuators from one to two and from two to four each resulted in about an order of magnitude decrease in the error cost function.

Number of Actuators	1	2	3	4	5
Actuator Length(s) (m)	0.5	0.25	0.1667	0.125	0.1
Optimum Actuator Location(s) (m)	0.0852	0.0600 0.4684	0.0450 0.3426 0.6432	0.0359 0.2646 0.4955 0.7265	0.0298 0.2155 0.4031 0.5906 0.7782
Optimum Actuator Voltage(s) (V)	3.429	3.824 4.159	3.993 4.355 4.350	4.087 4.461 4.462 4.456	4.147 4.528 4.529 4.529 4.522
Error ($\times 10^{-12}$)	408.9	54.38	14.15	5.166	2.310

Table 12. Optimization Algorithm Results for 50% Total Actuator Length for Parabolic Desired Shape

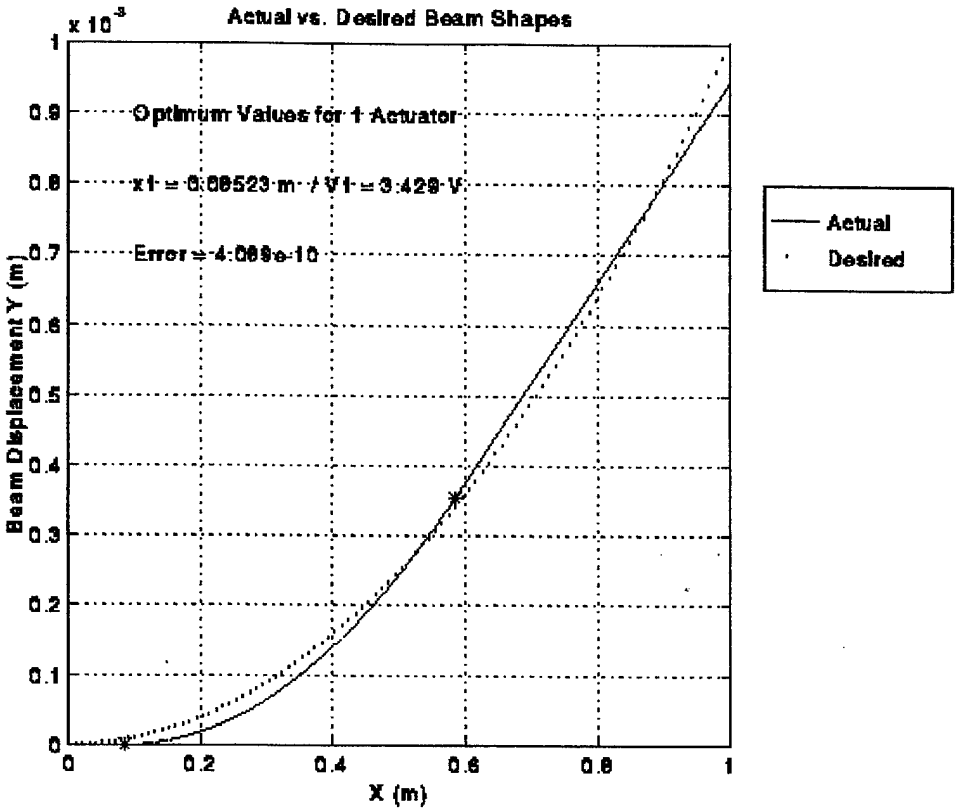

Figure 37. Optimal Location for One 50% Length Actuator

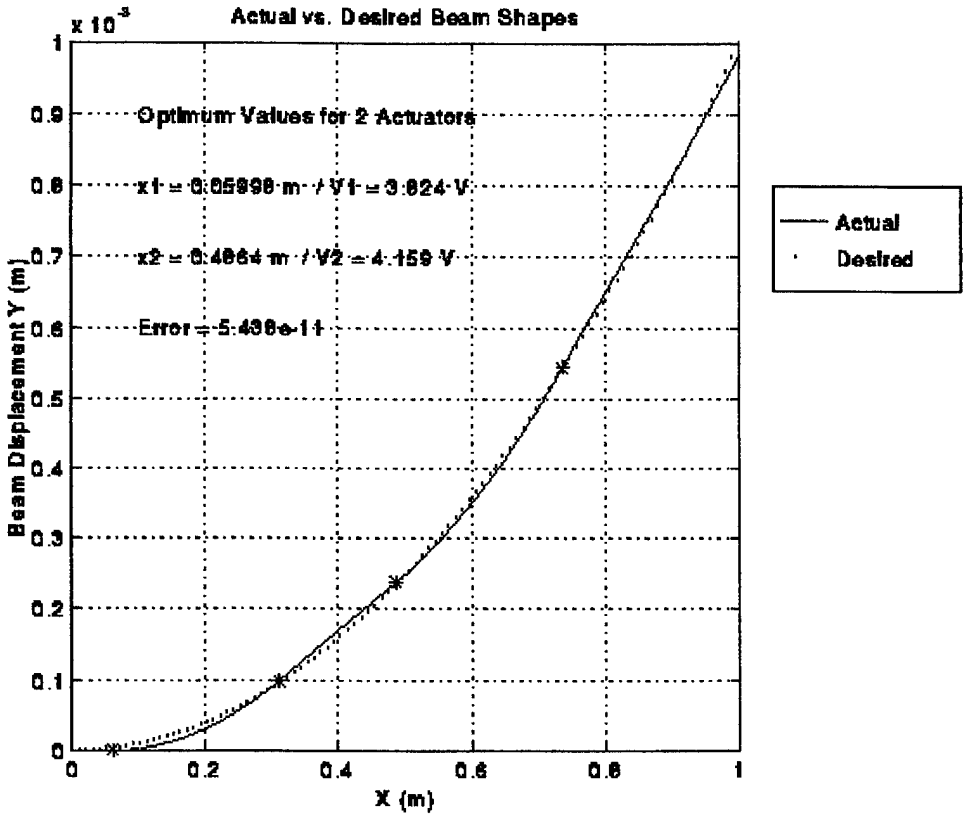

Figure 38. Optimal Location for Two 25% Length Actuators

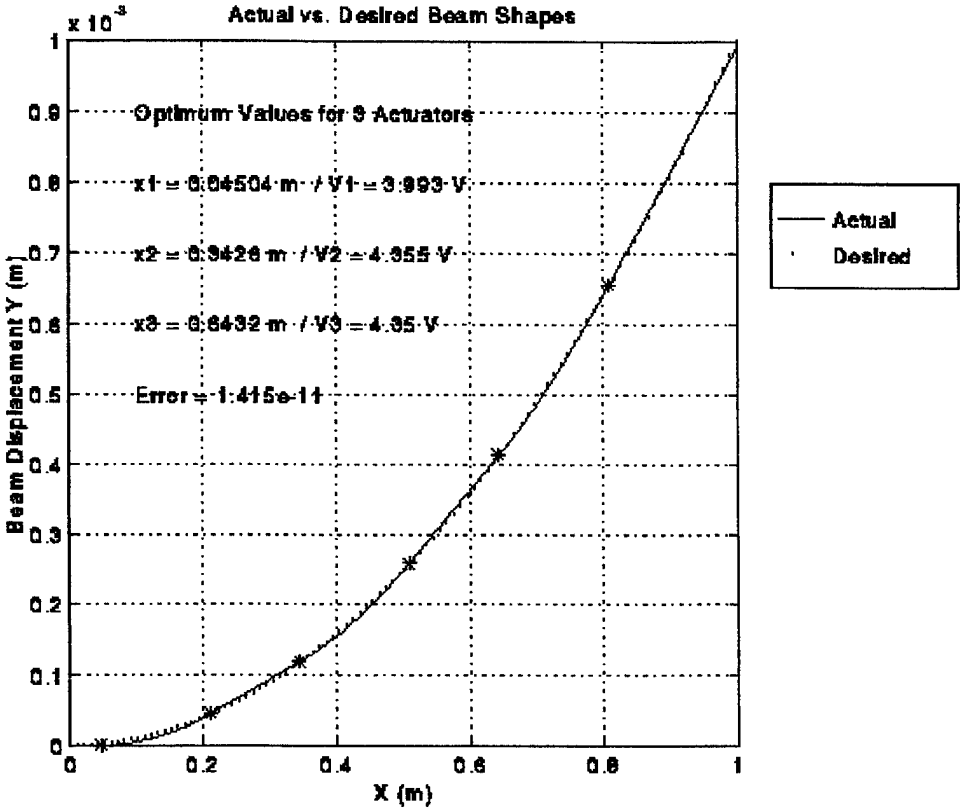

Figure 39. Optimal Location for Three 16.67% Length Actuators

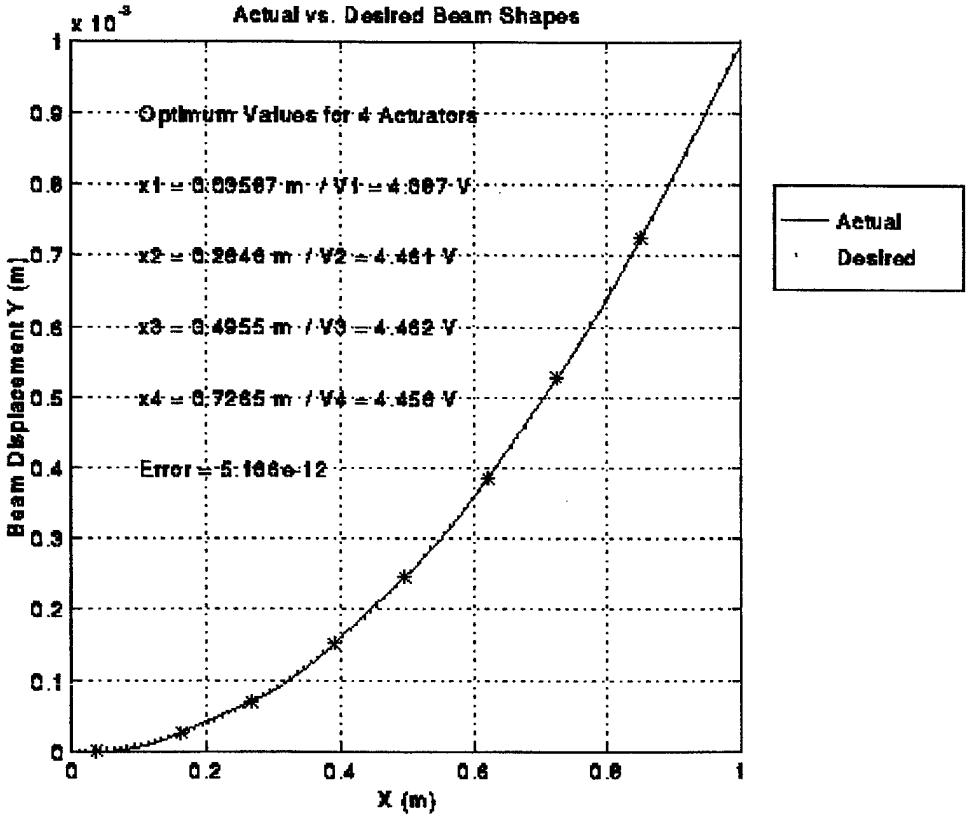

Figure 40. Optimal Location for Four 12.5% Length Actuators

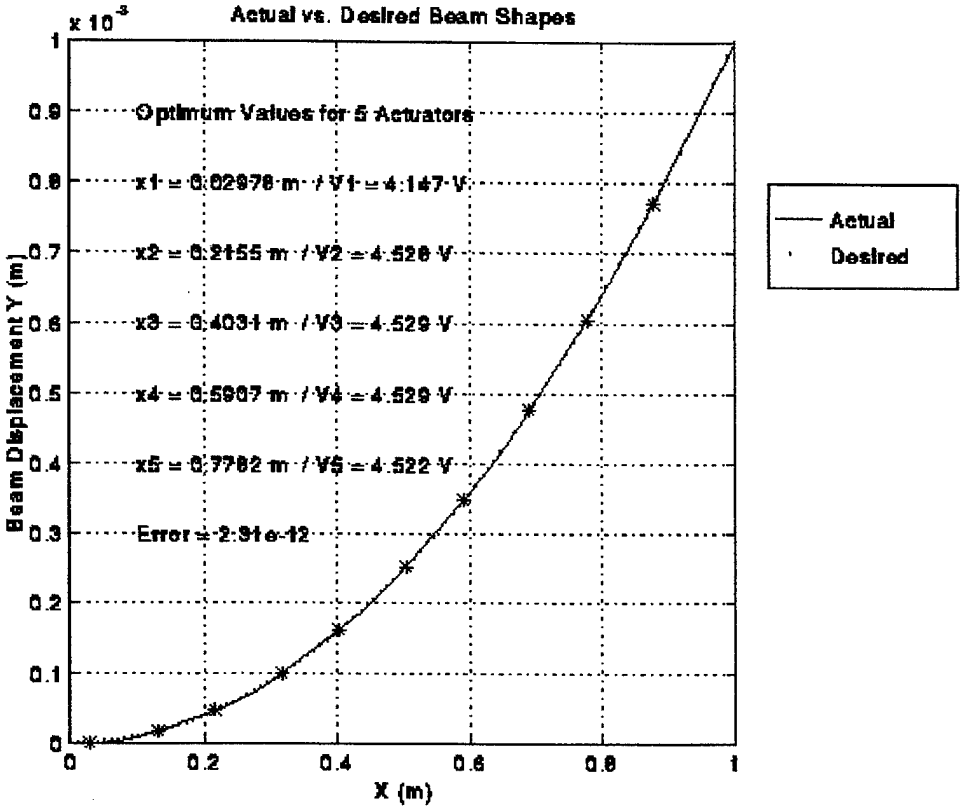

Figure 41. Optimal Locations for Five 10% Length Actuators

V. EXPERIMENTAL ANALYSIS

Experimental analysis was conducted in two parts. The first part consisted of comparison of the performance of several actuator configurations in producing beam curvature with the predictions from the corresponding Euler-Bernoulli models. The Euler-Bernoulli predictions neglected the effects of transverse stresses produced by the piezoceramic, assumed a linear strain distribution across the thickness of the composite actuator/beam and assumed a linear relationship between beam curvature and actuator input voltage. The second set of experiments examined the deformation of a beam due to four single actuators in the optimal locations to best approximate a parabolic displacement profile.

A. COMPARISON OF ACTUATOR CONFIGURATIONS

1. Physical Configuration

A schematic of the equipment setup for the experiment to compare the effectiveness of actuator configurations is shown in Figure 42. Piezoceramic actuators were bonded to a 0.031 in. (0.79 mm) thick 7075-T6 aluminum beam which was cantilevered such that its length was horizontal and width was vertical to allow bending of the beam to take place in the horizontal plane. The single actuator, symmetric pair and stacked pair configurations shown in Figure 5, Figure 6 and Figure 7, respectively, were each tested on separate beams. Each beam had an overall length of 24 in., 2 in. of which was held in the clamp, and a width of 0.875 in. All actuators were 2.5 in. long, 0.75 in. wide and 0.26 mm thick Navy Type II piezoceramic.

A XANALOG nonlinear dynamic systems modeling, simulation and real-time controls testing system was used to control actuator input and record experimental data. The XANALOG is a PC-based system incorporating an internal digital signal processor controlled by NL-SIM software running in a Windows environment. NL-SIM provides a

graphical interface which allows a control system model to be constructed using block diagrams and then compiled and operated in real time. System inputs and outputs can be displayed in both digital and graphical formats while the system is running and recorded to data files for post-experiment processing.

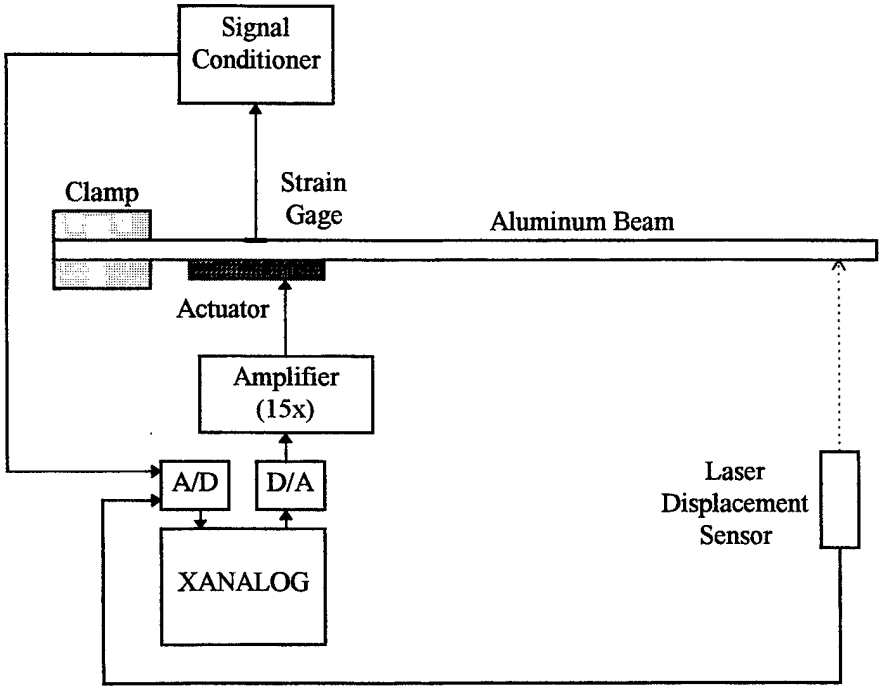

Figure 42. Experimental Setup for Comparison of Actuator Configurations

Beam tip displacement was measured at a distance of 20.125 in. from the center of each actuator using an NAiS ANL1651AC infrared laser analog displacement sensor with an output of 0.1 volts per millimeter of displacement. Beam surface strain was also measured directly opposite the center of the single and stacked pair actuator configurations in the beam length and width directions using Measurements Group Inc. CEA-13-125WT-350 bi-directional strain gages with a 2.16 gage factor. Each gage was connected to a Measurements Group Model 2120A Strain Gage Conditioner powered by a Model 2110A Power Supply. The Model 2120A output gains were set to 1732 to

provide an output of 4 volts per 1000 microstrain measured by each strain gage. Analog to digital conversion of the laser and strain gage conditioner outputs was performed by an eight-channel CIO-DAS16/330 A/D board and digital to analog conversion of the actuator command signal from the XANALOG system was performed by a six-channel CIO-DDA06 D/A board. Both boards were manufactured by Computer Boards, Inc. The ±10 volt analog output of the DDA06 was amplified by a 15:1 analog amplifier to provide a ±150 volt range of input to each actuator.

The command signal generator shown in Figure 43 was constructed using the NL-SIM software. The gain of 1.66667 was selected to allow integer command inputs to produce corresponding multiples of 25 volts input to the piezoceramic actuator when amplified by the analog amplifier. The second order filter shown was included to provide a gradual response to changes in the command input in order to prevent excitation of vibration in the beam. The filter's damping factor, ζ, was set to a value of 1 for critical damping and the filter's natural frequency, ω_n, was set to 0.1047 rad/s, corresponding to a value of 1/60 Hz. The response of the filter allowed the XANALOG output to the analog amplifier to reach steady state to four significant figures approximately 1.5 minutes after a change in the commanded input was entered.

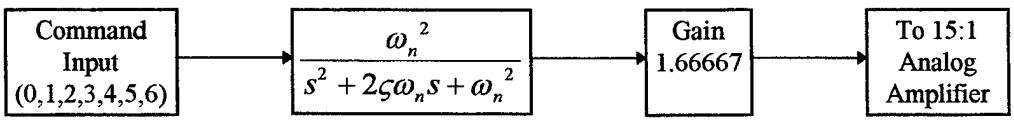

Figure 43. Block Diagram of XANALOG Actuator Command Signal Generator Implementation for Single Actuator Tests

2. Experimental Procedure

All of the experimental equipment was powered for at least 30 minutes prior to taking measurements to allow steady state conditions to be reached. The XANALOG system was configured to sample commanded actuator input and laser displacement sensor

and strain gage output at one second intervals to allow recorded data to be averaged in order to minimize the effects of noise in the sensor outputs. The laser and strain gage conditioner outputs were adjusted to indicate an average zero value as measured by the XANALOG system prior to the start of each measurement run. Each measurement run consisted of recording sensor outputs at actuator inputs of 0, 25, 50, 75, 100, 125, 150 and again 0 volts. Each actuator input was allowed to remain steady for 60 seconds to provide 60 sensor output data points for each actuator input to be averaged. The next voltage level was commanded immediately after each 60 second measurement and allowed two minutes to reach steady state before the next 60 second measurement was initiated. At least three measurement runs were conducted for each experiment to verify repeatability of the results. Data for each measurement run was saved to a MATLAB .MAT data file for processing and plotting. Measurements were taken for the single actuator acting in both compression and tension to compare the effectiveness of unsymmetric actuators for these two cases. Measurements for the stacked actuator pair were taken for the actuator acting in compression, while measurements for the symmetric actuator pair were taken with one actuator acting in tension and the other in compression.

3. Experimental Results

Measurement data for the single actuator beam is presented in Table 13 and plotted in Figure 44 for the actuator acting in compression and Table 14 and Figure 45 for the actuator acting in tension. Data for the symmetric actuator and stacked actuator pair experiments are presented in Table 15 and Figure 46 and Table 16 and Figure 47, respectively. Positive strain indicates tensile strain for the single actuator acting in tension and compressive strain for all other experiments. All runs indicated in the tables and figures were conducted consecutively with less than five minutes between the completion of one run and the start of the next. The first run for all experiments except the single actuator acting in compression was the first use of that actuator on the day of the experiment. The first measurement run for the single actuator acting in compression was

conducted immediately after preliminary testing of the experimental equipment which used the same actuator.

Significant hysteresis, or residual strain after the removal of applied voltage from the actuator, was apparent on the first run for all but the single actuator compression experiment. Udd [Ref. 14, p. 503] notes that hysteresis occurs in piezoceramic materials as the result of "energy dissipation due to internal sliding events in the polycrystaline piezoelectric body" and typically ranges from 0.1 to 10% of the strain due to an applied electric field prior to the removal of that field. Residual beam tip displacements of 31%, 23% and 36% of the displacement at maximum input voltage were noted here for the single, symmetric and stacked actuator beams respectively. The hysteresis effect is much less apparent in the following measurement runs for each actuator since the zero-displacement reference was adjusted at the start of each run. Measurements for the single actuator acting in compression and runs 2 through 4 of the other actuator experiments are therefore displacements and strains above any hysteresis level in the material at the start of the run. The displacement measurements for these runs demonstrated excellent repeatability for all of the actuators. The repeatability of strain measurements for all but the single actuator beam was also excellent. Strain measurements for the single actuator showed somewhat more variation from run to run but still reflected the same general trend as the other measurements.

The dashed lines in Figure 44 through Figure 47 depict the linear variation of beam tip displacement and beam surface strain predicted by the Euler-Bernoulli model, given by Equation 4.14 for one actuator:

$$y(x,V) = K_1 V_1 l_1 \left(x - x_1 - \frac{l_1}{2} \right) \cdot \quad \left(x_1 + l_1 \le x \le L \right) \tag{5.1}$$

where $\left(x - x_1 - \frac{l_1}{2} \right)$ is the distance between the center of the actuator and the measurement point at the beam tip. It can be seen from the figures that the Euler-

Bernoulli model provides a good approximation of the actual behavior of each actuator/beam combination at low actuator input voltage but differs increasingly from the actual behavior as voltage is increased. The actual relationship between beam tip displacement and actuator input voltage can be seen to be nonlinear. This is consistent with the fact that the published piezoelectric coefficient, d_{31}, of the piezoceramic represents a linear approximation of the material behavior over a specified operating range. The dotted lines in Figure 44 through Figure 47 represent second-order least squares curve fits of the form:

$$y(V) = c_0 V^2 + c_1 V + c_2 \tag{5.2}$$

to the observed displacements as a function of voltage. Coefficients determined for these curve fits and predicted values of c_1 from Equation 5.1 are given in Table 17. It should be noted that the values obtained for c_2 are negligibly small in magnitude. An expression for a second-order curve fit of actuator curvature as a function of actuator input voltage can be obtained by dividing Equation 5.2 by the actuator length l_1 and the measurement distance $\left(x - x_1 - \frac{l_1}{2}\right)$ and omitting the negligible constant term:

$$\kappa(V) = \frac{c_0 V^2 + c_1 V}{l_1\left(x - x_1 - \frac{l_1}{2}\right)} = k_0 V^2 + k_1 V \tag{5.3}$$

Values obtained for the k_0 and k_1 coefficients and the predicted curvature per unit voltage are given in Table 18.

The percentage of actual longitudinal strain in relation to the predicted strain was roughly 80% of the percentage of actual beam tip displacement in relation to the predicted displacement for the unsymmetric actuator configurations and roughly 140% for the symmetric actuator configuration. These percentages are too great to be explained by

measurement inaccuracies and variation of the beam and actuator material dimensions, which were determined to be within 2% of nominal values. Since strain was measured at the surface of the aluminum beam for the unsymmetric configurations and at the surface of the piezoceramic for the symmetric configuration, these results suggest that the strain distribution was not truly linear through the composite beam cross-section as shown in Figure 4. Rather, the strain at the aluminum beam surface was less than predicted by the assumed linear strain distribution but greater than predicted at the piezoceramic surface. The beam tip displacement measurements nonetheless provide a measure of the overall effect of the strain distribution over the entire actuator section of the beam at producing curvature of the beam's neutral axis.

Measured transverse strain tended to exceed the measured longitudinal strain by between 10% and 20%. The longitudinal strain had been expected to be significantly greater than the transverse strain due to the significantly larger moment of inertia of the beam cross-section about its longitudinal axis than about its transverse axis. The larger longitudinal moment of inertia should result in significantly less longitudinal curvature, and hence transverse strain, produced by the actuator. The strain gage conditioners for the longitudinal and transverse strain gages were swapped to eliminate the possibility of measurement equipment contributing to this result but found not to be a causing factor. The magnitude of the transverse strain measurements indicate that significant curvature about the beam's longitudinal axis does in fact occur at least locally near the center of the actuator.

Run	Predicted	1	2	3
Tip Displacement - mm (% of predicted)				
25 V	0.51	0.57 (112)	0.57 (112)	0.57 (113)
50 V	1.02	1.20 (118)	1.18 (116)	1.19 (116)
75 V	1.53	1.92 (125)	1.89 (124)	1.90 (124)
100 V	2.04	2.65 (130)	2.65 (130)	2.65 (130)
125 V	2.58	3.47 (134)	3.47 (134)	3.46 (134)
150 V	3.06	4.38 (143)	4.37 (143)	4.32 (141)
0 V	0.00	0.14	0.08	0.07
Longitudinal Strain - με (% of predicted)				
25 V	7.8	6.7 (85)	9.4 (120)	8.6 (110)
50 V	15.5	13.0 (84)	17.9 (115)	15.1 (98)
75 V	23.3	22.2 (95)	28.2 (121)	24.9 (107)
100 V	31.1	33.3 (107)	37.5 (120)	34.6 (111)
125 V	38.8	43.5 (112)	47.5 (122)	45.9 (118)
150 V	46.6	56.6 (121)	59.3 (127)	57.3 (123)
0 V	0.0	2.0	5.4	0.3
Transverse Strain -με				
25 V		8.6	10.3	9.3
50 V		17.9	20.4	17.7
75 V		28.7	32.3	29.3
100 V		41.7	43.5	41.1
125 V		54.0	56.0	54.2
150 V		69.3	71.1	68.9
0 V		1.4	4.9	0.0

Table 13. Beam Tip Displacement and Strain Measurements for Single Actuator Acting in Compression

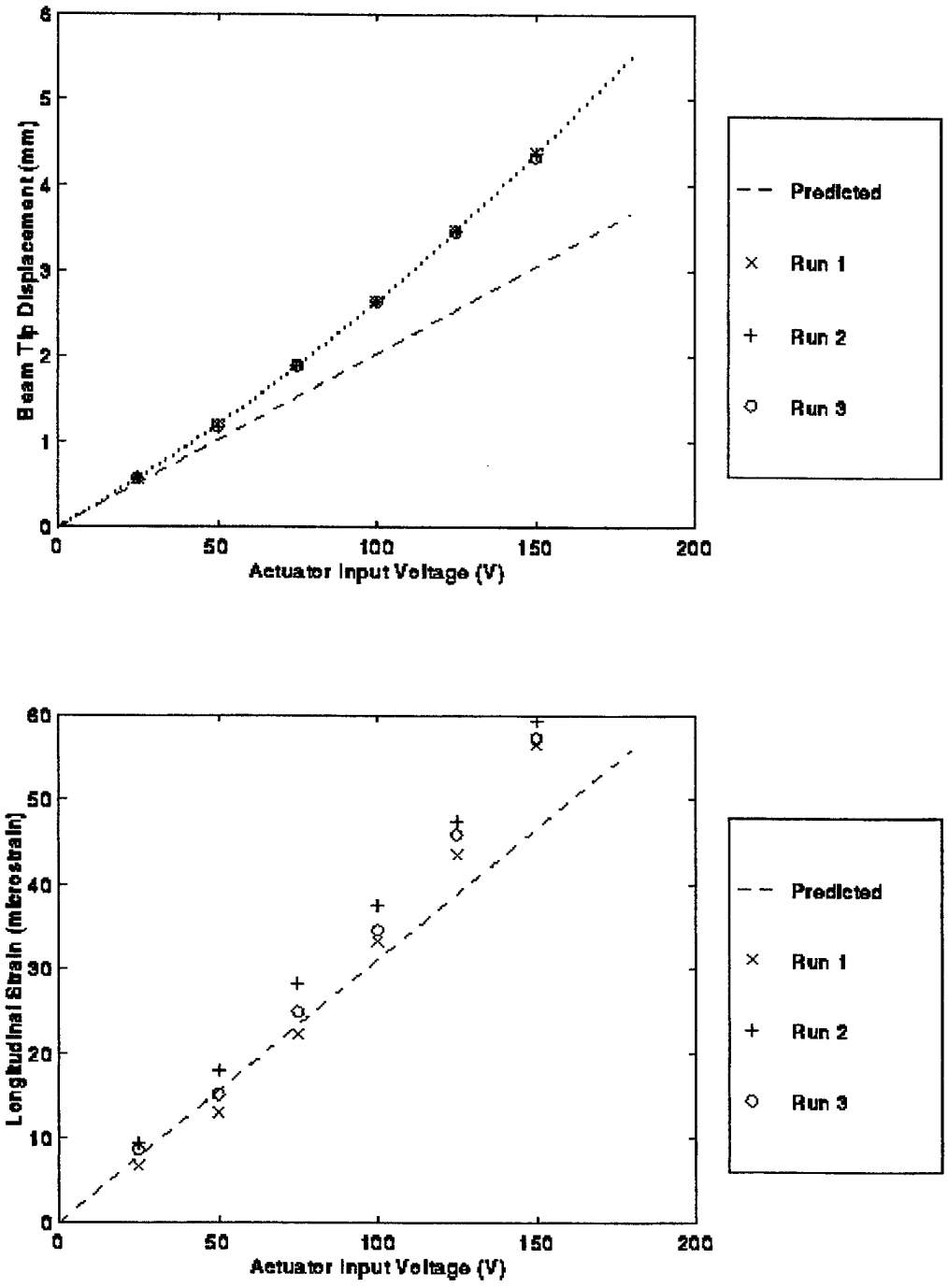

Figure 44. Beam Tip Displacement and Longitudinal Strain Measurements Single Actuator Acting in Compression

Run	Predicted	1	2	3	4
Tip Displacement - mm (% of predicted)					
25 V	0.51	0.87 (171)	0.56 (110)	0.58 (115)	0.58 (113)
50 V	1.02	1.87 (183)	1.23 (121)	1.23 (120)	1.22 (119)
75 V	1.53	2.92 (191)	1.95 (127)	1.94 (127)	1.94 (127)
100 V	2.04	4.03 (198)	2.72 (134)	2.71 (133)	2.70 (133)
125 V	2.58	5.18 (201)	3.55 (137)	3.53 (137)	3.54 (137)
150 V	3.06	6.33 (207)	4.50 (147)	4.45 (145)	4.42 (144)
0 V	0.00	1.94	0.14	0.09	0.09
Longitudinal Strain - με (% of predicted)					
25 V	7.8	5.2 (67)	6.6 (85)	7.1 (91)	7.8 (100)
50 V	15.5	11.4 (74)	13.8 (89)	17.2 (111)	16.7 (108)
75 V	23.3	19.3 (83)	23.2 (100)	26.0 (112)	26.2 (113)
100 V	31.1	30.5 (98)	33.1 (106)	35.8 (115)	35.8 (115)
125 V	38.8	45.2 (116)	42.9 (110)	46.3 (119)	46.8 (120)
150 V	46.6	59.2 (127)	55.3 (119)	58.2 (125)	57.5 (123)
0 V	0.0	1.0	-1.1	1.3	2.0
Transverse Strain -με					
25 V		14.8	8.9	9.2	9.1
50 V		29.7	18.3	20.2	18.8
75 V		42.3	29.8	30.6	30.1
100 V		63.5	41.6	43.0	41.9
125 V		80.9	54.3	54.7	54.4
150 V		97.9	68.6	69.0	66.9
0 V		30.7	2.2	2.5	2.0

Table 14. Beam Tip Displacement and Strain Measurements for Single Actuator Acting in Tension

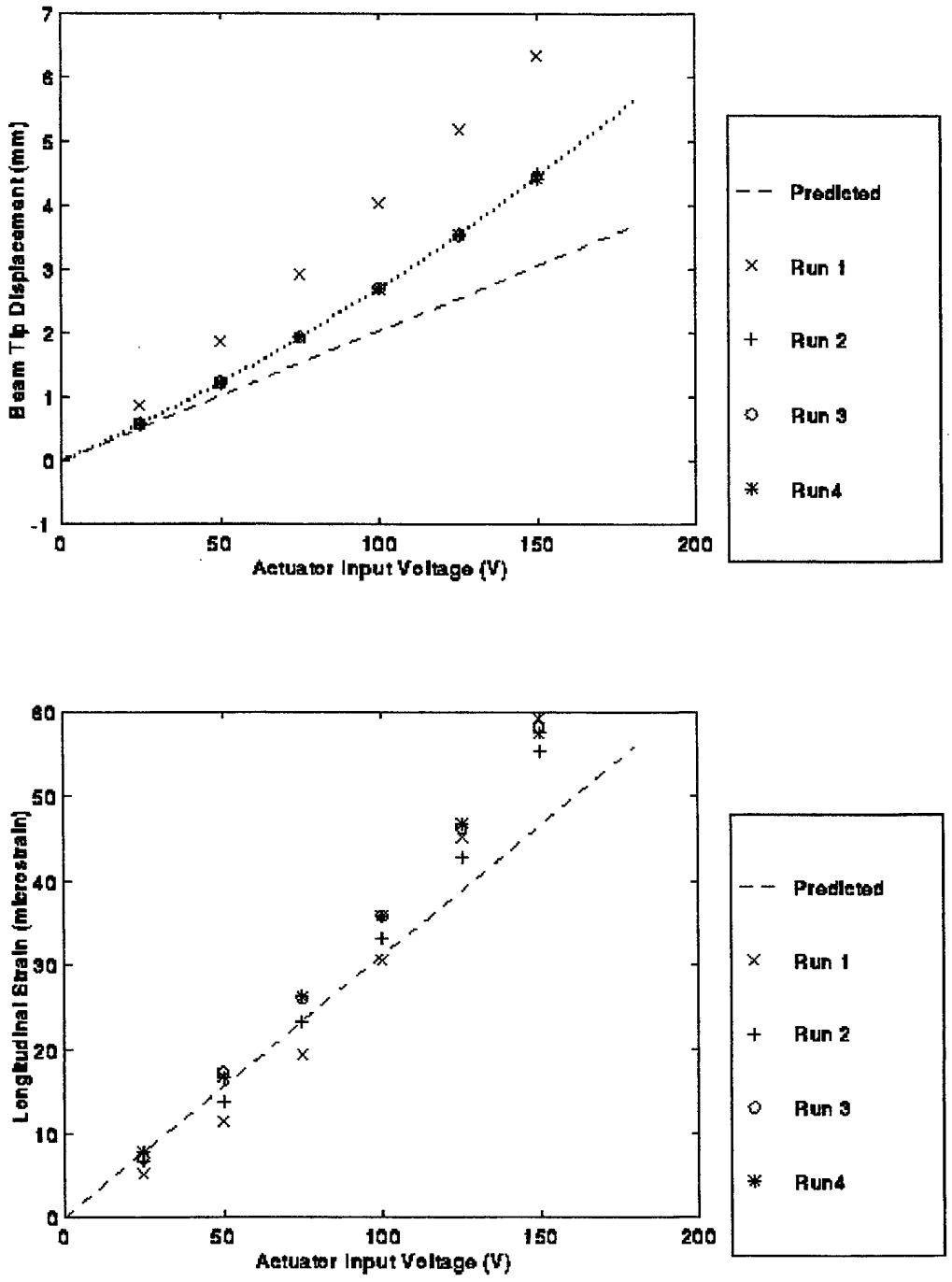

Figure 45. Beam Tip Displacement and Longitudinal Strain Measurements for Single Actuator Acting in Tension

Run	Predicted	1	2	3	4
Tip Displacement - mm (% of predicted)					
25 V	0.71	0.87 (122)	0.83 (117)	0.81 (114)	0.82 (115)
50 V	1.43	1.96 (137)	1.81 (127)	1.81 (126)	1.80 (126)
75 V	2.14	3.31 (155)	2.97 (139)	2.98 (139)	2.98 (139)
100 V	2.86	5.00 (175)	4.20 (147)	4.18 (146)	4.13 (144)
125 V	3.57	6.71 (188)	5.37 (150)	5.28 (148)	5.23 (146)
150 V	4.28	8.46 (198)	6.80 (158)	6.67 (156)	6.57 (153)
0 V	0.00	1.93	0.37	0.28	0.21
Longitudinal Strain - με (% of predicted)					
25 V	14.4	26.2 (182)	23.4 (163)	24.7 (172)	22.3 (155)
50 V	28.8	59.3 (206)	51.6 (179)	51.0 (177)	49.3 (171)
75 V	43.1	100.0 (232)	80.1 (186)	81.1 (188)	79.4 (184)
100 V	57.5	144.9 (252)	114.8 (200)	113.5 (197)	111.7 (194)
125 V	71.9	196.4 (273)	151.6 (211)	149.6 (208)	147.1 (205)
150 V	86.3	252.2 (292)	196.9 (228)	192.7 (223)	188.2 (218)
0 V	0.0	68.6	13.2	10.4	7.5
Transverse Strain -με					
25 V		28.0	24.7	26.1	25.0
50 V		61.6	54.9	54.6	53.3
75 V		102.6	85.9	87.1	85.6
100 V		148.9	122.8	122.2	120.7
125 V		201.7	162.3	160.8	159.2
150 V		260.6	211.1	207.0	202.8
0 V		59.4	11.6	10.3	7.5

Table 15. Beam Tip Displacement and Strain Measurements for Symmetric Actuator Pair

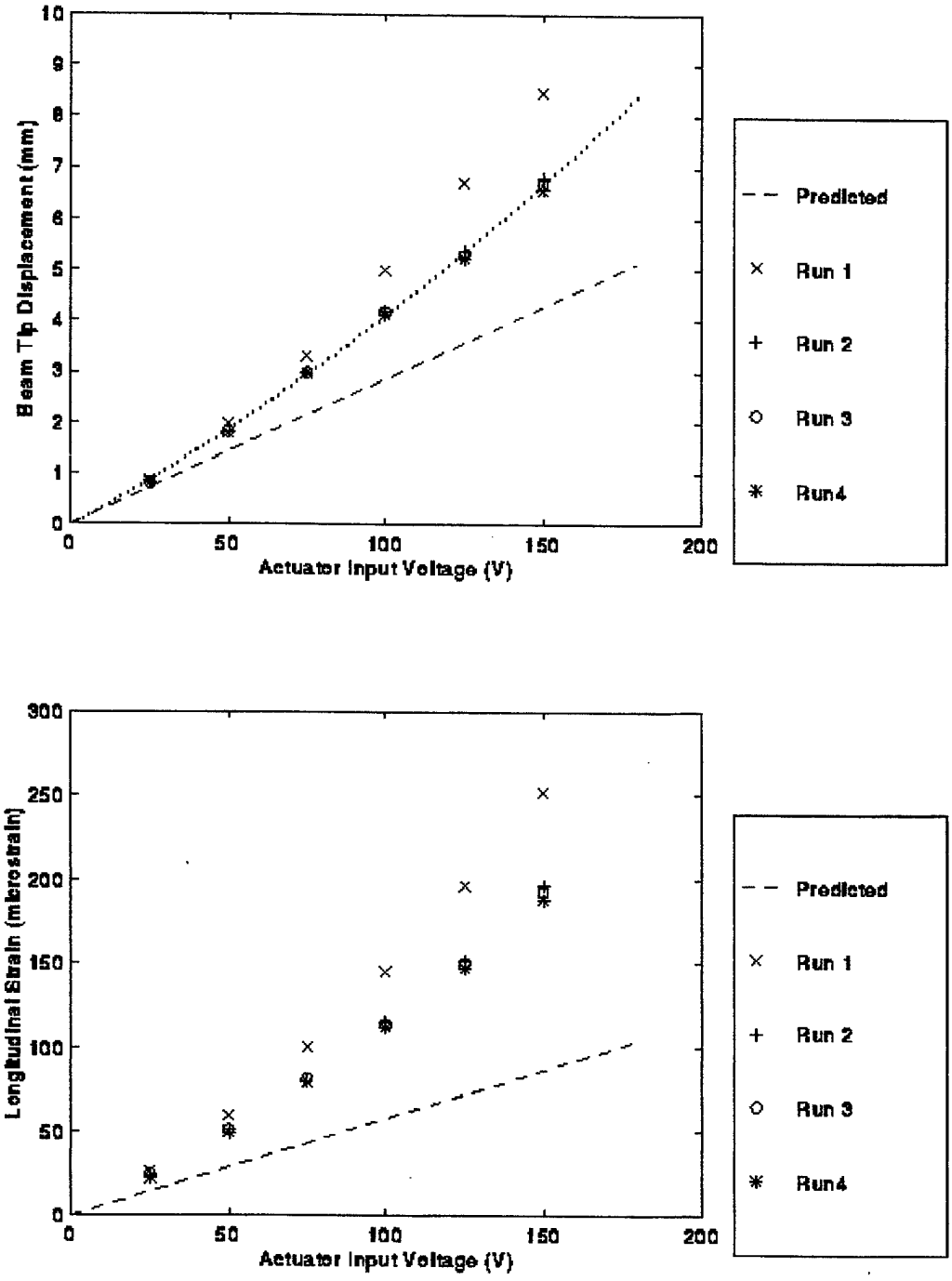

Figure 46. Beam Tip Displacement and Longitudinal Strain Measurements for Symmetric Actuator Pair

Run	Predicted	1	2	3	4
Tip Displacement - mm (% of predicted)					
25 V	0.56	1.03 (184)	0.57 (102)	0.58 (104)	0.57 (102)
50 V	1.12	2.23 (199)	1.25 (112)	1.26 (113)	1.26 (112)
75 V	1.69	3.43 (203)	2.05 (122)	2.02 (120)	2.01 (119)
100 V	2.25	4.74 (211)	2.95 (131)	2.90 (129)	2.88 (128)
125 V	2.81	6.17 (220)	3.96 (141)	3.87 (138)	3.81 (136)
150 V	3.37	7.70 (228)	5.18 (154)	4.99 (147)	4.94 (147)
0 V		2.79	0.35	0.19	0.16
Longitudinal Strain - με (% of predicted)					
25 V	8.5	14.1 (166)	8.2 (97)	6.2 (73)	7.2 (70)
50 V	17.0	29.0 (171)	16.3 (96)	14.4 (85)	17.5 (85)
75 V	24.5	45.0 (184)	26.2 (107)	24.7 (101)	28.0 (95)
100 V	33.9	65.8 (194)	37.0 (109)	34.6 (102)	40.4 (100)
125 V	42.4	83.2 (196)	49.2 (116)	45.9 (108)	54.7 (108)
150 V	50.9	102.7 (202)	63.9 (126)	59.8 (118)	70.4 (115)
0 V		43.4	5.7	2.8	1.5
Transverse Strain -με					
25 V		18.1	9.4	7.8	7.2
50 V		36.9	19.2	17.5	17.5
75 V		56.4	30.6	28.8	28.0
100 V		76.3	43.5	41.2	40.4
125 V		97.8	58.5	55.2	54.7
150 V		122.0	76.4	71.8	70.4
0 V		51.2	6.4	2.9	1.5

Table 16. Beam Tip Displacement and Strain Measurements for Stacked Actuator Pair Acting in Compression

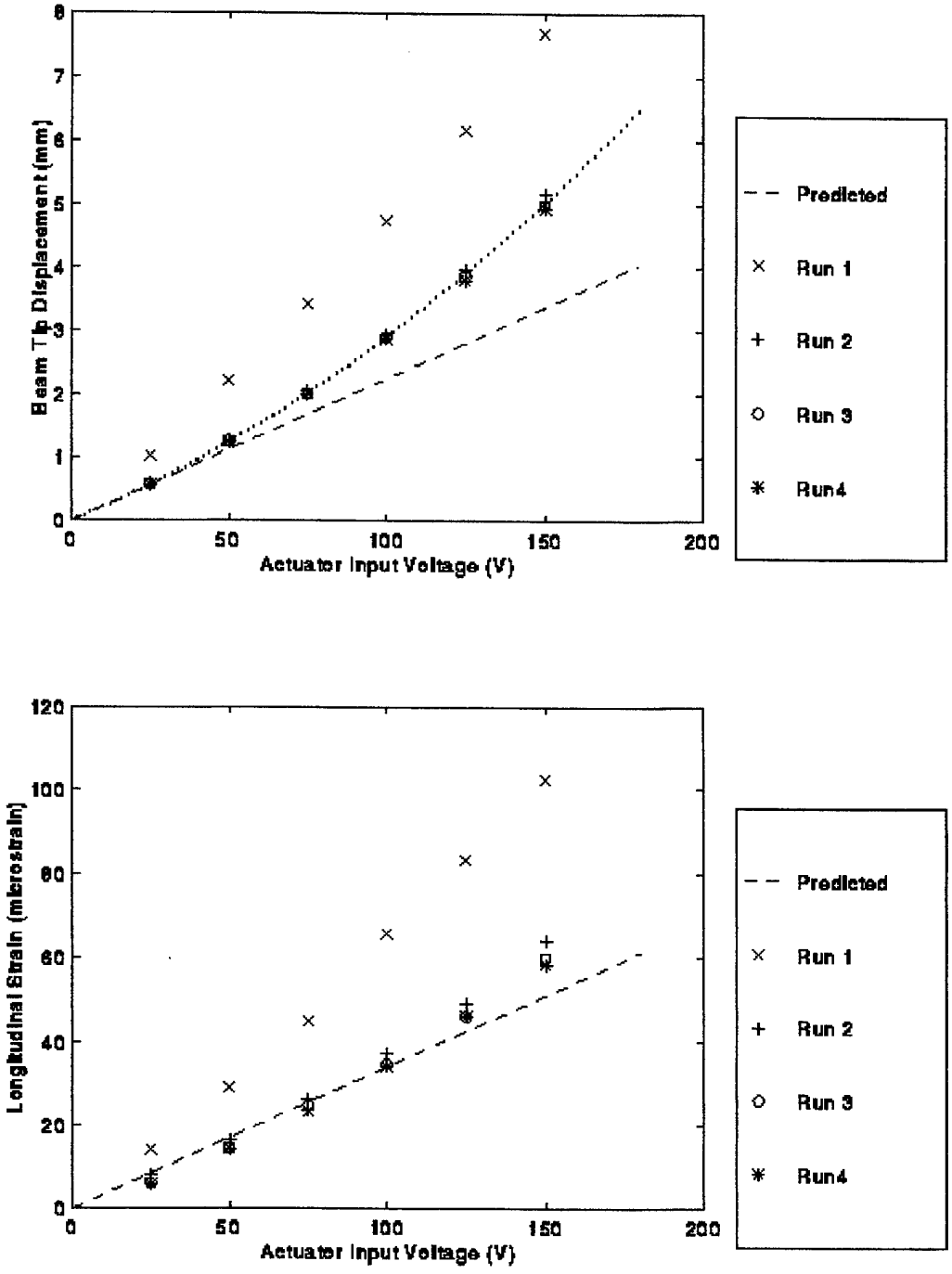

Figure 47. Beam Tip Displacement and Longitudinal Strain Measurements for Stacked Actuator Pair Acting in Compression

Beam	Predicted c_1 (10^{-2} mm/V)	c_0 (10^{-5} mm/V^2)	c_1 (10^{-2} mm/V)	c_2 (mm)
Single - Compression	2.04	5.05	2.15	0.00
Single - Tension	2.04	5.15	2.20	0.00
Symmetric Pair	2.86	6.79	3.46	-0.04
Stacked Pair	2.25	8.72	2.03	0.01

Table 17. Coefficients of Curve Fits for Observed Beam Tip Displacement as a Function of Actuator Input Voltage

Beam	Predicted $k_1 = K_1$ (10^{-4} rad/m/V)	k_0 (10^{-6} rad/m/V^2)	k_1 (10^{-2} rad/m/V)
Single - Compression	6.28	1.56	6.61
Single - Tension	6.28	1.58	6.77
Symmetric Pair	8.80	2.09	10.66
Stacked Pair	6.93	2.69	6.26

Table 18. Coefficients of Curve Fits for Observed Actuator Curvature as a Function of Actuator Input Voltage

B. BEAM SHAPE CONTROL WITH FOUR ACTUATORS

1. Physical Configuration

A schematic of the equipment setup for the four-actuator shape control experiment to compare the effectiveness of actuator configurations is shown in Figure 48. Eight piezoceramic actuator patches were bonded in four groups of two to one side of a 0.031 in. (0.79 mm) thick 7075-T6 aluminum beam which was cantilevered such that its length was horizontal and width was vertical to allow bending of the beam to take place in the

horizontal plane. The beam was also supported at approximately two-thirds of its length by an air pad riding on a granite table. The beam had an overall length of 45 in., 2 in. of which was held in the clamp, and a width of 1.625 in. All actuator patches were 2.5 in. long, 1.50 in wide and 0.26 mm thick Navy Type II piezoceramic, hence each of the four actuator groups had a total length of 5 in. The actuators were placed at locations on the beam shown in Table 19 which were determined by the optimization algorithm to best approximate a parabolic deflected beam shape with four 5 in. long actuators on a 43 in. long beam. The XANALOG system was again used to control actuator input and record experimental data and the ANL1651AC laser displacement sensor was used to measure displacement at selected points along the length of the beam. Beam surface strain was also measured directly opposite the center of the actuator patch nearer to the cantilevered end of the beam in each of the four actuator groups using a Measurements Group Inc. CEA-13-125WT-350 bi-directional strain gage opposite the first actuator and a CEA-13-125UW-350 unidirectional strain gage opposite the other three actuators. Strain gage output was obtained with a Gould Model 56-1301-00 DC/Bridge/Transducer Signal Conditioner for each gage. DAS16/330 and DDA06 boards were used for A/D and D/A conversion, respectively. Each ±10 volt analog output channel of the DDA06 was amplified by a 15:1 analog amplifier to provide a ±150 volt range of input to each actuator.

Actuator	Distance from Cantilevered End (in/cm)	Percentage of Actuator 3 Curvature for Parabolic Shape Approximation
1	1.70/4.31	91.4
2	11.52/29.26	100.0
3	21.43/54.43	100.0
4	31.34/79.60	99.9

Table 19. Actuator Locations and Curvature Ratios for Parabolic Shape Approximation

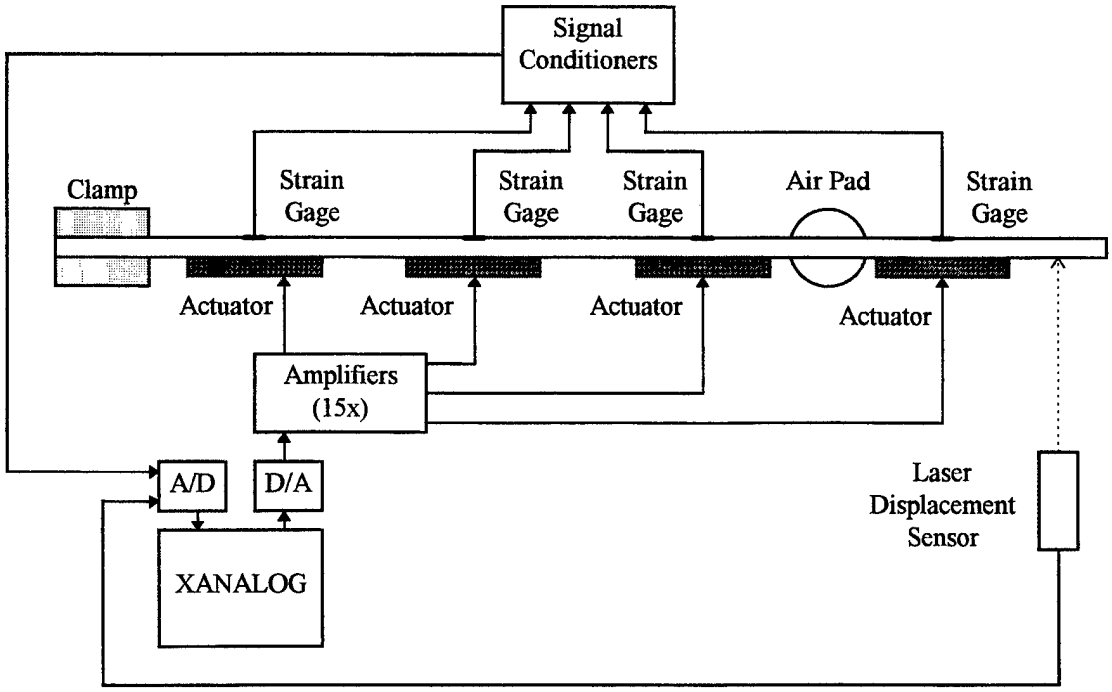

Figure 48. Setup of Four Actuator Shape Control Experiment

2. Experimental Procedure

A series of measurements was initially taken to characterize the relationship between actuator curvature and input voltage for the single actuator configuration on the beam used for this set of experiments. Beam tip displacement measurements were taken with voltage applied to the first actuator only and then with voltage applied to the second actuator only using the procedures described for the previous set of experiments. The beam tip displacement measurement point was 38 in. from the center of the first actuator and 28.13 in. from the center of the second actuator.

Two shape control experiments were then performed. Each experiment consisted of applying voltages predicted to produce the optimum approximation of a parabolic deformation profile along the beam's length from its initial undeformed shape. Voltages

for each experiment were calculated to produce curvature of the four actuators in the proportions listed in Table 19. Identical voltages were applied to actuators 2 through 4 since there was negligible difference between the curvatures required from these actuators. Corresponding input voltages for actuator 1 were determined for the first experiment by assuming a linear relationship between curvature and voltage as developed in Chapter II. Actuator 1 voltages for the second experiment were determined by solving Equation 5.3 for the curvature produced by each actuator 2-4 input voltage and then solving Equation 5.3 for the voltage to produce actuator 1 curvature equal to 91.4% of the actuator 2-4 curvature. Coefficients k_0 and k_1 for Equation 5.3 of 5.19×10^{-6} rad/m/V^2 and 6.26×10^{-4} rad/m/V, respectively, were obtained from a curve fit of beam tip displacement to actuator 1 input voltage as described in the following Experimental Results section.

Beam displacement was measured using the laser displacement sensor at locations of 18 in., 30 in. and 42.22 in. from the cantilevered end of the beam for each of the two experiments. It should be noted that the laser measurement axis was oriented perpendicular to the longitudinal axis of the *undeformed* beam. Increasing beam displacement therefore resulted in the displacement measurement points slightly further down the length of the beam than the nominal measurement locations. However, the small magnitude of the measured displacements relative to the length of the beam for these experiments made this effect insignificant.

Three sets of measurements were taken for each of the two experiments at each measurement point. Each measurement run consisted of recording sensor outputs at actuator inputs given for the input stages in Table 20 and Table 21 for the first and second experiment, respectively. Each actuator input was allowed to remain steady for 60 seconds to provide 60 sensor output data points for each actuator input to be averaged. The next input voltage stage was commanded immediately after each 60 second measurement and allowed two minutes to reach steady state before the next 60 second measurement was initiated. Data for each measurement run was saved to a MATLAB .MAT data file for processing and plotting. All measurements were taken with the actuators acting in compression. The actuators were cycled through the input voltages

corresponding to one measurement run prior to the recording of data to minimize the effects of hysteresis on the repeatability of the measurements.

Input Stage	Actuator 1 Input Voltage (V)	Actuator 2,3,4 Input Voltage (V)
1	0	0
2	45.7	50
3	91.4	100
4	137.2	150
5	0	0

Table 20. Linear Model Actuator Input Voltages for Shape Control Experiment 1

Input Stage	Actuator 1 Input Voltage (V)	Actuator 2,3,4 Input Voltage (V)
1	0	0
2	46.5	50
3	93.6	100
4	141.1	150
5	0	0

Table 21. Nonlinear Model Actuator Input Voltages for Shape Control Experiment 2

3. Experimental Results

Displacement and strain measurement data for beam deformation due to the first actuator is presented in Table 22 and plotted in Figure 50. Data for beam deformation due

to the second actuator is presented Table 23 and Figure 52. Positive strain values indicate compressive strain. All runs indicated in the tables and figures were conducted consecutively with less than five minutes between the completion of one run and the start of the next. The first run for each actuator was the first use of that actuator on the day of the experiment. Some hysteresis was observed on all measurement runs but most apparent on the first run for each actuator, with residual beam tip displacements of 16% and 24% of the displacement at maximum input voltage occurring on the first run for the first and second actuator, respectively. Repeatability of the displacement measurements for both actuators and strain measurements for the first actuator was good for runs 2 through 4, but the strain measurements for the second actuator were not as reliable. Strain measurements for runs 1 and 3 of the second actuator were substantially lower than corresponding measurements for other runs of the first and second actuator. The final zero input strain measurements for both of these runs indicated residual tensile rather than compressive strain, as denoted by the asterisks in Table 23. The combination of low measurement values and final tensile strain measurements suggest that either a shift in the strain gage conditioner zero strain output voltage occurred shortly after the start of each of these runs or the bond between the actuator 2 strain gage and the beam may have been poor, leading to inconsistent results.

The dashed lines in Figure 50 and Figure 52 represent the relationship between actuator input voltage and beam tip displacement predicted by the linear Euler-Bernoulli model, while the dotted lines represent second order least squares curve fits of the data from runs 2 through 4 for each actuator. Coefficients of Equation 5.2 for each of the curves are listed in Table 24 and the corresponding Equation 5.3 coefficients obtained are listed in Table 25. The k_0 and k_1 coefficients obtained for the two actuators agreed to within 6% and 2%, respectively.

It can be seen from the figures that the Euler-Bernoulli model again provides a reasonable approximation of the behavior of the beam as a function of input voltage, as was observed for the previous beams tested. However, unlike the previous experiments, the Euler-Bernoulli model overpredicted the tip displacement of the 1.625 in. wide beam

for actuator input voltages below about 75 volts and underpredicted the tip displacements at higher voltages. Comparison of the percentages of predicted displacement obtained for the 1.625 in. wide beam in Table 22 and Table 23 with the corresponding percentages of predicted displacement obtained for the 0.875 in. wide beam in Table 13 and Table 14 reveals that the percentage of predicted displacement obtained was always less for the wider beam. The reason for this is that the actuator produces curvature of the beam about both its transverse and *longitudinal* axes, a fact supported by the significant transverse strain measurements obtained. Curvature about the longitudinal axis increases the moment of inertia of the beam's cross-section, as shown in Figure 51, resulting in a greater resistance of the beam to bending about its transverse axis. The increase in moment of inertia is more significant for the wider beam than for the narrower beam.

The results of shape control experiment 1 are tabulated in Table 26 and plotted in Figure 52 and Figure 53. The "linear model predicted" column of Table 26 and the dashed lines on the figures represent the desired displacement of the beam along its length to approximate a parabolic shape predicted by the Euler-Bernoulli model of actuator curvature and Equations 4.10 through 4.14. The "nonlinear model predicted" column in the table and dotted lines on the figures represent the displacement of the beam predicted by Equations 4.10 through 4.14 with the curvature terms K_iV_i replaced by Equation 5.3 with the empirical coefficients k_0 and k_1 equal to those obtained from the experiment to characterize the first actuator given in Table 25. The measured displacements displayed excellent repeatability and can be seen to agree much more closely with the beam shape profile predicted using the nonlinear empirical model of actuator curvature than for the profile predicted by the linear model. As for the single actuator tests, the linear model overestimates the actuator performance for the low input voltages and underestimates actuator performance at higher voltages.

The results of shape control experiment 2 are presented in Table 27, Figure 54 and Figure 55. The "nonlinear model predicted" column in the table and dotted lines on the figures represent the desired displacement of the beam to approximate a parabolic shape determined using Equations 4.10 through 4.14 with the curvature terms K_iV_i replaced by

Equation 5.3, with the empirical coefficients k_0 and k_1 equal to those for the first actuator in Table 25. The "linear model predicted" column in the table and dashed lines on the figures represent the displacement of the beam predicted by the linear Euler-Bernoulli model of actuator curvature and Equations 4.10 through 4.14 for the specified input voltages. The measured displacements at the 18 in. and 30 in. measurement points displayed excellent repeatability, but the displacements at the 42.22 in. measurement point showed somewhat more variation. The latter measurements were the first series taken for this experiment and therefore the most affected by hysteresis. Residual displacements of about 6% of the displacement at maximum input voltage were observed for runs 1 and 2 at the 42.22 in. measurement point, but less than 2% residual displacement was observed on run 3 and for the measurements at the other measurement points. With the exception of runs 1 and 2 at the 42.22 in. measurement point, the measured displacements displayed much better agreement with the desired beam shape profile predicted using the nonlinear empirical model of actuator curvature than with the profile predicted by the linear model.

The results of the shape control experiments demonstrate the importance of considering the nonlinear behavior of the piezoceramic in determining the appropriate actuator inputs for precision shape control applications. The significant effects of hysteresis observed indicate that this effect must also be considered. Actual shape control applications should incorporate some form of feedback of the beam's shape to ensure that the desired deformation profile is attained.

Run	Predicted	1	2	3	4
Tip Displacement - mm (% of predicted)					
25 V	1.98	2.27 (115)	1.13 (57)	1.33 (67)	1.26 (64)
50 V	3.96	4.60 (116)	3.20 (81)	3.49 (88)	3.52 (89)
75 V	5.94	7.33 (123)	5.97 (100)	5.71 (96)	5.69 (96)
100 V	7.92	10.12 (128)	8.89 (112)	8.71 (110)	8.19 (103)
125 V	9.90	13.33 (135)	11.55 (117)	11.81 (119)	10.84 (110)
150 V	11.88	17.54 (148)	15.21 (128)	15.59 (131)	14.73 (124)
0 V	0.00	2.78	0.93	1.29	0.19
Longitudinal Strain - με (% of predicted)					
25 V	8.0	7.2 (90)	5.5 (69)	5.4 (68)	6.5 (82)
50 V	16.0	14.5 (91)	13.7 (85)	12.7 (80)	13.3 (83)
75 V	24.0	23.4 (97)	21.2 (88)	21.2 (89)	21.5 (90)
100 V	32.0	32.1 (100)	30.3 (95)	29.4 (92)	30.4 (95)
125 V	40.0	42.2 (106)	40.1 (100)	39.2 (98)	39.5 (99)
150 V	48.0	54.1 (113)	51.5 (106)	50.3 (105)	49.8 (104)
0 V	0.0	4.6	1.8	2.4	0.9
Transverse Strain -με					
25 V		8.2	8.2	8.0	8.1
50 V		17.6	17.1	17.0	16.3
75 V		27.5	26.8	26.8	26.5
100 V		38.8	37.5	37.3	36.6
125 V		51.6	49.7	49.8	48.7
150 V		67.0	63.7	63.4	60.8
0 V		5.7	3.4	3.2	-0.6

Table 22. Beam Tip Displacement and Strain Measurements for First Actuator Acting in Compression

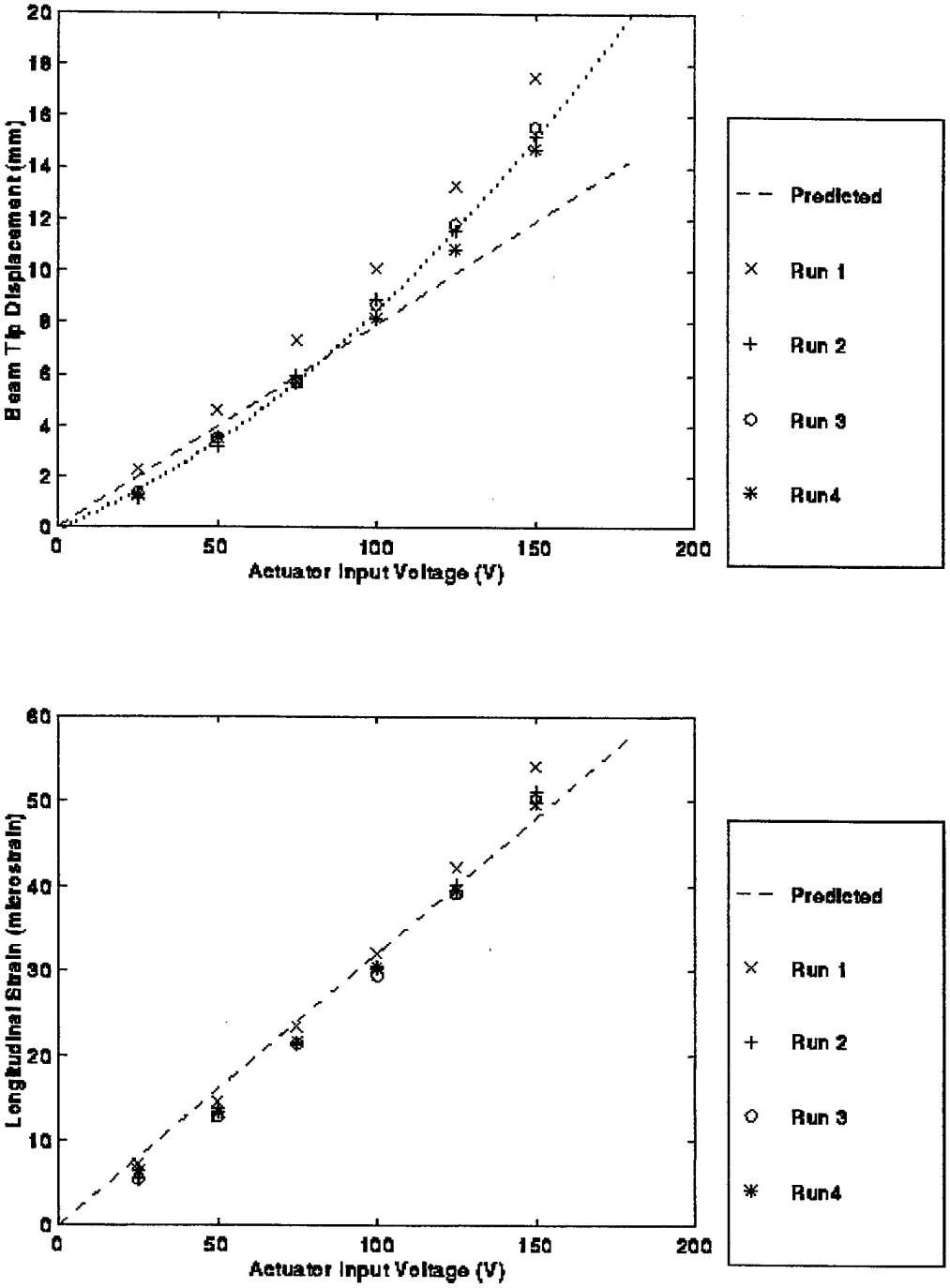

Figure 49. Beam Tip Displacement and Longitudinal Strain Measurements for First Actuator Acting in Compression

Run	Predicted	1	2	3	4
Tip Displacement - mm (% of predicted)					
25 V	1.47	1.29 (88)	1.31 (89)	1.12 (76)	1.27 (86)
50 V	2.93	3.06 (104)	2.71 (93)	2.67 (91)	2.76 (94)
75 V	4.40	5.45 (124)	4.54 (103)	4.38 (100)	4.45 (101)
100 V	5.86	8.08 (138)	6.44 (110)	6.41 (109)	6.22 (106)
125 V	7.33	11.22 (153)	8.88 (121)	8.47 (116)	8.81 (120)
150 V	8.79	15.05 (171)	11.81 (134)	11.40 (130)	11.62 (132)
0 V	0.00	3.57	0.81	0.31	0.85
Longitudinal Strain - με (% of predicted)					
25 V	8.0	3.3 (41)	5.7 (72)	4.9 (62)	5.9 (74)
50 V	16.0	7.9 (49)	11.8 (74)	10.3 (64)	12.2 (76)
75 V	24.0	16.6 (69)	18.9 (79)	16.5 (69)	19.6 (82)
100 V	32.0	25.6 (80)	27.2 (85)	23.6 (74)	27.0 (84)
125 V	40.0	34.1 (85)	36.9 (92)	31.2 (78)	36.4 (91)
150 V	48.0	44.7 (93)	47.3 (99)	40.2 (84)	45.6 (95)
0 V	0.0	-3.6*	0.8	-5.5*	0.8

Table 23. Beam Tip Displacement and Strain Measurements for Second Actuator Acting in Compression

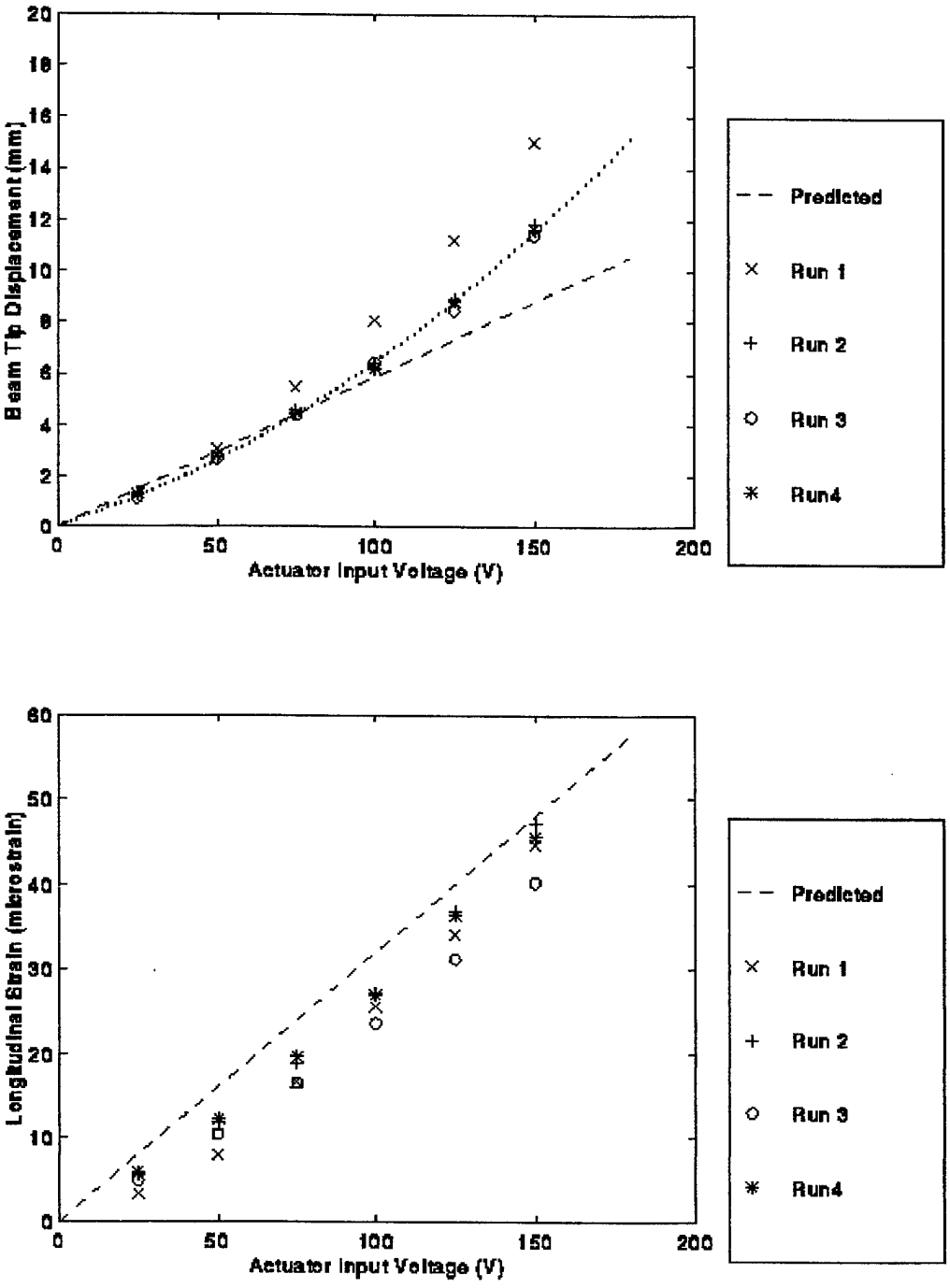

Figure 50. Beam Tip Displacement and Longitudinal Strain Measurements for Second Actuator Acting in Compression

Actuator	Predicted c_1 (10^{-2} mm/V)	c_0 (10^{-4} mm/V^2)	c_1 (10^{-2} mm/V)	c_2 (mm)
First	7.92	3.18	5.38	-0.10
Second	5.86	2.48	3.91	0.06

Table 24. Coefficients of Curve Fits for Observed Beam Tip Displacement as a Function of Actuator Input Voltage

Actuator	Predicted $k_1 = K_1$ (10^{-4} rad/m/V)	k_0 (10^{-6} rad/m/V^2)	k_1 (10^{-2} rad/m/V)
First	6.46	2.59	4.39
Second	6.46	2.74	4.31

Table 25. Coefficients of Curve Fits for Observed Actuator Curvature as a Function of Actuator Input Voltage

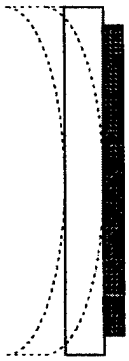

Figure 51. Graphic Depiction of Deformation of Beam Cross-Section due to Piezoceramic Actuator Acting in Compression

Beam Displacement at Measurement Locations - mm	Linear Model Predicted	Nonlinear Model Predicted	Run 1	Run 2	Run 3
45.7/50/50/50 Volts Input					
x = 18.0 in	1.73	1.50	1.47	1.25	1.32
x = 30.0 in	4.76	4.14	3.97	3.91	4.00
x = 42.2 in	9.33	8.16	8.45	8.20	8.12
91.4/100/100/100 Volts Input					
x = 18.0 in	3.46	3.65	3.57	3.40	3.42
x = 30.0 in	9.51	10.11	9.86	9.88	9.91
x = 42.2 in	18.67	19.94	20.63	20.21	20.36
137.2/150/150/150 Volts Input					
x = 18.0 in	5.19	6.45	6.03	5.88	5.86
x = 30.0 in	14.27	17.91	17.20	17.07	17.07
x = 42.2 in	28.02	35.35	35.18	34.73	34.82

Table 26. Beam Displacement Measurements for Shape Control Experiment 1 (Linear Model Voltages)

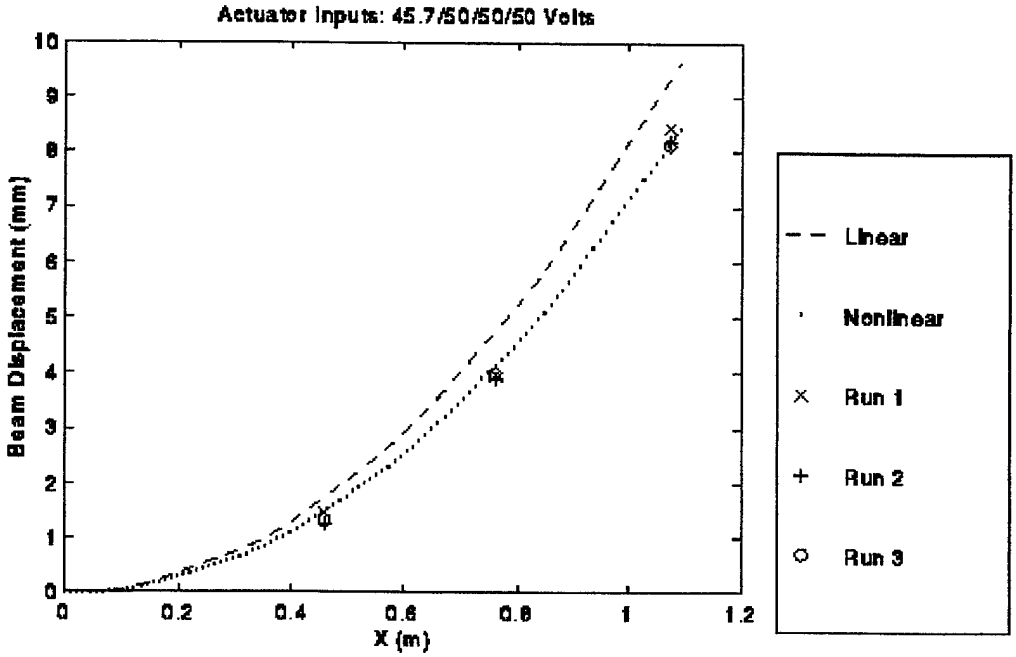

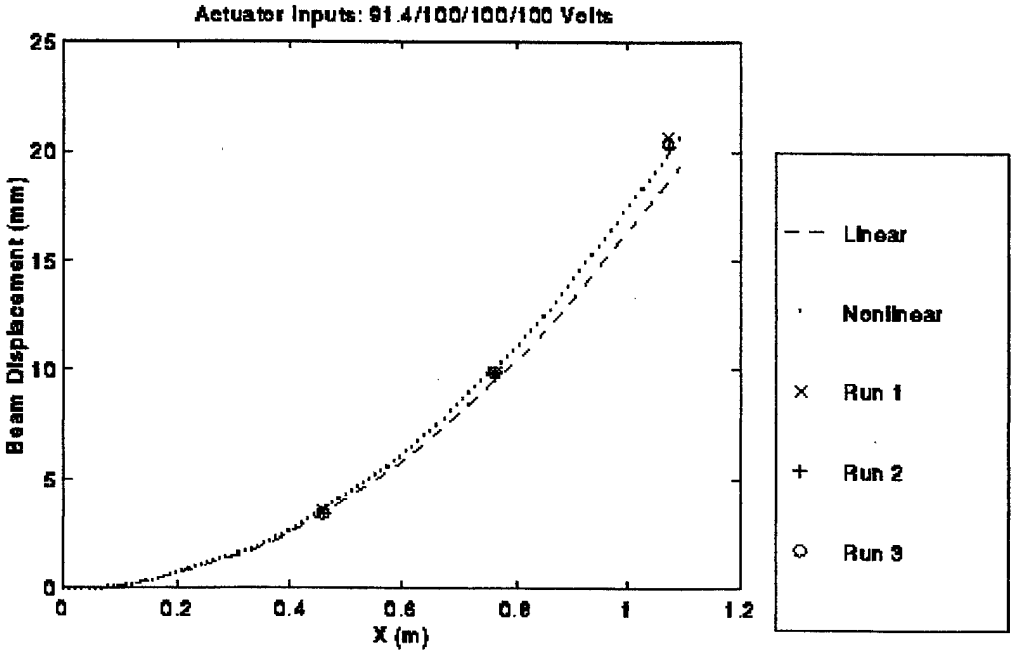

Figure 52. Beam Displacement Measurements for Shape Control Experiment 1 (Linear Model Voltages) (1,2 of 3)

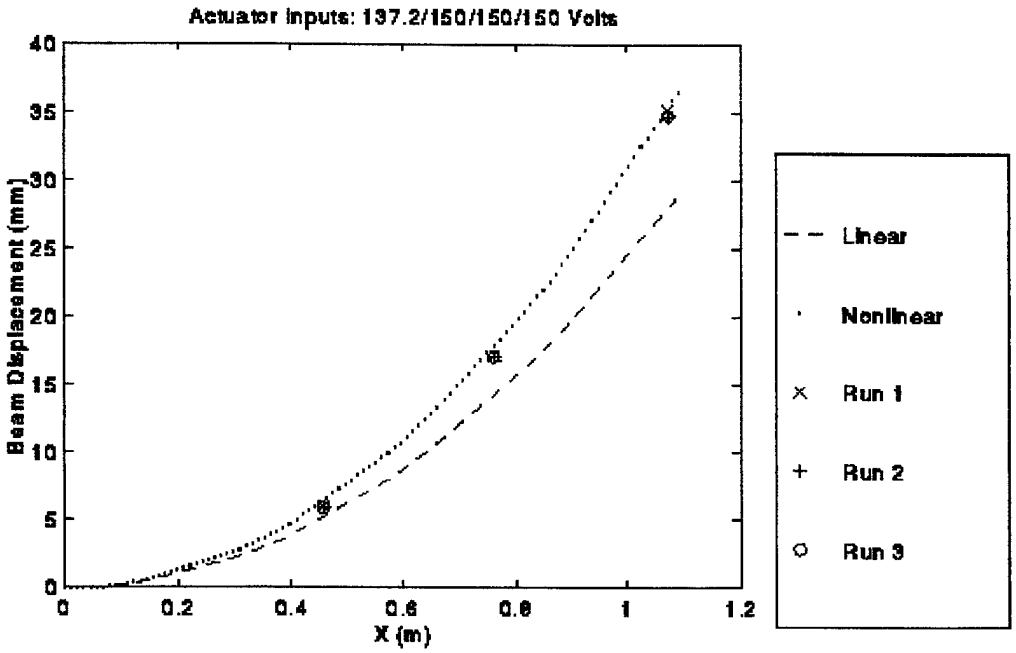

Figure 53. Beam Displacement Measurements for Shape Control Experiment 1 (Linear Model Voltages) (3 of 3)

Beam Displacement at Measurement Locations - mm	Linear Model Predicted	Nonlinear Model Predicted	Run 1	Run 2	Run 3
46.5/50/50/50 Volts Input					
x = 18.0 in	1.75	1.52	1.37	1.25	1.30
x = 30.0 in	4.80	4.19	4.10	3.85	3.87
x = 42.2 in	9.40	8.22	8.99	9.46	8.26
93.6/100/100/100 Volts Input					
x = 18.0 in	3.52	3.74	3.60	3.48	3.49
x = 30.0 in	9.63	10.28	10.10	9.85	9.66
x = 42.2 in	18.85	20.18	22.18	22.04	20.27
141.1/150/150/150 Volts Input					
x = 18.0 in	5.30	6.65	6.23	6.16	6.17
x = 30.0 in	14.48	18.29	17.76	17.54	17.08
x = 42.2 in	28.33	35.91	37.98	37.54	35.45

Table 27. Beam Displacement Measurements for Shape Control Experiement 2 (Nonlinear Model Voltages)

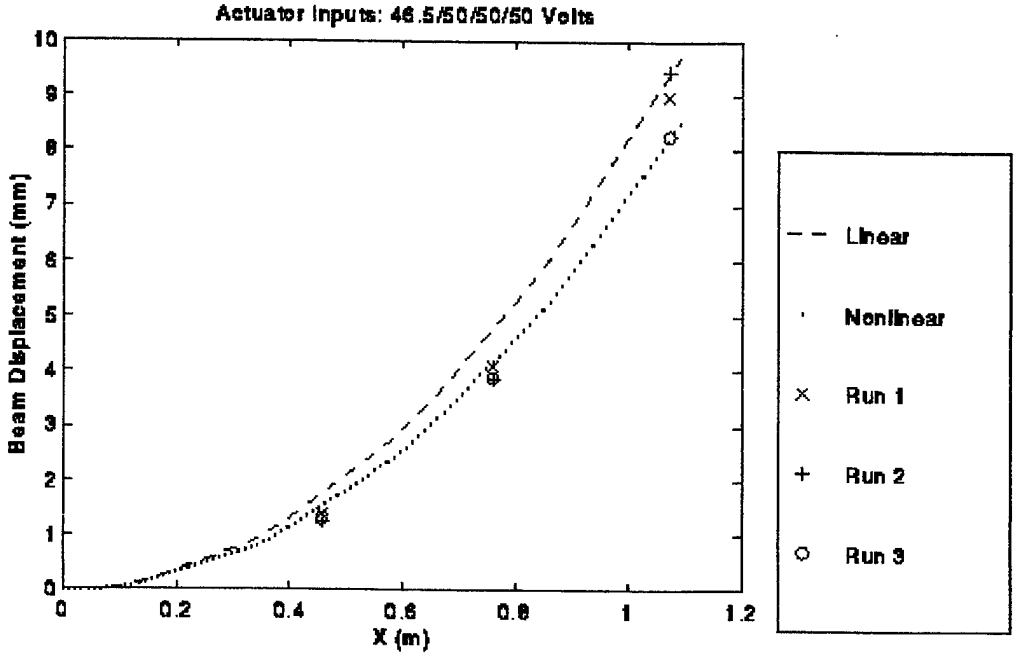

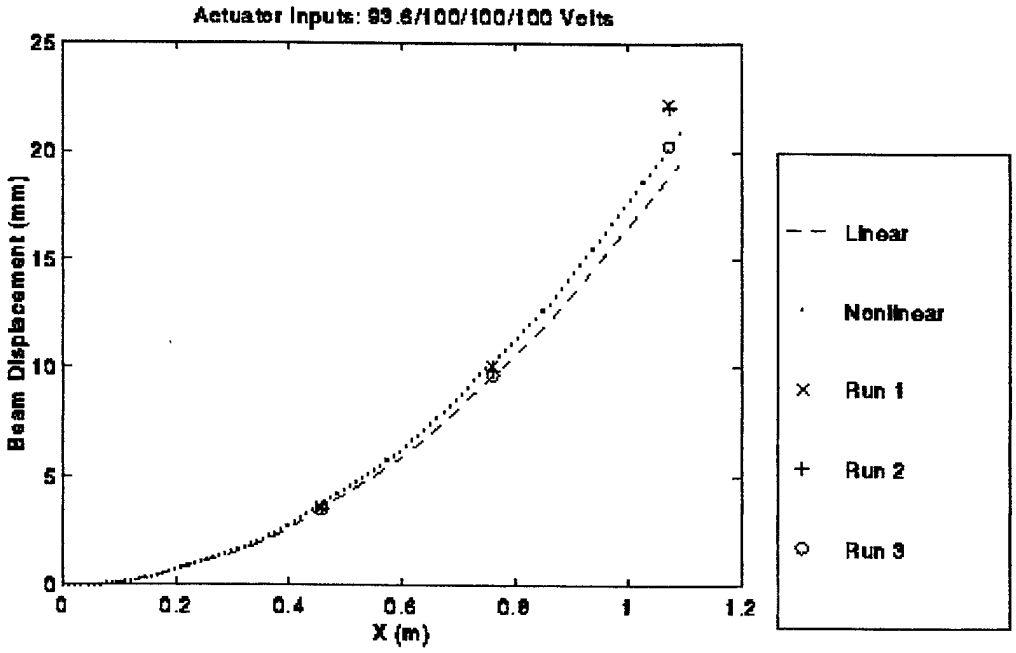

Figure 54. Beam Displacement Measurements for Shape Control Experiment 2 (Nonlinear Model Voltages) (1,2 of 3)

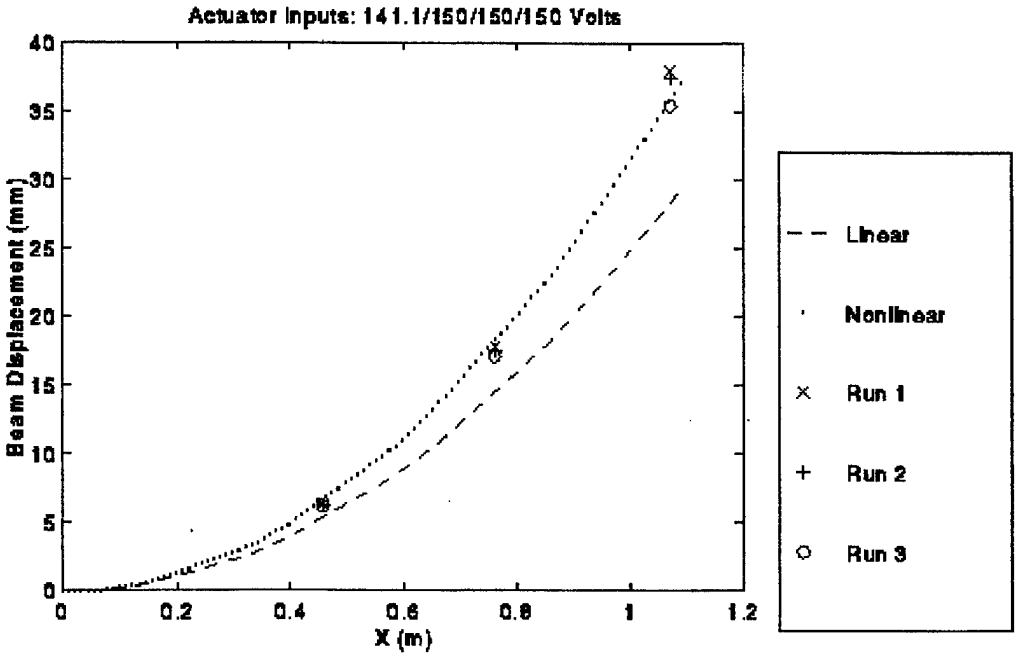

Figure 55. Beam Displacement Measurements for Shape Control Experiment 2 (Nonlinear Model Voltages) (3 of 3)

VI. CONCLUSIONS

Piezoceramic actuators have been shown to provide an effective means of controlling the shape of a thin flexible beamlike structure. Experimental analysis has demonstrated that the Euler-Bernoulli model provides a good measure of the relative effectiveness of various actuator configurations and a reasonable model of actuator performance at low input voltage. However, the true nonlinear behavior of piezoceramic actuators and the effects of hysteresis and transverse stresses not accounted for by the Euler-Bernoulli model have been shown to have significant ramifications for the use of piezoceramics in shape control. Hysteresis resulted in residual beam deformation in excess of 20% of full deformation after the removal of the initial actuator input voltage for the Navy Type II piezoceramics tested, but following displacement measurements were found to be highly repeatable. Nonlinear voltage-strain behavior of the piezoceramic produced significantly higher displacements than predicted by the Euler-Bernoulli model at higher actuator input voltages. Transverse stresses were found to result in reduced effectiveness for a given thickness of actuator on wider beams due to the resulting increase in the moment of inertia of the beam cross-section. All of these effects result in variation of the relationship between actuator curvature and input voltage from the linear behavior predicted by the Euler-Bernoulli model. Precision shape control applications must therefore consider these effects and should employ a control system incorporating some form of strain and/or position feedback to ensure the desired deformation of the beam is achieved.

The amount of beam deformation available from a piezoceramic actuator has been shown to depend on the dimensions and material properties of the structure and piezoceramic. High piezoceramic elastic modulus, piezoelectric coefficient and operating voltage are all desired actuator properties. The optimum total actuator thickness for a given beam/actuator configuration has been shown to be equal to a fixed percentage of the beam thickness, while the total beam curvature attainable for the optimum beam/actuator thickness ratio has been shown to be inversely related to the thickness of the beam.

The location of actuators on a beam structure is crucial to determining how closely a desired deformation profile can be approximated. Simultaneous optimization of the locations and input voltages of a fixed set of actuators to achieve a desired beam deformation profile proved to be unreliable due to the differences in the order of the actuator location and voltage terms in the optimization cost function. Using embedded Nelder and Mead simplex algorithms to separately optimize actuator locations and input voltages was found to produce much more reliable results, converging to the same optimum solution for a variety of initial conditions. Optimization of locations for different numbers of actuators making up a fixed total actuator length has shown that dividing a given actuator length into multiple small actuators allows a desired beam shape to be approximated more closely than can be achieved with a lesser number of longer actuators.

Certain sets of initial conditions were found to cause the optimization algorithm to fail to converge or converge to an erroneous result. The algorithm was also found to be susceptible to converging to a local minimum of the cost function, when one existed and initial conditions near the local minimum were selected. Consideration must therefore be given to the presence of inflection points in the desired shape function, which can result in local minima of the cost function, when selecting initial actuator locations for the optimization algorithm. Knowledge of the approximate values of the optimum actuator locations should be used in selecting initial conditions whenever possible. Multiple runs of the optimization program should be performed using different sets of initial conditions to ensure that the globally optimum actuator locations are attained.

Recommendations for further research include improving the mathematical model of the beam to consider transverse effects, incorporating constraints and techniques to avoid local minima in the optimization algorithm and exploring the use of feedback to control the shape of the beam. A plate theory model can be used to consider the effects of the curvature about the beam's longitudinal axis caused by the actuator acting in both the longitudinal and transverse directions for beam's with high width-to-thickness ratios. Modifying the optimization algorithm to include constraints would allow for the possibility of desired shape functions which can be most closely approximated by placing actuators

end to end or by actuators providing the maximum possible curvature. Techniques such as genetic algorithms or simulated annealing could also be included in the optimization algorithm to improve the probability of attaining the global minimum rather than a local minimum of the cost function. Multiple strain and/or displacement sensors could be utilized to provide feedback of the beam's shape to control inputs to the piezoceramic actuators. Sensors such as the laser displacement sensor used in the experiments conducted for this thesis and state-of-the-art fiber optic strain sensors are strong candidates for this application.

APPENDIX

```
% PROGRAM TO COMPARE PERFORMANCE OF PIEZOCERAMIC ACTUATOR
% CONFIGURATIONS
%
% This program calculates and plots the following data:
%   1) Beam curvature per unit voltage
%   2) Beam curvature at 20 Volts/mil of piezo thickness
%   3) Beam surface strain per unit voltage (Side of beam
%      opposite actuator for unsymmetric configurations)
%   4) Neutral axis distance from center of beam
% versus actuator thickness or actuator width for piezoceramic
% actuators bonded to a cantilever beam, given input properties
% of the beam, actuators and the bond between the actuator and
% the beam.
%
% The following actuator configurations are evaluated:
%   1) A single actuator bonded to one side of the beam
%   2) A single actuator bonded to each side of the beam
%   3) A dual (stacked) actuator bonded to one side of the beam
%   4) A dual (stacked) actuator bonded to each side of the beam

% Set number of points for plots
Numpts = 100;

% Set properties of beam
% Material name
 Beammatl = '7075-T6 Aluminum';
% Width (m)
 w = 0.0381;   % 1.5 inches
% Thickness
 t = 0.001575;
% Elastic modulus (N/m^2)
 E = 7.2e10;

% Set properties of PZT actuator
% Material name
 Piezonam = 'DOD Type II PZT';
% Constant width (m) for plots vs. actuator thickness
 wp = 0.0381;   % 1.5 inches
% Width range (m) for plots vs. actuator width
 wprange = linspace(0.1,1.0,Numpts)*w;
% Constant thickness (m) for plots vs. actuator width
 tp = 0.00026;
```

```
% Thickness range (m) for plots vs. actuator thickness
  tprange = linspace(0.0001,0.002,Numpts);
% Elastic modulus (N/m^2)
  Ep = 6.1e10;
% Piezoelectric coefficient (m/V)
  d31 = 1.71e-10;  % DOD Type II PZT

% Set properties of bond
% Width (m)
  wb = wp;
% Thickness (m)
  tb = 0;
% Elastic modulus (N/m^2)
  Eb = 1.78e9;

% Set electric field limitation of piezoceramic (volts/mil)
Volt_mil = 20;                  % Volts/mil

% Calculate electric field limitation of piezoceramic (volts/m)
V_tlimit = Volt_mil/0.0000254;   % Volts/m = Volts/mil/(0.0000254m/mil)

% Allow plots to be generated vs actuator width or thickness
Plottype = input('Generate plots vs actuator thickness (t) or width (w)?  ','s');

% Allow actuator thickness to be plotted as % of beam thickness
% or actual thickness for plots vs actuator thickness
if Plottype ~= 'w'
  Axistype = input('Plot actuator thickness as % of beam thickness (p) or actual thickness
(a)?  ','s');
end

% Create actuator width or thickness range in accordance
% with plot type
if Plottype == 'w'
  w = w*ones(1,Numpts);
  wp = wprange;
  wb = wp;
else
  t = t*ones(1,Numpts);
  tb = tb*ones(1,Numpts);
  tp = tprange;
end

% Calculate parameters for Crawley/Anderson formulation
```

```
% Single Actuator
EA1 = E*w.*t + Eb*wb.*tb + Ep*wp.*tp;
ES1 = Eb*wb.*tb.*(t/2+tb/2) + Ep*wp.*tp.*(t/2+tb+tp/2);
EI1 = E*w.*t.^3/12 + Eb*wb.*tb.*((t/2).^2 + (t/2).*tb + tb.^2/3) + ...
    Ep*wp*tp.*((t/2+tb).^2 + (t/2+tb).*tp + tp.^2/3);
P1 = Ep*d31*wp;
M1 = Ep*d31*wp.*(t/2 + tb + tp/2);
Eps0_1 = (P1.*EI1-M1.*ES1)./(EA1.*EI1-ES1.^2);
K_V1 = M1./EI1 - ES1./EI1.*(P1.*EI1 - M1.*ES1)./(EA1.*EI1 - ES1.^2);
y0_1 = Eps0_1./K_V1;

% Symmetric Pair of Actuators
EA2 = E*w.*t + 2*Eb*wb.*tb + 2*Ep*wp.*tp;
EI2 = E*w.*t.^3/12 + 2*Eb*wb.*tb.*((t/2).^2 + (t/2).*tb + tb.^2/3) + ...
    2*Ep*wp.*tp.*((t/2+tb).^2 + (t/2+tb).*tp + tp.^2/3);
M2 = 2*Ep*d31*wp.*(t/2 + tb + tp/2);
K_V2 = M2./EI2;

% Stacked Pair of Actuators
EA12 = E*w.*t + 2*Eb*wb.*tb + 2*Ep*wp.*tp;
ES12 = Eb*wb.*tb.*(t+2*tb + tp) + Ep*wp.*tp.*(t+3*tb+2*tp);
EI12 = E*w.*t.^3/12 + Eb*wb.*tb.*((t/2).^2 + (t/2+tb+tp).^2 + ...
    (t+5/3*tb+tp).*tb) + Ep*wp.*tp.*((t/2+tb).^2 + ...
    (t/2+2*tb+tp).^2 + (t+3*tb+5/3*tp).*tp);
P12 = 2*Ep*d31*wp;
M12 = Ep*d31*wp.*(t/2 + tb + tp/2 + t/2 + 2*tb + 3/2*tp);
Eps0_12 = (P12.*EI12-M12.*ES12)./(EA12.*EI12-ES12.^2);
K_V12 = M12./EI12 - ES12./EI12.*(P12.*EI12 - M12.*ES12)./ ...
     (EA12.*EI12 - ES12.^2);
y0_12 = Eps0_12./K_V12;

% Symmetric Pair of Stacked Actuators
EA22 = E*w.*t + 4*Eb*wb.*tb + 4*Ep*wp.*tp;
EI22 = E*w.*t.^3/12 + 2*Eb*wb.*tb.*((t/2).^2 + (t/2+tb+tp).^2 + ...
    (t+5/3*tb+tp).*tb) + 2*Ep*wp.*tp.*((t/2+tb).^2 + ...
    (t/2+2*tb+tp).^2 + (t+3*tb+5/3*tp).*tp);
M22 = 2*Ep*d31*wp.*(t/2 + tb + tp/2 + t/2 + 2*tb + 3/2*tp);
K_V22 = M22./EI22;

% Calculate strain per unit actuator input voltage at beam surface
% for each actuator configuration
StrainV1 = Eps0_1+K_V1.*t/2;     % Single Actuator
StrainV2 = K_V2.*t/2;            % Symmetric Pair of Actuators
StrainV12 = Eps0_12+K_V12.*t/2;  % Stacked Pair of Actuators
```

```
StrainV22 = K_V22.*t/2;          % Symmetric Pair of Stacked Actuators

% Plot results
figure
if Plottype == 'w'
  plot(wp./w*100,K_V1,'b--',wp./w*100,K_V12,'m-.',wp./w*100,K_V2,'r-', ...
      wp./w*100,K_V22,'g.')
  text(0.15,0.6,[num2str(tp*1000) ' mm Thick Actuator/' num2str(tb(1)*1000) ...
      ' mm Bond Thickness'],'Units','Normalized')
  xlabel('Actuator Width (%)')
elseif Axistype == 'p'
  plot(tp./t*100,K_V1,'b--',tp./t*100,K_V12,'m-.',tp./t*100,K_V2,'r-', ...
      tp./t*100,K_V22,'g.')
  text(0.15,0.6,[num2str(wp/w*100) '% Width Actuator/' num2str(tb(1)*1000) ...
      ' mm Bond Thickness'],'Units','Normalized')
  xlabel('Actuator Thickness (% of Beam Thickness)')
else
  plot(tp*1000,K_V1,'b--',tp*1000,K_V12,'m-.',tp*1000,K_V2,'r-', ...
      tp*1000,K_V22,'g.')
  text(0.15,0.6,[num2str(wp/w*100) '% Width Actuator/' num2str(tb(1)*1000) ...
      ' mm Bond Thickness'],'Units','Normalized')
  xlabel('Actuator Thickness (mm)')
end
ylabel('(rad/m/V)')
title('Beam Curvature per Unit Voltage')
legend('Single','1 Stacked','Sym. Pair','Sym. Stacked',-1)
text(0.15,0.9,Piezonam,'Units','Normalized')
text(0.15,0.8,['Ep = ' num2str(Ep) ' N/m^2   d31 = ' num2str(d31) ' m/V'], ...
    'Units','Normalized')
text(0.15,0.7,[num2str(t(1)*1000) ' mm Thick ' Beammatl ' Beam'],'Units', ...
    'Normalized')
grid

figure
if Plottype == 'w'
  plot(wp./w*100,V_tlimit*tp.*K_V1,'b--',wp./w*100,V_tlimit*tp.*K_V12,'m-.', ...
      wp./w*100,V_tlimit*tp.*K_V2,'r-',wp./w*100,V_tlimit*tp.*K_V22,'g.')
  text(0.15,0.6,[num2str(tp*1000) ' mm Thick Actuator/' num2str(tb(1)*1000) ...
      ' mm Bond Thickness'],'Units','Normalized')
  xlabel('Actuator Width (%)')
elseif Axistype == 'p'
  plot(tp./t*100,V_tlimit*tp.*K_V1,'b--',tp./t*100,V_tlimit*tp.*K_V12,'m-.', ...
      tp./t*100,V_tlimit*tp.*K_V2,'r-',tp./t*100,V_tlimit*tp.*K_V22,'g.')
  text(0.15,0.6,[num2str(wp/w*100) '% Width Actuator/' num2str(tb(1)*1000) ...
```

```
    ' mm Bond Thickness'],'Units','Normalized')
  xlabel('Actuator Thickness (% of Beam Thickness)')
else
  plot(tp*1000,V_tlimit*tp.*K_V1,'b--',tp*1000,V_tlimit*tp.*K_V12,'m-.', ...
     tp*1000,V_tlimit*tp.*K_V2,'r-',tp*1000,V_tlimit*tp.*K_V22,'g.')
  text(0.15,0.6,[num2str(wp/w*100) '% Width Actuator/' num2str(tb(1)*1000) ...
     ' mm Bond Thickness'],'Units','Normalized')
  xlabel('Actuator Thickness (mm)')
end
ylabel('Curvature (rad/m)')
title(['Beam Curvature at ' num2str(Volt_mil) ' Volts/mil'])
legend('Single','1 Stacked','Sym. Pair','Sym. Stacked',-1)
text(0.15,0.9,Piezonam,'Units','Normalized')
text(0.15,0.8,['Ep = ' num2str(Ep) ' N/m^2   d31 = ' num2str(d31) ' m/V'], ...
    'Units','Normalized')
text(0.15,0.7,[num2str(t(1)*1000) ' mm Thick ' Beammatl ' Beam'],'Units', ...
    'Normalized')
grid

figure
if Plottype == 'w'
  plot(wp./w*100,StrainV1*1e6,'b--',wp./w*100,StrainV12*1e6,'m-.', ...
     wp./w*100,StrainV2*1e6,'r-',wp./w*100,StrainV22*1e6,'g.')
  text(0.15,0.6,[num2str(tp*1000) ' mm Thick Actuator/' num2str(tb(1)*1000) ...
     ' mm Bond Thickness'],'Units','Normalized')
  xlabel('Actuator Width (%)')
elseif Axistype == 'p'
  plot(tp./t*100,StrainV1*1e6,'b--',tp./t*100,StrainV12*1e6,'m-.', ...
     tp./t*100,StrainV2*1e6,'r-',tp./t*100,StrainV22*1e6,'g.')
  text(0.15,0.6,[num2str(wp/w*100) '% Width Actuator/' num2str(tb(1)*1000) ...
     ' mm Bond Thickness'],'Units','Normalized')
  xlabel('Actuator Thickness (% of Beam Thickness)')
else
  plot(tp*1000,StrainV1*1e6,'b--',tp*1000,StrainV12*1e6,'m-.', ...
     tp*1000,StrainV2*1e6,'r-',tp*1000,StrainV22*1e6,'g.')
  text(0.15,0.6,[num2str(wp/w*100) '% Width Actuator/' num2str(tb(1)*1000) ...
     ' mm Bond Thickness'],'Units','Normalized')
  xlabel('Actuator Thickness (mm)')
end
ylabel('Strain/Voltage (microstrain/V)')
title('Surface Axial Strain per Unit Actuator Voltage')
legend('Single','1 Stacked','Sym. Pair','Sym. Stacked',-1)
text(0.15,0.9,Piezonam,'Units','Normalized')
text(0.15,0.8,['Ep = ' num2str(Ep) ' N/m^2   d31 = ' num2str(d31) ' m/V'], ...
```

```
    'Units','Normalized')
text(0.15,0.7,[num2str(t(1)*1000) ' mm Thick ' Beammatl ' Beam'],'Units', ...
    'Normalized')
grid

figure
if Plottype == 'w'
  plot(wp./w*100,y0_1*1000,'b--',wp./w*100,y0_12*1000,'m-.')
  text(0.15,0.6,[num2str(tp*1000) ' mm Thick Actuator/' num2str(tb(1)*1000) ...
      ' mm Bond Thickness'],'Units','Normalized')
  xlabel('Actuator Width (%)')
  ylabel('y0 (mm)')
elseif Axistype == 'p'
  plot(tp./t*100,y0_1./t*100,'b--',tp./t*100,y0_12./t*100,'m-.')
  text(0.15,0.6,[num2str(wp/w*100) '% Width Actuator/' num2str(tb(1)*1000) ...
      ' mm Bond Thickness'],'Units','Normalized')
  xlabel('Actuator Thickness (% of Beam Thickness)')
  ylabel('y0 (% of Beam Thickness)')
else
  plot(tp*1000,y0_1*1000,'b--',tp*1000,y0_12*1000,'m-.')
  text(0.15,0.6,[num2str(wp/w*100) '% Width Actuator/' num2str(tb(1)*1000) ...
      ' mm Bond Thickness'],'Units','Normalized')
  xlabel('Actuator Thickness (mm)')
  ylabel('y0 (mm)')
end
title('Neutral Axis Distance from Center of Beam')
legend('Single','1 Stacked',-1)
text(0.15,0.9,Piezonam,'Units','Normalized')
text(0.15,0.8,['Ep = ' num2str(Ep) ' N/m^2   d31 = ' num2str(d31) ' m/V'], ...
    'Units','Normalized')
text(0.15,0.7,[num2str(t(1)*1000) ' mm Thick ' Beammatl ' Beam'],'Units', ...
    'Normalized')
grid
```

```
% PROGRAM TO DETERMINE OPTIMUM ACTUATOR LOCATIONS
%
% This program determines the optimum actuator locations and input
% voltages to achieve the minimum error between the actuator deformed
% beam shape and a desired beam shape function for a cantilever
% beam with piezoceramic actuators of specified length, width, thickness
% and material properties bonded to both sides of the beam.

% Set desired shape function and coefficients
Shapfunc = 1  % y = C*x^2
% Shapfunc = 2  % y = C*(1-cos(mx))
C = 0.001;
% C = 0.0005;
m = pi;

% Set beam properties
L = 1;              % Beam length (m)
w = 0.0508;         % Beam width (m)
% t = 0.001575;       % Beam thickness (m)
t = 0.001575/2      % Beam thickness (m)
E = 7.2e10;         % Beam modulus of elasticity (N/m^2)

% Set piezoceramic actuator properties
% Navy Type II PZT
n = 4               % Number of actuators
la = 0.1*ones(n,1);   % Actuator lengths (m)
wp = 0.0381;        % Piezoceramic actuator width (m)
tp = 0.00027;       % Piezoceramic actuator thickness (m)
Ep = 6.1e10;        % Piezoceramic actuator modulus of elasticity (N/m^2)
d31 = 1.71e-10;     % Piezoelectric constant (m/V)
Vmax = 150;         % Maximum actuator input voltage (V)
Vmin = -150;        % Minimum actuator input voltage (V)

% Enter properties of bond between piezoceramic actuator and beam
wb = wp;            % Bond width (m)  (equal to actuator width)
tb = 0;             % Bond thickness (m)
Eb = 1.78e9;        % Bond modulus of elasticity (N/m^2)

% Calculate properties of beam cross-section
area = w.*t;        % Beam cross-sectional area (m^2)
areab = wb*tb;      % Bond cross-sectional area (m^2)
areap = wp*tp;      % Piezoceramic actuator cross-sectional area (m^2)
moi = w.*t.^3/12;   % Beam cross-section moment of inertia (m^4)
% Bond cross-section moment of inertia (m^4)
```

```
moib = wb*tb*(t^2/2 + t*tb + 2*tb^2/3);
% Piezoceramic actuator cross-section moment of inertia (m^4)
moip = wp*tp*((t+2*tb)^2/2 + (t+2*tb)*tp + 2*tp^2/3);
EI = E*moi+Eb*moib+Ep*moip; % Beam stiffness
K = Ep*d31*wp*(t+2*tb+tp)/EI;  % (Moment per unit voltage)/(Beam stiffness)
K = K*ones(n,1);

% Set options for unconstrained voltage optimization algorithm
Options = foptions';
Options(14) = 2000;    % Maximum number of iterations (0 -> 100*n)

% Set initial actuator locations for optimization algorithm
x0 = [0.05 0.25 0.5 0.75]'   % 4 Actuators

% Determine optimum voltage for initial actuator positions
if Shapfunc == 1
 V0 = fmins('beamerVu',zeros(n,1),Options,[],x0,la,K,C,L,n)
 % V0 = zeros(n,1)
else
 V0 = fmins('bercosVu',zeros(n,1),Options,[],x0,la,K,C,m,L,n)
end

% Calculate error cost function for initial actuator positions
if Shapfunc == 1
 J0 = beamerVu(V0,x0,la,K,C,L,n)
else
 J0 = bercosVu(V0,x0,la,K,C,m,L,n)
end

% Determine optimum actuator locations
if Shapfunc == 1
 flops(0)  % Reset floating point operations counter
 Optx = fmins('beamerxu',x0,Options,[],V0,la,K,C,L,n,Options)
 Ops = flops  % Output number of floating point operations
else
 flops(0)  % Reset floating point operations counter
 % Unconstrained locations
 Optx = fmins('bercosxu',x0,Options,[],V0,la,K,C,m,L,n,Options)
 Ops = flops  % Output number of floating point operations
end

% Determine optimum input voltages for optimum actuator locations
if Shapfunc == 1
 OptV = fmins('beamerVu',V0,Options,[],Optx,la,K,C,L,n)
```

```
else
 OptV = fmins('bercosVu',V0,Options,[],Optx,la,K,C,m,L,n)
end

% Calculate error cost function for optimum actuator locations
if Shapfunc == 1
 J = beamerVu(OptV,Optx,la,K,C,L,n)
else
 J = bercosVu(OptV,Optx,la,K,C,m,L,n)
end

% Plot results
% Set plot x range along beam length
x = linspace(0,L,100);
% Calculate beam displacement for optimum actuator locations and voltages
y = beamdisp(x,Optx,OptV,la,n,K);
% Calculate beam displacement at actuator actuator endpoints
yact = beamdisp([Optx;Optx+la],Optx,OptV,la,n,K);
% Calculate desired beam displacement along beam length
if Shapfunc == 1
 yf = C*x.^2;
else
 yf = C*(ones(size(x))-cos(m*x));
end
figure
plot(x,y,'r-',x,yf,'g.',[Optx;Optx+la],yact,'r*')
legend('Actual','Desired',-1)
grid
title('Actual vs. Desired Beam Shapes')
xlabel('X (m)')
ylabel('Beam Displacement Y (m)')
if n == 1
 text(0.1,0.9,['Optimum Values for 1 Actuator'],'Units','Normalized')
else
 text(0.1,0.9,['Optimum Values for ' int2str(n) ' Actuators'],'Units', ...
    'Normalized')
end
if n == 1
 text(0.1,0.8,['x1 = ' num2str(Optx(1)) ' m  / V1 = ' num2str(OptV(1)) ...
    ' V'],'Units','Normalized')
 text(0.1,0.7,['Error = ' num2str(J)],'Units','Normalized')
elseif n == 2
 text(0.1,0.8,['x1 = ' num2str(Optx(1)) ' m  / V1 = ' num2str(OptV(1)) ...
    ' V'],'Units','Normalized')
```

```
  text(0.1,0.7,['x2 = ' num2str(Optx(2)) ' m  / V2 = ' num2str(OptV(2)) ...
     ' V'],'Units','Normalized')
  text(0.1,0.6,['Error = ' num2str(J)],'Units','Normalized')
elseif n == 3
  text(0.1,0.8,['x1 = ' num2str(Optx(1)) ' m  / V1 = ' num2str(OptV(1)) ...
     ' V'],'Units','Normalized')
  text(0.1,0.7,['x2 = ' num2str(Optx(2)) ' m  / V2 = ' num2str(OptV(2)) ...
     ' V'],'Units','Normalized')
  text(0.1,0.6,['x3 = ' num2str(Optx(3)) ' m  / V3 = ' num2str(OptV(3)) ...
     ' V'],'Units','Normalized')
  text(0.1,0.5,['Error = ' num2str(J)],'Units','Normalized')
elseif n == 4
  text(0.1,0.8,['x1 = ' num2str(Optx(1)) ' m  / V1 = ' num2str(OptV(1)) ...
     ' V'],'Units','Normalized')
  text(0.1,0.7,['x2 = ' num2str(Optx(2)) ' m  / V2 = ' num2str(OptV(2)) ...
     ' V'],'Units','Normalized')
  text(0.1,0.6,['x3 = ' num2str(Optx(3)) ' m  / V3 = ' num2str(OptV(3)) ...
     ' V'],'Units','Normalized')
  text(0.1,0.5,['x4 = ' num2str(Optx(4)) ' m  / V4 = ' num2str(OptV(4)) ...
     ' V'],'Units','Normalized')
  text(0.1,0.4,['Error = ' num2str(J)],'Units','Normalized')
else  % (n = 5)
  text(0.1,0.8,['x1 = ' num2str(Optx(1)) ' m  / V1 = ' num2str(OptV(1)) ...
     ' V'],'Units','Normalized')
  text(0.1,0.7,['x2 = ' num2str(Optx(2)) ' m  / V2 = ' num2str(OptV(2)) ...
     ' V'],'Units','Normalized')
  text(0.1,0.6,['x3 = ' num2str(Optx(3)) ' m  / V3 = ' num2str(OptV(3)) ...
     ' V'],'Units','Normalized')
  text(0.1,0.5,['x4 = ' num2str(Optx(4)) ' m  / V4 = ' num2str(OptV(4)) ...
     ' V'],'Units','Normalized')
  text(0.1,0.4,['x5 = ' num2str(Optx(5)) ' m  / V5 = ' num2str(OptV(5)) ...
     ' V'],'Units','Normalized')
  text(0.1,0.3,['Error = ' num2str(J)],'Units','Normalized')
end

% Allow data to be saved
Savedata = input('Save data? (y/n)  ','s');
if Savedata == 'y'
  Savefile = input('Enter filename (without .MAT extension)  ','s');
  eval(['save ' Savefile])
end
```

```
% FUNCTION TO DETERMINE ERROR BETWEEN ACTUAL BEAM SHAPE AND
% DESIRED PARABOLIC SHAPE FOR UNCONSTRAINED ACTUATOR
% LOCATION OPTIMIZATION
%
% function f = beamerxu(x,V0,la,K,C,L,n,Options)
%
% This function calculates the value of the cost function 'f'
% for a cantilever beam of length 'L' with 'n' attached
% piezoceramic actuators at locations 'x' with lengths 'la' and
% curvature per unit input voltage 'K' and a desired parabolic
% beam shape function y = C*x^2.

function f = beamerxu(x,V0,la,K,C,L,n,Options)

% Determine optimum actuator input voltages for input actuator
% locations 'x'
V = fmins('beamerVu',V0,Options,[],x,la,K,C,L,n);

% Calculate summations for use in calculating beam shape
% polynomial coefficients
sumKVl = zeros(n,1);
sumKVlxl = zeros(n,1);
for i = 1:n
  sumKVl(i) = sum(K(1:i).*V(1:i).*la(1:i));    % Sum of Ki*Vi*li
  sumKVlxl(i) = sum(K(1:i).*V(1:i).*la(1:i).*(x(1:i)+la(1:i)/2));
            % Sum of Ki*Vi*li*(xi+li/2)
end

% Calculate beam shape polynomial coefficients
a2 = K.*V/2;
a1 = -K.*V.*x;
a1(2:n) = a1(2:n) + sumKVl(1:n-1);
a0 = K.*V.*x.^2/2;
a0(2:n) = a0(2:n) - sumKVlxl(1:n-1);
b1 = sumKVl;
b0 = -sumKVlxl;

% Create nx1 vector containing value of 'C'
Cvect = C*ones(n,1);

% Calculate value of cost function
f = C^2*x(1)^5/5;
f = f + sum((a2-Cvect).^2.*((x+la).^5 - x.^5))/5;
f = f + sum((a2-Cvect).*a1.*((x+la).^4 - x.^4))/2;
```

```
f = f + sum((2*(a2-Cvect).*a0+a1.^2).*((x+la).^3 - x.^3))/3;
f = f + sum(a1.*a0.*((x+la).^2 - x.^2));
f = f + sum(a0.^2.*la);
f = f + C^2*sum(x(2:n).^5 - (x(1:n-1)+la(1:n-1)).^5)/5;
f = f - C*sum(b1(1:n-1).*(x(2:n).^4 - (x(1:n-1)+la(1:n-1)).^4))/2;
f = f + sum((-2*C*b0(1:n-1)+b1(1:n-1).^2).*(x(2:n).^3 - ...
   (x(1:n-1)+la(1:n-1)).^3))/3;
f = f + sum(b1(1:n-1).*b0(1:n-1).*(x(2:n).^2 - (x(1:n-1)+la(1:n-1)).^2));
f = f + sum(b0(1:n-1).^2.*(x(2:n) - x(1:n-1)-la(1:n-1)));
f = f + C^2*(L^5-(x(n)+la(n))^5)/5;
f = f - C*b1(n)*(L^4-(x(n)+la(n))^4)/2;
f = f + (-2*C*b0(n)+b1(n)^2)*(L^3-(x(n)+la(n))^3)/3;
f = f + b1(n)*b0(n)*(L^2-(x(n)+la(n))^2);
f = f + b0(n)^2*(L-x(n)-la(n));


% FUNCTION TO DETERMINE ERROR BETWEEN ACTUAL BEAM SHAPE AND
% DESIRED PARABOLIC SHAPE FOR UNCONSTRAINED ACTUATOR
% VOLTAGE OPTIMIZATION
%
% function f = BeamerVu(V,x,la,K,C,L,n)
%
% This function calculates the values of the cost function 'f'
% for a cantilever beam of
% length 'L' with 'n' attached piezoceramic actuators and a
% desired parabolic beam shape function y = C*x^2, where the
% elements of the input vector 'V' are the actuator input
% voltages, the elements of 'x' are the distances
% of the actuators from the root of the beam, and the
% elements of 'la' are the actuator lengths.

function f = BeamerVu(V,x,la,K,C,L,n)

% x = Actuator locations (m)
% V = Actuator voltages (V)
% la = Actuator lengths (m)

% Calculate summations for use in calculating beam shape
% polynomial coefficients
sumKVl = zeros(n,1);
sumKVlxl = zeros(n,1);
for i = 1:n
  sumKVl(i) = sum(K(1:i).*V(1:i).*la(1:i));    % Sum of Ki*Vi*li
  sumKVlxl(i) = sum(K(1:i).*V(1:i).*la(1:i).*(x(1:i)+la(1:i)/2));
```

```
        % Sum of Ki*Vi*li*(xi+li/2)
end

% Calculate beam shape polynomial coefficients
a2 = K.*V/2;
a1 = -K.*V.*x;
a1(2:n) = a1(2:n) + sumKVl(1:n-1);
a0 = K.*V.*x.^2/2;
a0(2:n) = a0(2:n) - sumKVlxl(1:n-1);
b1 = sumKVl;
b0 = -sumKVlxl;

% Create nx1 vector containing value of 'C'
Cvect = C*ones(n,1);

% Calculate value of cost function
f = C^2*x(1)^5/5;
f = f + sum((a2-Cvect).^2.*((x+la).^5 - x.^5))/5;
f = f + sum((a2-Cvect).*a1.*((x+la).^4 - x.^4))/2;
f = f + sum((2*(a2-Cvect).*a0+a1.^2).*((x+la).^3 - x.^3))/3;
f = f + sum(a1.*a0.*((x+la).^2 - x.^2));
f = f + sum(a0.^2.*la);
f = f + C^2*sum(x(2:n).^5 - (x(1:n-1)+la(1:n-1)).^5)/5;
f = f - C*sum(b1(1:n-1).*(x(2:n).^4 - (x(1:n-1)+la(1:n-1)).^4))/2;
f = f + sum((-2*C*b0(1:n-1)+b1(1:n-1).^2).*(x(2:n).^3 - ...
   (x(1:n-1)+la(1:n-1)).^3))/3;
f = f + sum(b1(1:n-1).*b0(1:n-1).*(x(2:n).^2 - (x(1:n-1)+la(1:n-1)).^2));
f = f + sum(b0(1:n-1).^2.*(x(2:n) - x(1:n-1)-la(1:n-1)));
f = f + C^2*(L^5-(x(n)+la(n))^5)/5;
f = f - C*b1(n)*(L^4-(x(n)+la(n))^4)/2;
f = f + (-2*C*b0(n)+b1(n)^2)*(L^3-(x(n)+la(n))^3)/3;
f = f + b1(n)*b0(n)*(L^2-(x(n)+la(n))^2);
f = f + b0(n)^2*(L-x(n)-la(n));
```

```
% FUNCTION TO DETERMINE ERROR BETWEEN ACTUAL BEAM SHAPE AND
% DESIRED C*(1-cos(mx)) SHAPE FOR UNCONSTRAINED ACTUATOR
% LOCATION OPTIMIZATION
%
% function f = bercosxu(x,V0,la,K,C,m,L,n,Options)
%
% This function calculates the value of the cost function 'f'
% for a cantilever beam of length 'L' with 'n' attached
% piezoceramic actuators at locations 'x' with lengths 'la' and
% curvature per unit input voltage 'K' and a desired sinusoidal
% beam shape function y = C*(1-cos(mx)).

function f = bercosxu(x,V0,la,K,C,m,L,n,Options)

% Determine optimum actuator input voltages for input actuator
% locations 'x'
V = fmins('bercosVu',V0,Options,[],x,la,K,C,m,L,n);

% Calculate summations for use in calculating beam shape
% polynomial coefficients
sumKVl = zeros(n,1);
sumKVlxl = zeros(n,1);
for i = 1:n
  sumKVl(i) = sum(K(1:i).*V(1:i).*la(1:i));    % Sum of Ki*Vi*li
  sumKVlxl(i) = sum(K(1:i).*V(1:i).*la(1:i).*(x(1:i)+la(1:i)/2));
            % Sum of Ki*Vi*li*(xi+li/2)
end

% Calculate beam shape polynomial coefficients
a2 = K.*V/2;
a1 = -K.*V.*x;
a1(2:n) = a1(2:n) + sumKVl(1:n-1);
a0 = K.*V.*x.^2/2;
a0(2:n) = a0(2:n) - sumKVlxl(1:n-1);
b1 = sumKVl;
b0 = -sumKVlxl;

% Create nx1 vector containing value of 'C'
Cvect = C*ones(n,1);

% Calculate value of cost function
f = C^2*(x(1)-2/m*sin(m*x(1)) + L/2 + 1/4/m*sin(2*m*L));
f = f + sum(a2.^2.*((x+la).^5 - x.^5))/5;
f = f + sum(a2.*a1.*((x+la).^4 - x.^4))/2;
```

```
f = f + sum((2*a2.*(a0-Cvect)+a1.^2).*((x+la).^3 - x.^3))/3;
f = f + sum(a1.*(a0-Cvect).*((x+la).^2 - x.^2));
f = f + sum((a0-Cvect).^2.*la);
f = f + 2*C*sum(a2.*(2/m^2*((x+la).*cos(m*(x+la))-x.*cos(m*x))));
f = f + 2*C*sum(a2.*(((x+la).^2/m-2/m^3*ones(n,1)).*sin(m*(x+la))- ...
   (x.^2/m-2/m^3*ones(n,1)).*sin(m*x)));
f = f + 2*C*sum(a1.*((cos(m*(x+la))-cos(m*x))/m^2 + ...
   ((x+la).*sin(m*(x+la))-x.*sin(m*x))/m));
f = f + 2/m*C*sum((a0-Cvect).*(sin(m*(x+la))-sin(m*x)));
f = f + sum(b1(1:n-1).^2.*(x(2:n).^3 - (x(1:n-1)+la(1:n-1)).^3))/3;
f = f + sum(b1(1:n-1).*(b0(1:n-1)-Cvect(1:n-1)).*(x(2:n).^2 - ...
   (x(1:n-1)+la(1:n-1)).^2));
f = f + sum((b0(1:n-1)-Cvect(1:n-1)).^2.*(x(2:n) - x(1:n-1)-la(1:n-1)));
f = f + 2*C*sum(b1(1:n-1).*(cos(m*x(2:n))-cos(m*(x(1:n-1)+la(1:n-1)))))/m^2;
f = f + 2*C*sum(b1(1:n-1).*(x(2:n).*sin(m*x(2:n))-(x(1:n-1)+la(1:n-1)).* ...
   sin(m*(x(1:n-1)+la(1:n-1)))))/m;
f = f + 2*C/m*sum((b0(1:n-1)-Cvect(1:n-1)).*(sin(m*x(2:n))- ...
   sin(m*(x(1:n-1)+la(1:n-1)))));
f = f + b1(n).^2.*(L.^3 - (x(n)+la(n)).^3)/3;
f = f + b1(n).*(b0(n)-C).*(L.^2 - (x(n)+la(n)).^2);
f = f + (b0(n)-C).^2.*(L - x(n)-la(n));
f = f + 2*C*b1(n).*(cos(m*L)-cos(m*(x(n)+la(n))))/m^2;
f = f + 2*C*b1(n).*(L.*sin(m*L)-(x(n)+la(n)).*sin(m*(x(n)+la(n))))/m;
f = f + 2*C/m*(b0(n)-C).*(sin(m*L)-sin(m*(x(n)+la(n))));


% FUNCTION TO DETERMINE ERROR BETWEEN ACTUAL BEAM SHAPE AND
% DESIRED C*(1-cos(mx)) SHAPE FOR UNCONSTRAINED ACTUATOR
% VOLTAGE OPTIMIZATION
%
% function f = bercosVu(x,V0,la,K,C,m,L,n,Options)
%
% This function calculates the value of the cost function 'f'
% for a cantilever beam of length 'L' with 'n' attached
% piezoceramic actuators at locations 'x' with lengths 'la' and
% curvature per unit input voltage 'K' and a desired sinusoidal
% beam shape function y = C*(1-cos(mx)).

function f = bercosVu(V,x,la,K,C,m,L,n,Options)

% x = Actuator locations (m)
% V = Actuator voltages (V)
% la = Actuator lengths (m)
```

```
% Calculate summations for use in calculating beam shape
% polynomial coefficients
sumKVl = zeros(n,1);
sumKVlxl = zeros(n,1);
for i = 1:n
  sumKVl(i) = sum(K(1:i).*V(1:i).*la(1:i));    % Sum of Ki*Vi*li
  sumKVlxl(i) = sum(K(1:i).*V(1:i).*la(1:i).*(x(1:i)+la(1:i)/2));
            % Sum of Ki*Vi*li*(xi+li/2)
end

% Calculate beam shape polynomial coefficients
a2 = K.*V/2;
a1 = -K.*V.*x;
a1(2:n) = a1(2:n) + sumKVl(1:n-1);
a0 = K.*V.*x.^2/2;
a0(2:n) = a0(2:n) - sumKVlxl(1:n-1);
b1 = sumKVl;
b0 = -sumKVlxl;

% Create nx1 vector containing value of 'C'
Cvect = C*ones(n,1);

% Calculate value of cost function
f = C^2*(x(1)-2/m*sin(m*x(1)) + L/2 + 1/4/m*sin(2*m*L));
f = f + sum(a2.^2.*((x+la).^5 - x.^5))/5;
f = f + sum(a2.*a1.*((x+la).^4 - x.^4))/2;
f = f + sum((2*a2.*(a0-Cvect)+a1.^2).*((x+la).^3 - x.^3))/3;
f = f + sum(a1.*(a0-Cvect).*((x+la).^2 - x.^2));
f = f + sum((a0-Cvect).^2.*la);
f = f + 2*C*sum(a2.*(2/m^2*((x+la).*cos(m*(x+la))-x.*cos(m*x))));
f = f + 2*C*sum(a2.*(((x+la).^2/m-2/m^3*ones(n,1)).*sin(m*(x+la))- ...
   (x.^2/m-2/m^3*ones(n,1)).*sin(m*x)));
f = f + 2*C*sum(a1.*((cos(m*(x+la))-cos(m*x))/m^2 + ...
   ((x+la).*sin(m*(x+la))-x.*sin(m*x))/m));
f = f + 2/m*C*sum((a0-Cvect).*(sin(m*(x+la))-sin(m*x)));
f = f + sum(b1(1:n-1).^2.*(x(2:n).^3 - (x(1:n-1)+la(1:n-1)).^3))/3;
f = f + sum(b1(1:n-1).*(b0(1:n-1)-Cvect(1:n-1)).*(x(2:n).^2 - ...
   (x(1:n-1)+la(1:n-1)).^2));
f = f + sum((b0(1:n-1)-Cvect(1:n-1)).^2.*(x(2:n) - x(1:n-1)-la(1:n-1)));
f = f + 2*C*sum(b1(1:n-1).*(cos(m*x(2:n))-cos(m*(x(1:n-1)+la(1:n-1)))))/m^2;
f = f + 2*C*sum(b1(1:n-1).*(x(2:n).*sin(m*x(2:n))-(x(1:n-1)+la(1:n-1)).* ...
   sin(m*(x(1:n-1)+la(1:n-1)))))/m;
f = f + 2*C/m*sum((b0(1:n-1)-Cvect(1:n-1)).*(sin(m*x(2:n))- ...
   sin(m*(x(1:n-1)+la(1:n-1)))));
```

```
f = f + b1(n).^2.*(L.^3 - (x(n)+la(n)).^3)/3;
f = f + b1(n).*(b0(n)-C).*(L.^2 - (x(n)+la(n)).^2);
f = f + (b0(n)-C).^2.*(L - x(n)-la(n));
f = f + 2*C*b1(n).*(cos(m*L)-cos(m*(x(n)+la(n))))/m^2;
f = f + 2*C*b1(n).*(L.*sin(m*L)-(x(n)+la(n)).*sin(m*(x(n)+la(n))))/m;
f = f + 2*C/m*(b0(n)-C).*(sin(m*L)-sin(m*(x(n)+la(n))));


% FUNCTION TO DETERMINE THE DEFLECTED SHAPE OF A CANTILEVER
% BEAM DUE TO ATTACHED PIEZOCERAMIC ACTUATORS
%
% function y = beamdisp(x,xa,v,la,n,K)
%
% This function returns a vector of transverse displacements, y,
% of a cantilever beam with 'n' attached piezoceramic actuators,
% given the starting locations of the actuators, 'xa', the lengths
% of the actuators, 'la', the actuator input voltages, 'v', and the
% vector 'K' containing the actuator curvatures per unit voltage.
%  'x' is a vector containing a range of axial distances from the
% root of the beam at which 'y' is to be evaluated and 'xa', 'v'
% and 'la' are all nx1 vectors.

function y = beamdisp(x,xa,v,la,n,K)
y = zeros(size(x));
for m = 1:length(x)
 if x(m) <= xa(1)    % x prior to start of actuator
  y(m) = 0;
 elseif xa(1) < x(m) & x(m) <= xa(1)+la(1)
  y(m) = K(1)*v(1)/2*(x(m)-xa(1))^2;
 elseif x(m) <= xa(n)+la(n)
  for k = 1:n
   if xa(k) <= x(m) & x(m) <= xa(k)+la(k)
    y(m) = K(k)*v(k)/2*(x(m)-xa(k))^2+sum(K(1:k-1).*v(1:k-1).* ...
        la(1:k-1).*(x(m)*ones(size(xa(1:k-1)))-xa(1:k-1)-la(1:k-1)/2));
   elseif k<n
    if xa(k)+la(k) <= x(m) & x(m) <= xa(k+1)
     y(m) = sum(K(1:k).*v(1:k).*la(1:k).*(x(m)*ones(size(xa(1:k)))- ...
         xa(1:k)-la(1:k)/2));
    end
   end
  end
 else
  y(m) = sum(K(1:n).*v(1:n).*la(1:n).*(x(m)*ones(size(xa(1:n)))- ...
      xa(1:n)-la(1:n)/2));
```

```
 end
end


% PROGRAM TO DETERMINE OPTIMUM ACTUATOR LOCATIONS
% FROM A GIVEN DISCRETE SET OF POSSIBLE LOCATIONS
%
% This program determines the optimum actuator location and input
% voltage from a specified discrete range of possible actuator
% locations to achieve the minimum error between the actuator deformed
% beam shape and a desired parabolic shape function for a cantilever
% beam with piezoceramic actuators bonded to both sides of the beam.
% 1, 2 or 3 actuators can be specified

% Coefficient of desired parabolic shape function
C = 0.001;

% Enter beam properties
L = 1;              % Beam length (m)
w = 0.0508;         % Beam width (m)
t = 0.001575;       % Beam thickness (m)
E = 7.2e10;         % Beam modulus of elasticity (N/m^2)

% Enter piezoceramic actuator properties
% Navy Type II PZT
n = 3;              % Number of actuators
la = 0.1*ones(n,1);   % Actuator lengths (m)
wp = 0.0381;        % Piezoceramic actuator width (m)
tp = 0.00027;       % Piezoceramic actuator thickness (m)
Ep = 6.1e10;        % Piezoceramic actuator modulus of elasticity (N/m^2)
d31 = 1.71e-10;     % Piezoelectric constant (m/V)

% Enter properties of bond between piezoceramic actuator and beam
wb = wp;            % Bond width (m)  (equal to actuator width)
tb = 0;             % Bond thickness (m)
Eb = 1.78e9;        % Bond modulus of elasticity (N/m^2)

% Calculate properties of beam cross-section
area = w.*t;        % Beam cross-sectional area (m^2)
areab = wb*tb;      % Bond cross-sectional area (m^2)
areap = wp*tp;      % Piezoceramic actuator cross-sectional area (m^2)
moi = w.*t.^3/12;   % Beam cross-section moment of inertia (m^4)
% Bond cross-section moment of inertia (m^4)
moib = wb*tb*(t^2/2 + t*tb + 2*tb^2/3);
```

```
% Piezoceramic actuator cross-section moment of inertia (m^4)
moip = wp*tp*((t+2*tb)^2/2 + (t+2*tb)*tp + 2*tp^2/3);
EI = E*moi+Eb*moib+Ep*moip;  % Beam stiffness
K = Ep*d31*wp*(t+2*tb+tp)/EI;  % (Moment per unit voltage)/(Beam stiffness)
K = K*ones(n,1);

% Set run number, minimum and maximum locations for actuators
% and spacing between actuator locations in range of positions
% evaluated between minimum and maximum locations for each actuator
Run = 6;                    % Run number
Savefile = 'NTII3_6';
xmin = [0.055 0.355 0.655];          % Run 6 (0.005 spacing)
xmax = [0.095 0.395 0.695];          % Run 6 (0.005 spacing)
Spacing = [0.005 0.005 0.005];       % Run 6

% Set initial voltages for unconstrained voltage optimization algorithm
V0 = zeros(n,1);

% Set options for unconstrained voltage optimization algorithm
Options = foptions';
Options(14) = 2000;    % Maximum number of iterations (0 -> 100*n)

% Divide each actuator location range into up to 9 equally spaced
% possible locations separated by the interval set in 'Spacing'
if n == 1       % 1 Actuator
  xrange = [xmin:Spacing:xmax];
elseif n == 2   % 2 Actuators
  xrange = [xmin(1):Spacing(1):xmax(1);xmin(2):Spacing(2):xmax(2)];
else            % 3 Actuators
  xrange = [xmin(1):Spacing(1):xmax(1);xmin(2):Spacing(2):xmax(2); ...
          xmin(3):Spacing(3):xmax(3)];
end

% Evaluate optimum actuator voltages and beam shape error
% for each combination of actuator locations
x = zeros(n,1);
Maxindex = length(xrange);
if n == 1                       % 1 Actuator
  Ermatrix = zeros(Maxindex,1);
  Voltage1 = zeros(Maxindex,1);
  for k = 1:Maxindex
    fprintf(['\nk = ' int2str(k) '\n'])
    x = xrange(k);
    V = fmins('beamerVu',V0,Options,[],x,la,K,C,L,n);
```

```
  Voltage1(k) = V;
  Ermatrix(k) = beamerVu(V,x,la,K,C,L,n);
  if k ~= 1
   if Ermatrix(k) < Minerror
    Optloc = k;
    OptV = V;
    Minerror = Ermatrix(k)
   end
  else
   Optloc = 1;
   OptV = V;
   Minerror = Ermatrix(k)
  end
 end
 clear k
 Optx = xrange(Optloc)
 OptV
 Minerror

elseif n == 2                    % 2 Actuators
 Ermatrix = zeros(10);
 Voltage1 = zeros(10);
 Voltage2 = zeros(10);
 Voltsum = zeros(10);
 for j = 1:Maxindex
  x(1) = xrange(1,j);
  for k = 1:Maxindex
   fprintf(['\njk = ' int2str(j) ' ' int2str(k) '\n'])
   x(2) = xrange(2,k);
   if (x(1)+la(1)<=x(2))
    V = fmins('beamerVu',V0,Options,[],x,la,K,C,L,n);
    Voltage1(j,k) = V(1);
    Voltage2(j,k) = V(2);
    Ermatrix(j,k) = beamerVu(V,x,la,K,C,L,n);
    if j+k ~= 2
     if Ermatrix(j,k) < Minerror
      Optloc = [j k];
      OptV = V;
      Minerror = Ermatrix(j,k)
     end
    else
     Optloc = [1 1];
     OptV = V;
     Minerror = Ermatrix(j,k)
```

```
      end
    else
      Voltage1(j,k) = 0;
      Voltage2(j,k) = 0;
      Ermatrix(j,k) = 0;
    end
  end
end
clear j k
Optx = [xrange(1,Optloc(1));xrange(2,Optloc(2))]
OptV
Minerror
Voltsum = Voltage1+Voltage2;

else                          % 3 Actuators
 Ermatrix = zeros(100,10);
 Voltage1 = zeros(100,10);
 Voltage2 = zeros(100,10);
 Voltage3 = zeros(100,10);
 Voltsum = zeros(100,10);
 for i = 1:Maxindex
  x(1) = xrange(1,i);
  for j = 1:Maxindex
   x(2) = xrange(2,j);
   for k = 1:Maxindex
    fprintf(['\nijk = ' int2str(i) ' ' int2str(j) ' ' int2str(k) '\n'])
    x(3) = xrange(3,k);
    if (x(1)+la(1)<=x(2)) & (x(2)+la(2)<=x(3))
     V = fmins('beamerVu',V0,Options,[],x,la,K,C,L,n);
     Voltage1(10*(i-1)+j,k) = V(1);
     Voltage2(10*(i-1)+j,k) = V(2);
     Voltage3(10*(i-1)+j,k) = V(3);
     Ermatrix(10*(i-1)+j,k) = beamerVu(V,x,la,K,C,L,n);
     if i+j+k ~= 3
      if Ermatrix(10*(i-1)+j,k) < Minerror
       Optloc = [i j k];
       OptV = V;
       Minerror = Ermatrix(10*(i-1)+j,k)
      end
     else
      Optloc = [1 1 1];
      OptV = V;
      Minerror = Ermatrix(10*(i-1)+j,k)
     end
```

```
      else
        Voltage1(10*(i-1)+j,k) = 0;
        Voltage2(10*(i-1)+j,k) = 0;
        Voltage3(10*(i-1)+j,k) = 0;
        Ermatrix(10*(i-1)+j,k) = 0;
      end
    end
  end
 end
 clear i j k
 Optx = [xrange(1,Optloc(1));xrange(2,Optloc(2));xrange(3,Optloc(3))]
 OptV
 Minerror
 Voltsum = Voltage1+Voltage2+Voltage3;
end

% Plot results
x = linspace(0,L,100);
y = beamdisp(x,Optx,OptV,la,n,K);          % Fixed length actuators
yact = beamdisp([Optx;Optx+la],Optx,OptV,la,n,K);
yf = C*x.^2;
figure
plot(x,y,'r-',x,yf,'g.',[Optx;Optx+la],yact,'r*')
legend('Actual','Desired',-1)
grid
title('Actual vs. Desired Beam Shapes')
xlabel('X (m)')
ylabel('Beam Displacement Y (m)')
if n == 1
 text(0.1,0.9,['Run ' int2str(Run) ' Optimum Values for 1 Actuator:'], ...
    'Units','Normalized')
 text(0.1,0.8,['x1 = ' num2str(Optx(1)) ' m  / V1 = ' num2str(OptV(1)) ...
    ' V'],'Units','Normalized')
 text(0.1,0.7,['Error = ' num2str(Minerror,4)],'Units','Normalized')
elseif n == 2
 text(0.1,0.9,['Run ' int2str(Run) ' Optimum Values for 2 Actuators:'], ...
    'Units','Normalized')
 text(0.1,0.8,['x1 = ' num2str(Optx(1)) ' m  / V1 = ' num2str(OptV(1)) ...
    ' V'],'Units','Normalized')
 text(0.1,0.7,['x2 = ' num2str(Optx(2)) ' m  / V1 = ' num2str(OptV(2)) ...
    ' V'],'Units','Normalized')
 text(0.1,0.6,['Error = ' num2str(Minerror,4)],'Units','Normalized')
elseif n == 3
 text(0.1,0.9,['Run ' int2str(Run) ' Optimum Values for 3 Actuators:'], ...
```

```
    'Units','Normalized')
 text(0.1,0.8,['x1 = ' num2str(Optx(1)) ' m  / V1 = ' num2str(OptV(1)) ...
    ' V'],'Units','Normalized')
 text(0.1,0.7,['x2 = ' num2str(Optx(2)) ' m  / V1 = ' num2str(OptV(2)) ...
    ' V'],'Units','Normalized')
 text(0.1,0.6,['x3 = ' num2str(Optx(3)) ' m  / V1 = ' num2str(OptV(3)) ...
    ' V'],'Units','Normalized')
 text(0.1,0.5,['Error = ' num2str(Minerror,4)],'Units','Normalized')
end

% Save data to .MAT file
eval(['save ' Savefile])


% PROGRAM TO DETERMINE OPTIMUM ACTUATOR INPUT VOLTAGES
% FROM A GIVEN DISCRETE SET OF POSSIBLE VOLTAGES
%
% This program determines the optimum actuator input voltages
% from a specified discrete range of possible actuator
% voltages to achieve the minimum error between the actuator deformed
% beam shape and a desired parabolic shape function for a cantilever
% beam with piezoceramic actuators bonded to both sides of the beam.
% 1, 2 or 3 actuators can be specified

% Coefficient of desired parabolic shape function
C = 0.001;

% Enter beam properties
L = 1;              % Beam length (m)
w = 0.0508;         % Beam width (m)
t = 0.001575;       % Beam thickness (m)
E = 7.2e10;         % Beam modulus of elasticity (N/m^2)

% Enter piezoceramic actuator properties
% Navy Type II PZT
n = 3;              % Number of actuators
la = 0.1*ones(n,1);   % Actuator lengths (m)
wp = 0.0381;        % Piezoceramic actuator width (m)
tp = 0.00027;       % Piezoceramic actuator thickness (m)
Ep = 6.1e10;        % Piezoceramic actuator modulus of elasticity (N/m^2)
d31 = 1.71e-10;     % Piezoelectric constant (m/V)
Vmax = 150;         % Maximum actuator input voltage (V)
Vmin = -150;        % Minimum actuator input voltage (V)
```

```
% Enter properties of bond between piezoceramic actuator and beam
wb = wp;              % Bond width (m)  (equal to actuator width)
tb = 0;              % Bond thickness (m)
Eb = 1.78e9;          % Bond modulus of elasticity (N/m^2)

% Calculate properties of beam cross-section
area = w.*t;          % Beam cross-sectional area (m^2)
areab = wb*tb;        % Bond cross-sectional area (m^2)
areap = wp*tp;        % Piezoceramic actuator cross-sectional area (m^2)
moi = w.*t.^3/12;     % Beam cross-section moment of inertia (m^4)
% Bond cross-section moment of inertia (m^4)
moib = wb*tb*(t^2/2 + t*tb + 2*tb^2/3);
% Piezoceramic actuator cross-section moment of inertia (m^4)
moip = wp*tp*((t+2*tb)^2/2 + (t+2*tb)*tp + 2*tp^2/3);
EI = E*moi+Eb*moib+Ep*moip;  % Beam stiffness
K = Ep*d31*wp*(t+2*tb+tp)/EI;  % (Moment per unit voltage)/(Beam stiffness)
K = K*ones(n,1);

% Set run number, minimum and maximum voltages for actuators
% and increment between actuator voltages in range of positions
% evaluated between minimum and maximum locations for each actuator
Run = 1;                  % Run number
Savefile = 'NTII1_1V';
Vmin = [10];              % Run 1 (5 V increment)
Vmax = [50];              % Run 1 (5 V increment)
Incremnt = [5];           % Run 1

% Set actuator locations
if n == 1
  x = 0.2420;
elseif n == 2
  x = [0.1220;0.5394];
else
  x = [0.0728;0.3678;0.6641];
end

% Set initial voltages for unconstrained voltage optimization algorithm
V0 = zeros(n,1);

% Set options for unconstrained voltage optimization algorithm
Options = foptions';
Options(14) = 2000;    % Maximum number of iterations (0 -> 100*n)

% Divide each actuator voltage range into up to 9 equally spaced
```

```
% possible locations separated by the interval set in 'Spacing'
if n == 1       % 1 Actuator
  Vrange = [Vmin:Incremnt:Vmax];
elseif n == 2   % 2 Actuators
  Vrange = [Vmin(1):Incremnt(1):Vmax(1);Vmin(2):Incremnt(2):Vmax(2)];
else            % 3 Actuators
  Vrange =
[Vmin(1):Incremnt(1):Vmax(1);Vmin(2):Incremnt(2):Vmax(2);Vmin(3):Incremnt(3):Vma
x(3)];
end

% Evaluate optimum actuator voltages and beam shape error
% for each combination of actuator locations
Maxindex = length(Vrange);
if n == 1                       % 1 Actuator
  Ermatrix = zeros(Maxindex,1);
  Voltage1 = zeros(Maxindex,1);
  for k = 1:Maxindex
    fprintf(['\nk = ' int2str(k) '\n'])
    V = Vrange(k);
    Ermatrix(k) = beamerVu(V,x,la,K,C,L,n);
    if k ~= 1
      if Ermatrix(k) < Minerror
        OptV = V;
        Minerror = Ermatrix(k)
      end
    else
      OptV = V;
      Minerror = Ermatrix(k)
    end
  end
  clear k
  OptV
  Minerror

elseif n == 2                   % 2 Actuators
  Ermatrix = zeros(10);
  for j = 1:Maxindex
    for k = 1:Maxindex
      fprintf(['\njk = ' int2str(j) ' ' int2str(k) '\n'])
      V = [Vrange(1,j);Vrange(2,k)];
      Ermatrix(j,k) = beamerVu(V,x,la,K,C,L,n);
      if j+k ~= 2
        if Ermatrix(j,k) < Minerror
```

```
        OptV = V;
        Minerror = Ermatrix(j,k)
       end
      else
       OptV = V;
       Minerror = Ermatrix(j,k)
      end
     end
    end
    clear j k
    OptV
    Minerror

else                          % 3 Actuators
    Ermatrix = zeros(100,10);
    for i = 1:Maxindex
     for j = 1:Maxindex
      for k = 1:Maxindex
       fprintf(['\nijk = ' int2str(i) ' ' int2str(j) ' ' int2str(k) '\n'])
       V = [Vrange(1,i);Vrange(2,j);Vrange(3,k)];
       Ermatrix(10*(i-1)+j,k) = beamerVu(V,x,la,K,C,L,n);
       if i+j+k ~= 3
        if Ermatrix(10*(i-1)+j,k) < Minerror
         OptV = V;
         Optindex = [i j k];
         Minerror = Ermatrix(10*(i-1)+j,k)
        end
       else
        OptV = V;
        Optindex = [i j k];
        Minerror = Ermatrix(10*(i-1)+j,k)
       end
      end
     end
    end
    clear i j k
    OptV
    Minerror
end

% Plot results
if n == 1    % 1 Actuator
 % Plot variation in shape error vs. actuator voltage
 figure
```

```
plot(Vrange,Ermatrix)
title('Error vs. Actuator Input Voltage for 1 Actuator')
xlabel('Actuator Voltage (V)')
ylabel('Error')
text(0.15,0.95,['Run ' int2str(Run)],'Units','Normalized')
text(0.15,0.85,['Actuator Location:  ' num2str(x) ' m'],'Units','Normalized')
grid

elseif n == 2    % 2 Actuators
 % Plot variation in shape error vs. actuator positions
 figure
 meshz(Vrange(2,:),Vrange(1,:),Ermatrix(1:Maxindex,1:Maxindex))
 title('Error vs. Actuator Input Voltages for 2 Actuators')
 xlabel('Voltage 2 (V)')
 ylabel('Voltage 1 (V)')
 text(0.15,0.95,['Run ' int2str(Run)],'Units','Normalized')
 text(0.15,0.85,['Actuator Locations:  ' num2str(x(1)) ' m  ' ...
    num2str(x(2)) ' m'],'Units','Normalized')

else    % 3 Actuators
 % Plot variation in shape error for Actuator 1 fixed
 % at optimum location
 figure
 meshz(Vrange(3,:),Vrange(2,:),Ermatrix(10*(Optindex(1)-1)+1: ...
     10*(Optindex(1)-1)+Maxindex,1:Maxindex))
 title('Error vs. Actuator 2 & 3 Voltage at Optimum Actuator 1 Voltage')
 xlabel('Voltage 3 (V)')
 ylabel('Voltage 2 (V)')
 text(0.15,0.95,['Run ' int2str(Run)],'Units','Normalized')
 text(0.15,0.85,['Actuator Locations:  ' num2str(x(1)) ' m  ' ...
    num2str(x(2)) ' m  ' num2str(x(3)) ' m'],'Units','Normalized')

 % Plot variation in shape error for Actuator 2 fixed
 % at optimum location
 figure
 meshz(Vrange(3,:),Vrange(1,:),Ermatrix(10*[0:Maxindex-1]+ ...
     Optindex(2)*ones(1,Maxindex),1:Maxindex))
 title('Error vs. Actuator 1 & 3 Voltage at Optimum Actuator 2 Voltage')
 xlabel('Voltage 3 (V)')
 ylabel('Voltage 1 (V)')
 text(0.15,0.95,['Run ' int2str(Run)],'Units','Normalized')
 text(0.15,0.85,['Actuator Locations:  ' num2str(x(1)) ' m  ' ...
    num2str(x(2)) ' m  ' num2str(x(3)) ' m'],'Units','Normalized')
```

```
 % Plot variation in shape error for Actuator 3 fixed
 % at optimum location
 figure
 Ermesh = reshape(Ermatrix(:,Optindex(3)),10,10)';
 meshz(Vrange(2,:),Vrange(1,:),Ermesh(1:Maxindex,1:Maxindex))
 title('Error vs. Actuator 1 & 2 Voltage at Optimum Actuator 3 Voltage')
 xlabel('Voltage 2 (V)')
 ylabel('Voltage 1 (V)')
 text(0.15,0.95,['Run ' int2str(Run)],'Units','Normalized')
 text(0.15,0.85,['Actuator Locations:  ' num2str(x(1)) ' m  ' ...
     num2str(x(2)) ' m  ' num2str(x(3)) ' m'],'Units','Normalized')
end

% Save data to .MAT file
eval(['save ' Savefile])
```

LIST OF REFERENCES

1. Crawley, E. F. and Anderson, "Detailed Models of the Piezoceramic Actuation of Beams," *Journal of Intelligent Material Systems and Structures*, vol. 1, January, 1990.

2. *Guide to Modern Piezoelectric Ceramics*, Vernitron Division, Morgan Matroc, Inc., Bedford, Oh, 1991.

3. Crawley, E. F. and de Luis, J., "Use of Piezoelectric Actuators as Elements of Intelligent Structures," *AIAA Journal*, vol. 25, no. 10, pp. 1373-1385, October 1987.

4. Chaudry, Z. A. and Rogers, C. A., "A Mechanics Approach to Induced Strain Actuation of Structures," Third International Conference on Adaptive Structures, San Diego, CA, November, 1992.

5. Bronowicki A. J. and Betros, R. S., *Design and Implementation of Active Structures*, Active Structures Workshop course notes, TRW Space and Electronics Group, Redondo Beach, CA.

6. Griffin, S. F., Denoyer, K. K. and Yost, B. J., "Smart Patch Piezoceramic Actuator Issues," Seventh NASA/DoD CSI Conference, Lake Tahoe, CA, 1992.

7. Baz, A. and Poh, S., "Optimum Shape Control of Flexible Beams by Piezoelectric Actuators," Mechanical Engineering Department, The Catholic University of America, Washington, D.C.

8. Bazaraa, M. S. and Shetty, C. M., *Nonlinear Programming Theory and Algorithms*, John Wiley & Sons, 1979.

9. Grace, A., *Optimization Toolbox User's Guide*, The Mathworks, Inc., 1995.

10. Clark, R. L. and Fuller, C. R., "Optimal Placement of Piezoelectric Actuators and Polyvinylidene Fluoride Error Sensors In Active Structural Acoustic Control Approaches," *Journal of the Acoustical Society of America*, vol. 92, no. 3, September 1992.

11. Wang, B. T., Burdisso, R. A. and Fuller, C. R., "Optimal Placement of Piezoelectric Actuators for Active Structural Acoustic Control," *Journal of Intelligent Material Systems and Structures*, vol. 5, January, 1994.

12. Parkinson, J. M. and Hutchinson, D., "A Consideration of Non-gradient Algorithms for the Unconstrained Optimization of Functions of High Dimensionality", *Numerical Methods for Optimization*, Academic Press, 1972, F. A. Lootsma, editor.

13. Parkinson, J. M. and Hutchinson, D., "An Investigation into the Efficiency of Variants on the Simplex Method", *Numerical Methods for Optimization*, Academic Press, 1972, F. A. Lootsma, editor.

14. Udd, E., *Fiber Optic Smart Structures*, John Wiley & Sons, Inc., 1995.

BIBLIOGRAPHY

Agrawal, B. N., class notes for course AA4816, "Dynamics and Control of Smart Structures," Naval Postgraduate School, 1996.

Allen, D. H. and Haisler, W. E., *Introduction to Aerospace Structural Analysis*, John Wiley & Sons, Inc., 1985.

Jones, R. M., *Mechanics of Composite Materials*, Taylor and Francis, 1975.

Vanderplaats, G. N., *Numerical Optimization Techniques for Engineering Design: With Applications*, McGraw-Hill, Inc., 1984.

INITIAL DISTRIBUTION LIST

1. Defense Technical Information Center — 2
   8725 John J. Kingman Rd., STE 0944
   Ft. Belvoir, VA 22060-6218

2. Dudley Knox Library — 2
   Naval Postgraduate School
   411 Dyer Rd.
   Monterey, CA 93943-5002

3. Chairman, Code AA — 1
   Department of Aeronautics and Astronautics
   Naval Postgraduate School
   Monterey, CA 93943

4. Professor Brij N. Agrawal, Code AA/Ag — 2
   Department of Aeronautics and Astronautics
   Naval Postgraduate School
   Monterey, CA 93943

5. Dr. John L. Meyer — 2
   Code 8220
   Naval Research Laboratory
   4555 Overlook Ave., SW
   Washington, D.C. 20375

6. Professor Barry S. Leonard, Code AA/Ln — 1
   Department of Aeronautics and Astronautics
   Naval Postgraduate School
   Monterey, CA 93943

7. Professor Don A. Danielson, Code MA/Dd — 1
   Department of Mathematics
   Naval Postgraduate School
   Monterey, CA 93943

8. LT Kirk E. Treanor, USN — 1
   975 Linda Dr.
   Campbell, CA 95008